January 2012

Syntheses And Characterization Of Homo- And Heterometallic Tert-Butoxides/cyclopentadienides Of Group 4/14 Metals And Mixed Ligand (tert-Butoxides/cyclopentadienides) Coordination Polymers Of Group 1/14 Metals

Edmond Yong Njua

SYNTHESES AND CHARACTERIZATION OF HOMO- AND HETEROMETALLIC *TERT*-BUTOXIDES/CYCLOPENTADIENIDES OF GROUP 4/14 METALS AND MIXED LIGAND (*TERT*-BUTOXIDES/CYCLOPENTADIENIDES) COORDINATION POLYMERS OF GROUP 1/14 METALS

By

Edmond Yong Njua

Bachelor of Science, University of Buea, 2004

A Dissertation

Submitted to the Graduate School

of the

University of North Dakota

In partial fulfillment of the requirements

for the degree of

Doctor of Philosophy

Grand Forks, North Dakota

August 2012

This dissertation, submitted by Edmond Yong Njua in partial fulfillment of the requirements for the Degree of Doctor of Philosophy from the University of North Dakota, has been read by the Faculty Advisory Committee under whom the work has been done, and is hereby approved.

Dr. Lothar Stahl

Dr. Harmon Abrahamson

Dr. Irina Smoliakova

Dr. Kathryn Thomasson

Dr. William Schwalm

This dissertation is being submitted by the appointed advisory committee as having met all of the requirements of the Graduate School at the University of North Dakota and is hereby approved.

Dean Wayne Swisher

Date

PERMISSION

Title Syntheses and Characterization Of Homo- and Heterometallic *Tert*-Butoxides/Cyclopentadienides of Group 4/14 Metals
And
Mixed Ligand (*Tert*-Butoxides/Cyclopentadienides) Coordination Polymers of Group 1/14 Metals

Department Chemistry

Degree Doctor of Philosophy

In presenting this dissertation in partial fulfillment of the requirements for a graduate degree from the University of North Dakota, I agree that the library of this University shall make it freely available for inspection. I further agree that permission for extensive copying for schorlaly purposes may be granted by the professor who supervised my dissertation work or, in his absence, by the Chairperson of the department or the dean of the Graduate School. It is understood that any copying or publication or other use of this dissertation or part thereof for financial gain shall not be allowed without my written permission. It is also understood that due recognition shall be given to me and to the University of North Dakota in any scholarly use which may be made of any material in my dissertation.

Edmond Njua

07/26/2012

TABLE OF CONTENTS

LIST OF FIGURES

LIST OF TABLES

Table Page

LIST OF SCHEMES

Scheme Page

LIST OF SYMBOLS AND ABBREVIATIONS

Å = angstrom unit, 1 x 10^{-10} m

Alk = Alkyl group

°C = degrees celcius

Benzene-d_6 = deuterated benzene

Cp = cyclopentadiene

Cp* = Me_5C_5

C_2 = two-fold axis of rotation

C_3 = three-fold axis of rotation

DME = dimethoxyethane

Et_2O = diethyl ether

NMR = nuclear magnetic resonance

Me = methyl

^{t}Bu = *tert*-butyl

Ph = phenyl

OTf = triflate anion

Subl. = sublime

THF = tetrahydrofuran

THF-d_8 = deuterated tetrahydrofuran

ABSTRACT

In the first part of this work, the interaction of Group 4 metal tetrachlorides with group 14 alkoxometallates, $[NaM(O^tBu)_3]_2$, where M = Ge, Sn, Pb, is reported. Treatment of $MCl_4(THF)_2$, M = Hf, Zr, with ½ equivalent of $[NaSn(O^tBu)_3]_2$ led to the isolation of the the ionic complexes $\{M(O^tBu)_3(THF)_3](SnCl_3)\}$, **6** (M = Zr) and **7** (M = Hf). The neutral species $[MCl_2(O^tBu)_2(THF)_2]$, **8** (M = Zr) and **9** (M = Hf), were obtained with 1/3 equivalent of the ligand. Interference in attempted derivitization of **6** by the trichlorostannate unit led to its replacement with the triflate anion, thereby yielding *fac*-$\{Zr(O^tBu)_3(THF)_2(OTf)\}$, **11**. When a full equivalent of the ligand was used, the complexes *fac*-$\{Sn(O^tBu)_3M(O^tBu)_3\}$, **12** (M = Zr) and **13** (M = Hf), were isolated. The ligands, $[NaM(O^tBu)_3]_2$, where M = Ge, Pb, did not yield products akin to **6** and **7**, but gave products similar to **12** and **13**, namely, *fac*-$\{M(O^tBu)_3(THF)_3](ECl_3)\}$, **14**–**19** (where M = Zr, Hf and E = Ge, Pb). Titanium, on the other hand, did not form products similar to **14**–**19**, but $Ti(O^tBu)_3Cl$ reacted with silver triflate to give $[Ti(O^tBu)_2(OTf)_2(THF)_2]$, **10**. The structures of **6**–**14** were determined by X-ray crystallography.

Part two describes the syntheses and characterization of complexes obtained from the reactions between $CpZrCl_3$·dme and group 14 alkoxometallates. Interaction with $NaSn(O^tBu)_3$ and $NaGe(O^tBu)_3$ led to the displacement of the cyclopentadienide from

zirconium, albeit with the formation of different products. {[$(O^tBu)_2ClZr(\mu$-ClSnCp)(μ-$O^tBu)_2ZrCl$ $(O^tBu)_2]\cdot C_6D_6$}, **19** and CpSnCl were isolated with the former, while *fac*-[$Ge(\mu O^tBu)_3ZrCl(O^tBu)_2$], **21**, Cp_2Ge and $ZrCl_3(O^tBu)$ were the products from the interaction of the latter. The CpSnCl obtained reacted with NaO^tBu to give NaCp and $NaSn(O^tBu)_3$, which together crystallized as the coordination polymer, {(THF).NaCp.NaCp.$NaSn(O^tBu)_3]_2\cdot$THF}, **20**. On the other hand, the interaction of $CpZrCl_3\cdot$dme with $NaPb(O^tBu)_3$ failed to displace the Cp ligand and simply afforded the substitution products, $CpZr(O^tBu)_3$, **22**, and $PbCl_2$. Compounds **19**, **20** and **21** were characterized by X-ray crystallography.

In part three, the *tert*-butoxy transfer property of tri(*tert*-butoxy)stannate was exploited in the syntheses of homometallic *tert*-butoxides/chlorides of Group 4 (Ti, Zr) and 5 (Nb) metals from the metal tetrachlorides. Interaction of both $MCl_4(THF)_2$, M = Ti, Zr, with four equivalents of NaO^tBu in the presence of catalytic amounts of $NaSn(O^tBu)_3$ led to the isolation of $Ti(O^tBu)_4$, **24** and $Zr(O^tBu)_4$, **25** respectively, while interaction with three equivalents of NaO^tBu yielded the chloro-*tert*-butoxides, $TiCl(O^tBu)_3$, **26** and $ZrCl(O^tBu)_3$, **27** respectively. Treatment of $NbCl_4(THF)_2$ with four equivalents of NaO^tBu led to the isolation of $Nb(O^tBu)_5$, **28** and single-crystal X-ray study revealed a distorted trigonal bipyramidal geometry for the compound.

In part four, the syntheses and solid-state structures of groups 1/14 metal double salt coordination polymers are reported. Combinations of cyclopentadienide salts of the alkali metals (MCp) with alkali-metal alkoxometalates ($ME(O^tBu)_3$) (where M = Na, K and E = Sn, Ge) gave polymeric complexes of the type $[MCp(THF)ME(O^tBu)_3]_\infty$, **29**–**31**, and $[MCp(THF)_2ME(O^tBu)_3]_\infty$, **32**, in which the cyclopentadienide rings are bilaterally

η^5-coordinated by two alkali metal ions. All compounds were characterized by NMR spectroscopy and X-ray crystallography.

GENERAL INTRODUCTION

1. Overview

The chemistry of metal alkoxides has been extensively studied and a large number of articles and reviews have been published on these compounds.[1–11] The first synthesis of metal alkoxides dates back to the 1800s when Liebig synthesized sodium and potassium ethoxides from the respective metals and ethanol.[2] The synthesis of alkoxides of other metals such as boron and silicon followed subsequently.[1] A big contribution to this field was made in 1899 by V. E. Tishchenko who published his thesis on aluminum alkoxides, in which he reported the condensation of aldehydes to esters using aluminum alkoxides, a reaction known today as the Tishchenko reaction.[2] This was the first time a metal alkoxide was employed as a catalyst.[2] After Tishchenko's work, the use of metal alkoxides was restricted to organic chemistry, where metal alkoxides were used for the reduction of carbonyl compounds and as catalysts for the disproportionation of aldehydes.[2] Modern alkoxide chemistry as we know it today was pioneered by research begun in the 1950s by D. C. Bradley and co-workers.[2,12] They shaped the structure of modern metal alkoxide chemistry. Currently, alkoxide complexes have been reported for nearly all the elements of the periodic table. Although so much attention has been given to these compounds, the ease of syntheses and modification of alkoxide ligands still provides a vast pool of exploitable research. The popularity of these metal complexes has led to them being used for many different applications in areas such as organic synthesis, catalysis, material science, and biology.[13]

An important area of application of transition-metal alkoxides is their use as precursors for the production of highly pure metal oxide-based ceramic materials through sol-gel processing or chemical vapor deposition.[14–18] In the sol-gel technique, homogeneous solutions of the metal alkoxide in a suitable solvent, usually the parent alcohol, are prepared, and subsequently hydrolyzed under controlled conditions to yield inorganic gels that can be converted to oxide thin films and nanoparticles. This route of processing is usually reserved for highly soluble non-volatile alkoxides. The more volatile alkoxides are usually processed via the chemical vapor deposition technique, whereby the metal alkoxides are purified to a high degree by distillation or sublimation *in vacuo*. The pure metal alkoxide is then hydrolyzed to afford the metal oxide.

Another area of application of transition-metal alkoxides is in catalysis.[19,20] Alkoxides usually form very stable complexes with early-transition metals; hence they are good ancillary ligands for these metal complexes.[1,2] The propensity of metal alkoxides to form aggregates in solution and the non-stoichiometric use of these compounds slowed their application in catalysis.[21] It was not until the synthesis of monomeric alkoxides, which was achieved by the use of bulky alkoxides that do not bridge easily, that the application of transition-metal alkoxides in catalysis became popular.[21] Transition metal alkoxides were first used as catalysts in the 1980s, when Katsuki and Sharpless discovered that $Ti(O^{i}Pr)_4$ was able to catalyze the asymmetric epoxidation of allylic alcohols.[22] Notwithstanding this late use of transition metal alkoxides in catalysis, they have been extensively studied as catalysts for many different transformations with remarkable success.[1,2] Shortly after Katsuki and Sharpless, Schrock and co-workers achieved the metathesis and polymerization of alkenes and alkynes using

transition-metal alkoxy compounds.[23] Others research groups, Wolczanski and co-workers have demonstrated the use of bulky monodentate alkoxides of group 4 and 5 in the activation of different molecules,[24,25] while Shibasaki and co-workers have used zirconium alkoxides, such as $Zr(O^tBu)_4$, $Zr(O^nPr)_4$ and modifications thereof in transformations, such as oxidation of alcohols and phenols, conversion of olefins to β-cyanohydrins, asymmetric Mannich-type reactions, catalytic asymmetric aza-Diels-Alder reactions and many others.[26] These numerous applications demonstrate the ubiquitous nature of transition-metal alkoxide complexes.

2. Literature Review

2.1. Synthesis of Metal Alkoxides

Alkoxides are represented by the general formula $[M(OR)_x]_n$ (where M = metal of valency x, R = alkyl or aryl group, and n = degree of association).[1,2] They are obtained from alcohols by the replacement of the hydroxylic hydrogen with a metal cation.[1,2] The degree of association (n) usually depends on the size of the alkyl group on the alcohol and it is usually higher for lower primary or secondary groups.[1] Monomeric alkoxides are obtained with larger R groups.[1]

Metal alkoxides are moisture sensitive.[2] Their synthesis is usually carried out using air-free techniques and all solvents used are thoroughly dried to avoid decomposition. Many methods have been developed for the synthesis of metal alkoxides and the method of choice is usually dependent on the type of metal and alkoxide compound desired. Different routes are used for the synthesis of homometallic (one kind

of metal), heterometallic (different metals), homoleptic (same ligand) or heteroleptic (two or more different ligands) alkoxides.

2.1.1. Synthesis of Homometallic Alkoxides

Direct Reaction of Metals with Alcohols (Method 1)

Table 1. pK_a values of selected alcohols

Alcohols	pK_a
MeOH	15.8
EtOH	15.9
^{i}PrOH	17.1
^{t}BuOH	19.2
PhOH	9.95
CF_3CH_2OH	12.8
$CH_3(CF_3)_2COH$	9.6
$(CF_3)_2CHOH$	9.3
$(CF_3)COH$	5.4

$$\mathbf{M} + n\,\mathbf{ROH} \longrightarrow \mathbf{M(OR)}n + n/2\,\mathbf{H_2\,(g)} \quad (1.1)$$

This method works best for highly electropositive metals: alkali-metals, alkaline earth metals, lanthanides and aluminum.[1,2] The highly electropositive alkali-metals react vigorously, with the evolution of hydrogen (eq 1.1), while the reaction is slower with the alkaline earth, lanthanide metals and aluminum. These latter metals, therefore require a catalyst, usually I_2 or $HgCl_2$.[1,2] This route of synthesis also depends on the acidity of the alcohol. Alcohols are generally weak acids with pK_a values that are higher than that of

water (pK_a = 15.7).[1] Fluorinated alcohols are more reactive because of their electron-withdrawing substituents, but they are also poorer nucleophiles, Table 1.[1,27]

Anodic Oxidation of Metal in Alcohol (Method 2)

This method is preferentially used for less active metals (Sc, Y, Ti, Zr, Nb, Ta, Fe, Co, Ni, Cu, and Pb).[1,2] The anodic dissolution of metals in alcohols is usually done in the presence of electroconductive additives (LiCl, NaBr, NH_4Cl, and R_4NCl).[1,2] This method of preparation is favored for the synthesis of alkoxides of less electropositive metals and metalloids due to its ease and production of non-toxic hydrogen gas as the main by-product (Scheme 1).[1]

$$\mathbf{M} \longrightarrow \mathbf{M}^{n+} + n\mathbf{e}^- \qquad \text{(anode)} \quad (1.2)$$

$$n\,\mathbf{ROH} + n\mathbf{e}^- \longrightarrow n\,\mathbf{RO}^- + n\,\mathbf{H}\bullet$$

$$n\,\mathbf{H}\bullet \longrightarrow n/2\,\mathbf{H_2} \qquad \text{(cathode)} \quad (1.3)$$

$$\mathbf{M}^{n+} + n\,\mathbf{RO}^- \longrightarrow \mathbf{M(OR)}_n$$

Scheme 1. Mechanism for the production of alkoxides by the electrochemical technique (copied from reference 1).

Reaction of Metal Oxide or Hydroxide with Alcohols (Method 3)

$$\mathbf{MOH} + \mathbf{ROH} \rightleftharpoons \mathbf{MOR} + \mathbf{H_2O} \quad (1.4)$$

$$\mathbf{MO} + \mathbf{2\,ROH} \rightleftharpoons \mathbf{M(OR)_2} + \mathbf{H_2O} \quad (1.5)$$

This method has been employed in the synthesis of alkoxides of *s*-block metals (sodium), *p*-block metals (boron, thallium), as well as for metalloids (silicon, arsenic).[1,2] Both reactions are reversible. Hence, it is important to continuously remove the water by-product. For higher boiling alcohols, water is simply removed by distillation. When the

boiling point of the alcohol is lower than that of water, removal of the water is achieved by addition of benzene which forms an azeotrope with water.

Alcoholysis of MX_4 (X = H, Alk, C≡C, ≡N, NH_2, NR_2, $N(SiR_3)_2$, SH, ...), (Method 4)

$$\mathbf{MX_n} + n\mathbf{ROH} \longrightarrow \mathbf{M(OR)_n} + n\mathbf{HX} \quad (1.6)$$

The driving force in this technique lies in the formation of a stable HX by-product which is usually a liquid or a gas.[1,2] Using this technique, the alkoxides of very active metals, which otherwise react very explosively with alcohols, could be prepared safely by the alcoholysis of their metal hydrides. The drawback of this method is that sometimes the starting materials are not commercially available (such as metal amides) or are very expensive.

Direct Reaction of MX_4 with Alcohols (X = Halide) (Method 5)

$$\mathbf{MX_n} + (x+y)\,\mathbf{ROH} \rightleftharpoons \mathbf{MCl_{n-x}(OR)_x(ROH)_y} + x\,\mathbf{HX} \quad (1.7)$$

Metal halides usually undergo alcoholysis in the presence of a suitable base to give the appropriate homoleptic alkoxide or chloride-alkoxide derivatives.[1,2] The extent of alcoholysis depends on the valency of the metal and at times the product obtained incorporates additional alcohol molecules.

Metathesis Reactions of MX_4 with Alkali-Metal Alkoxides or Ammonia (X = Halide) (Method 6)

$$MX_n + n\,M^{I}OR \longrightarrow M(OR)_n + n\,MX \quad (1.8)$$

$$MX_n + n\,ROH + n\,NH_3 \xrightarrow{\text{benzene}} M(OR)_n + n\,NH_4X \quad (1.9)$$

The previous route (Method 5) does not always give complete substitution products. To synthesize pure homoleptic alkoxides, bases such alkali-metal alkoxides, pyridine, trialkylamines and ammonia are usually employed.[1,2] Ammonia is typically the preferred base.

Alcohol Interchange (Method 7)

$$M(OR)_x + n\,R'OH \rightleftharpoons M(OR)_{x-n}(OR')_n + n\,ROH \quad (1.10)$$

This method is mostly used to access alkoxide complexes that cannot be obtained using the other routes.[1] If the incoming alcohol has a higher boiling point than the one being eliminated, the reaction yield is increased by distilling the lower boiling alcohol (as a benzene azeotrope). On the other hand, if the incoming alcohol has a lower boiling point, the reaction yield is increased by using an excess of the incoming alcohol. Precipitation of the new alkoxide compound also maximizes the yield of the reaction. This route yields heteroleptic homometallic alkoxides if the substitution is incomplete. When the substitution is complete, a homoleptic alkoxide complex is obtained.

Transesterification of Metal Alkoxides (Method 8)

$$M(OR)_x + n\ R''COOR' \rightleftharpoons M(OR)_{x-n}(OR')_n + n\ R''COOR \quad (1.11)$$

This method is similar to the previous one, but it has the following advantages:[1] a) it is mostly unaffected by sterics and so it allows for the synthesis of tertiary alkoxides, b) sometimes the esters (silyl acetates) are more stable than their corresponding alcohols (silanols), and c) it allows for the easy synthesis of *tert*-butoxide derivatives. This approach is applicable for the synthesis of either homo- or heteroleptic alkoxide complexes.

2.1.2. Synthesis of Heterometallic Alkoxides

Two main routes have been developed for the synthesis of heterometallic alkoxide complexes.[1]

Reaction Between Two Alkoxide Complexes (Method 1)

$$M(OR)_n + x\ M'(OR)_y \longrightarrow MM'_x(OR)_{n+xy} \quad (1.12)$$

The reaction works well when one of the complexes is an alkali-metal or alkaline earth metal alkoxide and the other is either a main group metal, transition metal, actinide or lanthanide alkoxide complex.

Reaction Between a Metal Halide and an Alkali Alkoxometallate (Method 2)

$$MX_n + n\ M'M''(OR)_y \longrightarrow MM''_x(OR)_{ny} + n\ M'X\ (s) \quad (1.13)$$

The reaction is driven by the formation of a stable alkali-metal chloride, which is simply filtered off to yield pure samples of the desired metal alkoxide.

2.2. Structures of Metal Alkoxides

Alkoxide ligands are strong σ-donors; hence they usually form strong covalent bonds with electrophilic metal centers.[27] Owing to the fact that the donor oxygen atoms have three unpaired electrons, the alkoxide ligands can be bridging or non-bridging giving rise to the different possible structures shown in Figure 1.[1] The structures preferred by the alkoxide are usually dependent on the electronic and steric properties of the alkoxo group.

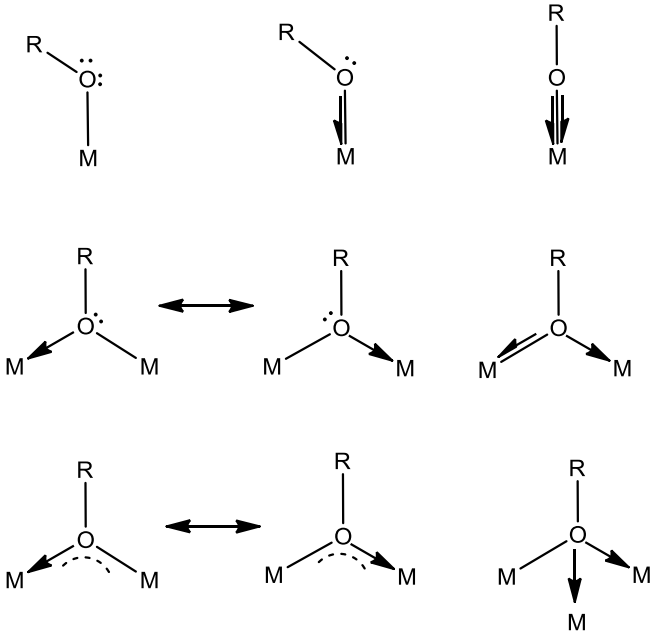

Figure 1. Coordination modes of alkoxo ligands (copied from reference 1).

The structures formed by metal alkoxides can range from simple monomeric compounds through oligomers to polymers. The formation of complex aggregates is made possible by the high donor ability of the oxygen atom of the alkoxide group. The most commonly encountered complexes are those with one to six metal atoms. Alkoxide

complexes with more than six metal centers are usually oligomers. Based on molecular complexity, these compounds can be classified as follows:

Mononuclear complexes – The compounds in this class are usually formed when the R group of the alkoxide is very bulky or the donor oxygen atom is functionally hindered due to the presence of other donor groups on the alkoxide ligand or the presence of donor solvent molecules.[1,2] The influence of the R-group size can be seen in the structures of $[Be(OC_6H_2{}^tBu_3\text{-}2,4,6)_2(Et_2O)]$ and $Be(O^tBu)Cl$.[28,29] The former compound is monomeric due to the bulkiness of the alkoxide, which discourages alkoxide bridging. The molecule is further stabilized by a coordinated solvent molecule. On the other hand, due to the reduction of the steric bulk on the alkoxide ligand and around the metal center, the latter compound is trimeric with alkoxide bridges. Monomeric alkoxides can also be formed when the oxidation number of the central atom is equivalent to its coordination number. Some other compounds with monomeric structures are $Zr(O^tBu)_4$,[1] $Hf(O^tBu)_4$,[1] and $M(OC_6H_2Me\text{-}4\text{-}{}^tBu_2\text{-}2\text{-}6)_2$, M = Ge, Sn.[30]

Binuclear complexes – Most alkoxide clusters formed fall into this category. The complexes are dimeric and are usually connected by bridging alkoxide units, Figure 2. In the case of metals like molybdenum and tungsten,[31] the complexes are usually stabilized by metal–metal bonds without bridging alkoxide units, Figure 2f. Examples of compounds with this structural configuration are $[Sn(O^tBu)_2]_2$,[32] $Sn(O^tBu)_3M$ (where M = In and Tl),[33,34] $[LiO^tBu_3]_2$[35] and $[Nb(OR)_5]_2$[36,37] (where R = Me and ^{i}Pr).

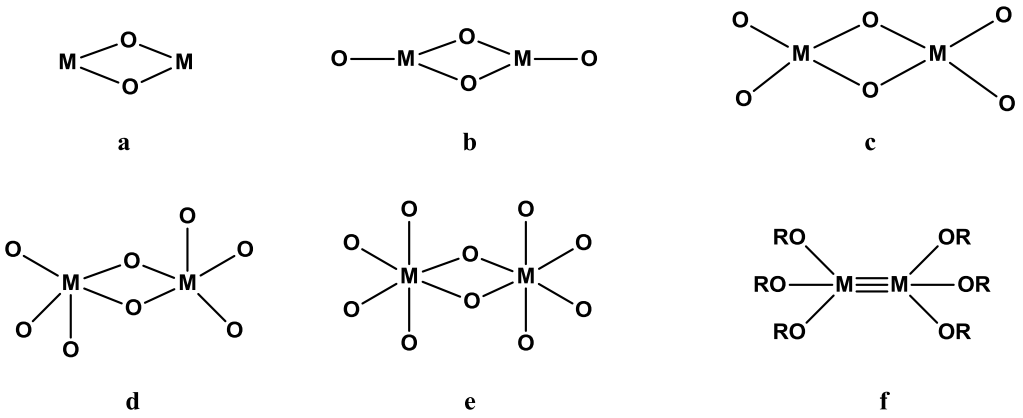

Figure 2. Sketches of observed binuclear structures.

Trinuclear complexes – These compounds are often triangular (Figure 3d), linear chains (Figure 3a,c,e), and non-linear chains (Figure 3b).[1,2] They are usually composed of bridging alkoxide units. Some trinuclear complexes are $[Pb(O^tBu)_2]_3$[38] and $Ba[(O^tBu)_3Zr(O^tBu)_2]_2$.[39]

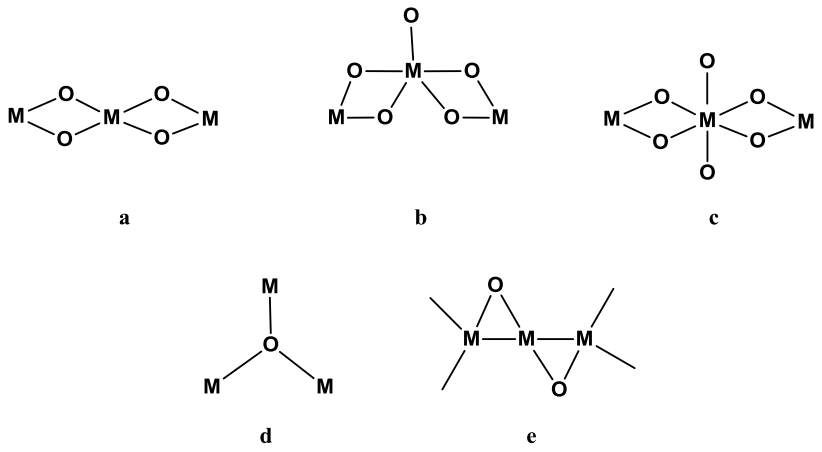

Figure 3. Sketches of observed trimeric structures.

Tetranuclear complexes – Several different configurations are possible in this class (Figure 4).[1,2] The tetrahedral configuration has a μ_4-O core that bridges four metal atoms. This configuration is uncommon and it has been reported only for $[Pb(\mu_4\text{-}O)(\mu\text{-}OSiPh)_6]$.[2]

The butterfly configurations are made up of M_4X_{12} clusters and usually contain metal –metal bonds.[1,2] They have been reported for Mo and W.[2] Cubane-like molecules have an $M_4(\mu_3\text{-}O)_4$ core and are common for alkali-metal alkoxides.[1,2] Examples are TlOEt and the *tert*-butoxides of K, Rb and Cs.[2,40] The rhombohedral configuration, which is of the $Ti_4(OR)_{16}$-type, is the most common of all tetrameric structures.[2] It is made up of an M_4-rhombus with two μ_3-O and four μ-O ligands.[2] Some compounds that adopt this structure type are $[Mg_4(OC_2H_4OMe)_6(DME)_2]^{2+}$,[41] $Sr_4(OPh)_8(PhOH)_2(THF)_6$[42] and $Li_2Nb_2(OCH_2SiMe_3)_{12}$.[43] The propeller configuration, which has been observed in $Al_4(O^iPr)_{12}$, has a central aluminum ion connected to three peripheral aluminum ions by alkoxide bridges.[2] All four aluminum metal atoms lie in a plane that is perpendicular to the main trigonal axis of the molecule. Examples are $[Al\{Al(OEt)_2R\}_3]$ (where R = Me or ^{t}Bu),[44,45] and $[M\{Al(O^iPr)_4\}_3]$ (where M = Er or Eu)[46,47].

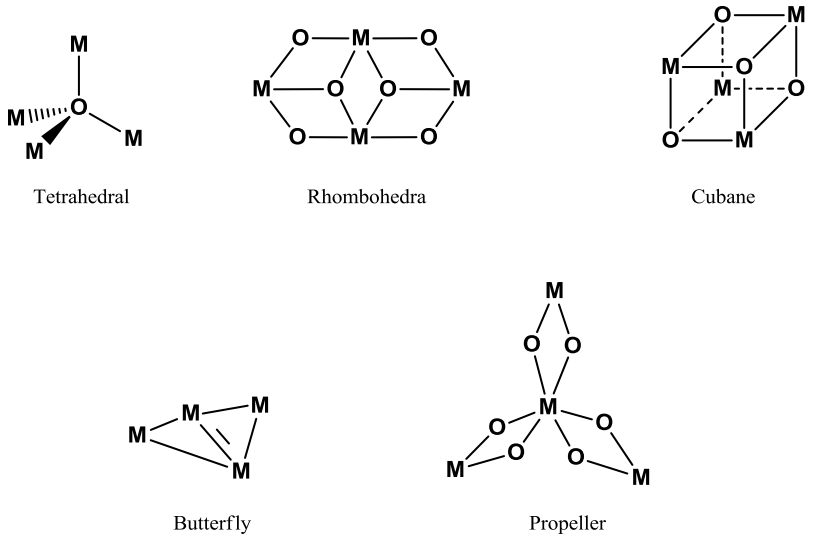

Figure 4. Sketches of observed tetrameric structures.

Pentanuclear complexes – Pentanuclear complexes have an M_5O core (Figure 5). They are either trigonal bipyramidal, like $[Na_3La_2(OC_6H_4Me\text{-}4)_9(THF)_5]$,[48] or square planar, like $[Y_4Pr(\mu_5\text{-}O)(O^iPr)_{13}]$.[49]

Hexanuclear complexes – They are either octahedral or trigonal prismatic with a μ_6-O center, or are of the double propeller type (Figure 5).

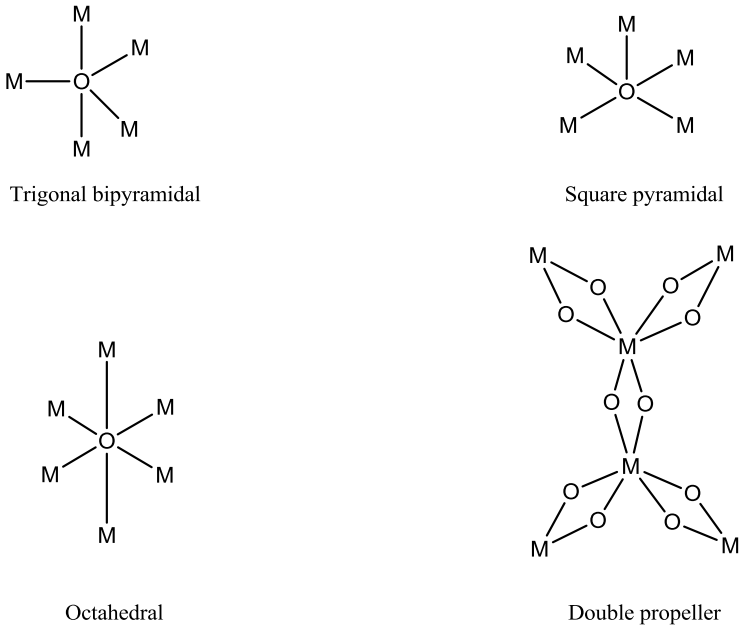

Figure 5. Sketches of observed pentanuclear and hexanuclear structures.

2.3. Electronic Properties of Alkoxide Ligands

Alkoxide ligands are connected to metal centers via a σ-type orbital (Figure 6a), but there are two π-orbitals that are perpendicular to the M–O bond and they could potentially form π-bonds with the metal.[5,50] In extreme cases, following the effective

atomic number (EAN) or 18 e^- rule, alkoxides can be considered as 5 e^- donors (Figure 6c).[5,50] This extreme case is not supported by experiment, and alkoxides are usually considered to be $3e^-$ donors (Figure 6b).[5,50] The evidence for the $3e^-$ donation is usually obtained from structural characterization. The angle of the M–O–R linkage and the M–O bond length are usually used to gauge the degree of π-bonding.[5,20] A near linearity of the M–O–R bond is most often associated with involvement of π-interaction, and the shorter the M–O bond, the stronger the π-interaction. However, it has been shown that in some cases there is little correlation between the M–O–R bond angle and the M–O bond length.[51] There is an ambiguity due to the fact that a combination of both the σ-effect and sterics could produce the same results as those usually associated with π-bonding. Generally, the strength of both the σ- and π-interactions depends on the electrophilicity of the metal center.

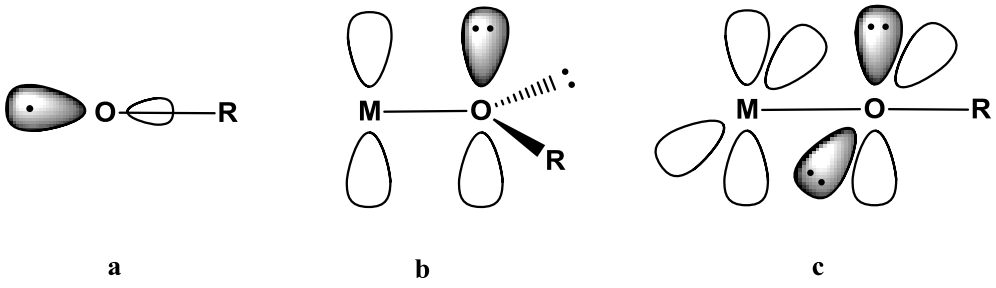

Figure 6. Donor orbitals of an alkoxide ($\sigma + 2\pi$) (copied from reference 5).

CHAPTER I

SYNTHESES AND STRUCTURES OF CATIONIC AND NEUTRAL, HOMOMETALLIC AND HETEROBIMETALLIC *TERT*-BUTOXIDES OF THE GROUP 4/14 METALS

Introduction

Group 14 alkoxometallates (Figure 7) are good chelating ligands for electropositive metals. The hard donor properties of these ligands make them suitable candidates for such metals. These ligands have been used to chelate many different metals, ranging from main group metals such as Mg, Ca, Ba, Sn, Pb, and Ge, to transition metals such as Cr, Co, Mn, Ni, Zn, and Cd, to give cage-like structures akin to those shown in Figure 8.[52–55]

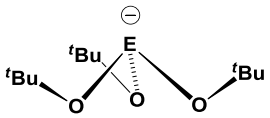

E = Sn (**1**), Ge (**2**), Pb(**3**)

Figure 7. Group 14 alkoxometallates.

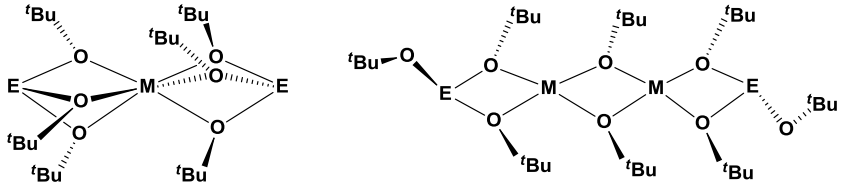

E = Ge, Sn, Pb and M = main group or transition metal

Figure 8.Cage structures of main group and transition metal group 14 alkoxometalate chelates.

The syntheses of the group 14 alkoxometallates were first reported by the Veith research group.[52–55] The ease of syntheses and possible modification of these ligands makes them very attractive. Another desirable feature of the ligands is that they are monoanaionic chelating alkoxides, hence they are similar to successful ligands, such as tris(pyrazolyl)borate ligands. Lastly, the ligands possess minimal steric bulk, therefore simplifying interpretation of experimental findings.

Although the group 14 alkoxometallates have been used to chelate many metals, no work has been reported on the interaction of these ligands with group 4 and 5 metals. The fact that Caulton and coworkers[56] (Scheme 2) reported the syntheses of *fac*-{[E(μ-O^{t}Bu)$_3$Zr(O^{t}Bu)] (E = Sn, Pb) makes this exclusion suprising, since these compounds could be formally viewed as formed from [Zr(O^{t}Bu)$_3$]$^+$ and [E(O^{t}Bu)$_3$]$^-$ (group 14 alkoxometallate). This suggested that *fac*-{[E(μ-O^{t}Bu)$_3$Zr(O^{t}Bu)] could be synthesized by treating group 4 tetrachlorides with the dimeric sodium salts, [NaE(O^{t}Bu)$_3$]$_2$ (where E = Ge, Sn, or Pb).

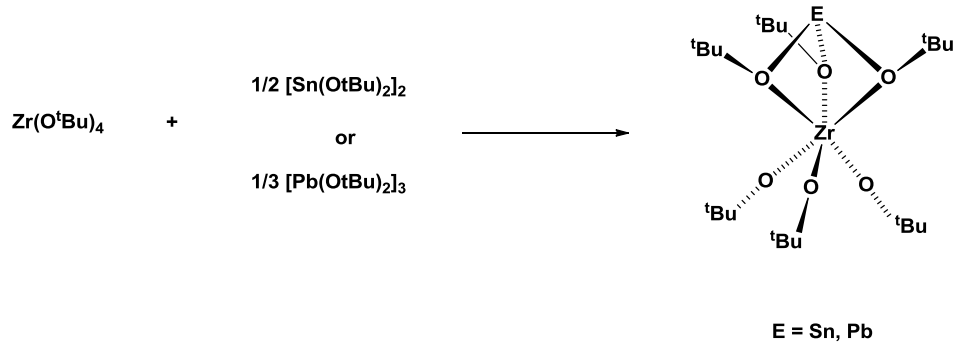

Scheme 2. Syntheses of *fac*-{[E(μ-O^{t}Bu)$_3$Zr(O^{t}Bu)$_3$].

The syntheses of group 4/14 *tert*-butoxides were sought by treating group 4 metal tetrachlorides with either a half- or a full equivalent of the dimeric group 14

alkoxometallates in THF. The goal of this study was to synthesize and characterize these compounds by NMR spectroscopy and X-ray crystallography.

Experimental

Description of Techniques and Chemicals Used

General Procedures

All experiments were performed under an atmosphere of argon, using standard Schlenk techniques. Solvents were dried and freed of molecular oxygen by distillation under an atmosphere of nitrogen from sodium- or potassium-benzophenone ketyl immediately before use. NMR spectra were recorded on a Bruker AVANCE-500 NMR spectrometer at 25 °C. The ^{1}H and $^{13}C\{^{1}H\}$ NMR spectra are referenced relative to (i) C_6D_5H (7.16 ppm) and C_6D_6 (128.39 ppm), (ii) $O(CDHCD_2)_2$ (3.58 ppm), $O(CD_2CDH)_2$ (1.73 ppm), $O(CD_2CD_2)_2$ (67.57 ppm), and $O(CD_2CD_2)_2$ (25.37 ppm), respectively. Melting points were obtained on a Mel-Temp apparatus and are uncorrected. Midwest Microanalytical Services, Indianapolis, Indiana performed the elemental analyses. The reagents $ZrCl_4$, $HfCl_4$, $SnCl_2$, $Ti(O^tBu)_4$, and AgOTf were purchased from Aldrich or Alfa Aesar, while *cis*-$MCl_4(THF)_2$,[57] M = Ti, Zr, or Hf, $[NaE(O^tBu)_3]_2$ (where E = Ge[53], Sn[58], or Pb[53]) and $Ti(O^tBu)_3Cl$[59] were prepared according to published procedures.

X-ray Crystallography

Suitable single crystals were coated with Paratone N oil, affixed to Mitegen or Litholoop crystal holders, and centered on the diffractometer in a stream of cold nitrogen. Reflection intensities were collected with a Bruker Apex diffractometer, equipped with an Oxford Cryosystems, 700 Series Cryostream cooler, operating at 173 K. Data were measured using ω scans of 0.3° per frame for 20 seconds until a complete hemisphere of data had been collected. Cell parameters were retrieved using SMART[60] software and refined with SAINT[61] on all observed reflections. Data were reduced with SAINTplus, which corrects for Lorentz and polarization effects and crystal decay. Empirical absorption corrections were applied with SADABS.[62] The structures were solved by direct methods and refined by full-matrix least squares methods on F^2 with SHELXL-97[63] incorporated in SHELXTL Version 5.10.[64]

Synthesis of *fac*-{[Zr(O^{t}Bu)$_3$(THF)$_3$](SnCl$_3$)]}, 6

A 100 mL, 2-neck flask equipped with an inlet was charged with *cis*-$ZrCl_4(THF)_2$ (2.00 g, 5.30 mmol) and 20 mL of THF. The solution was chilled to –78 °C in an acetone/dry ice bath. $[NaSn(O^tBu)_3]_2$, dissolved in THF (25 mL), was then added drop-wise. The reaction mixture was stirred overnight and then concentrated to 10 mL. It was stored at –10 °C for several days, upon which time colorless hexagonal crystals were isolated. Yield: 93 % (3.70 g, 4.92 mmol).

Mp: 69–72 °C. ^{1}H NMR (THF-d_8): δ 3.62 (t, $^3J_{HH}$ = 12 Hz, 12H, OCH_2CH$_2$), 1.77 (t, $^3J_{HH}$ = 12 Hz, 12H, OCH$_2$CH_2), 1.27 (s, 27H, OC(CH_3)$_3$). ^{13}C{^{1}H} NMR (THF-d_8): δ

75.4 (s, O*C*$(CH_3)_3$), 68.3 (s, O*C*H_2CH_2), 33.0 (s, OC(CH_3)$_3$), 26.4 (s, OCH_2*C*H_2). Anal. Calcd for $C_{24}H_{51}Cl_3O_6SnZr$: C, 38.33; H, 6.84. Found: C, 37.98; H, 7.89.

Synthesis of *fac*-{[Hf(O^{t}Bu)$_3$(THF)$_3$](SnCl$_3$)]}, 7

To a cold (–78 °C) solution of *cis*-$HfCl_4(THF)_2$ (1.58 g, 3.40 mmol) in THF (30 mL) was added drop-wise a solution of [NaSn(O^{t}Bu)$_3$]$_2$ (1.23 g, 1.70 mmol) in THF (20 mL). The precipitated NaCl was filtered using a medium porosity frit and the filtrate was concentrated to 10 mL. Storage of the solution at –10 °C afforded hexagonal colorless crystals. Yield: 87 % (2.50 g, 2.98 mmol).

Mp: 58–60 °C. ^{1}H NMR (THF-d_8): δ 3.62 (t, $^3J_{HH}$ = 12 Hz, 12H, OCH_2CH$_2$), 1.77 (t, $^3J_{HH}$ = 12 Hz, 12H, OCH$_2$CH_2), 1.27 (s, 27H, OC(CH_3)$_3$). ^{13}C{^{1}H} NMR (THF-d_8): δ 75.2 (s, O*C*$(CH_3)_3$), 68.4 (s, O*C*H_2CH_2), 33.4 (s, OC(CH_3)$_3$), 26.5 (s, OCH_2*C*H_2). Anal. Calcd for $C_{24}H_{51}Cl_3O_6SnHf$: C, 34.35; H, 6.13. Found: C, 34.28; H, 5.92.

Synthesis of [ZrCl$_2$(O^{t}Bu)$_2$(THF)$_2$], 8

A solution of [NaSn(O^{t}Bu)$_3$]$_2$ (0.23 g, 0.44 mmol) in THF (20 mL) was added drop-wise to a pre-cooled (–78 °C) solution of *cis*-$ZrCl_4(THF)_2$ (0.500 g, 1.33 mmol) in THF (20 mL). The mixture was allowed to warm to room temperature, and then it was stirred for 16 h. The precipitated salt was filtered off. Concentration and storage at –10 °C afforded colorless, hexagonal, plate-like crystals. Yield: 77 % (0.46 g, 1.02 mmol).

Mp: 120 °C. ^{1}H NMR (THF-d_8): δ 3.62 (t, $^3J_{HH}$ = 12 Hz, 8H, OCH_2CH$_2$), 1.77 (t, $^3J_{HH}$ = 12 Hz, 8H, OCH$_2$CH_2), 1.31 (s, 18H, OC(CH_3)$_3$). ^{13}C{^{1}H} NMR (THF-d_8): δ 78.9 (s, O*C*$(CH_3)_3$), 68.4 (s, O*C*H_2CH_2), 32.3 (s, OC(CH_3)$_3$), 26.6 (s, OCH_2*C*H_2). Anal. Calcd for $C_{16}H_{34}Cl_2O_4Zr$: C, 42.46; H, 7.57. Found: C, 41.96; H, 7.26.

Synthesis of $[HfCl_2(O^tBu)_2(THF)_2]$, 9

To a cold (–78 °C) solution of *cis*-$HfCl_4(THF)_2$ (0.643 g, 2.00 mmol) in THF (20 mL) was added drop-wise a solution of $[NaSn(O^tBu)_3]_2$ (0.722 g, 1.00 mmol) in THF (20 mL). The resulting colorless mixture was stirred at room temperature overnight. Filtration, concentration and storage of the solution at –10 °C afforded colorless, hexagonal, plate-like crystals. Yield: 91 % (0.981 g, 1.82 mmol).

Mp: 132–135 °C. ^{1}H NMR (THF-d_8): δ 3.62 (t, 8H, OCH_2CH$_2$), 1.77 (t, $^3J_{HH}$ = 12 Hz, 8H, OCH$_2$CH_2), 1.30 (s, 18H, OC(CH_3)$_3$). ^{13}C{^{1}H} NMR (THF-d_8): δ 77.8 (s, O*C*(CH$_3$)$_3$), 68.4 (s, O*C*H$_2$CH$_2$), 32.6 (s, OC(*C*H$_3$)$_3$), 26.6 (s, OCH$_2$*C*H$_2$). Anal. Calcd for $C_{16}H_{34}Cl_2O_4Hf$: C, 35.60; H, 6.35. Found: C, 35.52; H, 5.98.

Synthesis of $[Ti(O^tBu)_2(OTf)_2(THF)_2]$, 10

To a solution of AgOTf (0.85 g, 3.3 mmol) in THF (10 mL) at room temperature was added at once a THF (20 mL) solution of $Ti(O^tBu)_3Cl$ (1.00 g, 3.3 mmol). The resulting milky-white reaction mixture was stirred for 30 min and the precipitated silver chloride was removed with a medium-porosity frit. Concentration and storage of the clear filtrate at –4 °C afforded colorless, hexagonal crystals after 3 days. Yield: 71 % (1.51 g, 2.34 mmol).

Mp: 82–84 °C. ^{1}H NMR (THF-d_8): δ 3.62 (t, $^3J_{HH}$ = 12 Hz, 8H, OCH_2CH$_2$), 1.77 (t, $^3J_{HH}$ = 12 Hz, 8H, OCH$_2$CH_2), 1.52 (s, 18H, OC(CH_3)$_3$). ^{13}C{^{1}H} NMR (THF-d_8): δ 120.8 (q, $J_{C–F}$ = 319 Hz, CF_3), 96.1 (s, O*C*(CH$_3$)$_3$), 68.3 (s, O*C*H$_2$CH$_2$), 31.4 (s, OC(*C*H$_3$)$_3$), 26.4 (s, OCH$_2$*C*H$_2$). Anal. Calcd for $C_{18}H_{34}F_6O_{10}S_2Ti$: C, 33.97; H, 5.38. Found: C, 34.45; H, 5.62.

Synthesis of *fac*-[Zr(O^{t}Bu)$_3$(OTf)(THF)$_2$], 11

A THF (20 mL) solution of *fac*-{[Zr(O^{t}Bu)$_3$(THF)$_3$](SnCl$_3$)} (1.36 g, 1.82 mmol) was treated drop-wise with a THF (20 mL) solution of AgOTf (0.47 g, 1.8 mmol) at room temperature. The reaction mixture was stirred for 15 min and the precipitated AgSnCl$_3$ was removed by filtration. The filtrate was then concentrated *in vacuo* to 10 mL. Storage of the solution at –4 °C afforded colorless crystals after 3 days. Yield: 84 % (0.92 g, 1.52 mmol).

Mp: 114–116 °C. ^{1}H NMR (THF-d_8): δ 3.62 (t, $^3J_{HH}$ = 12 Hz, 8H, OCH_2CH$_2$), 1.77 (t, $^3J_{HH}$ = 12 Hz, 8H, OCH$_2$CH_2), 1.30 (s, 18H, OC(CH_3)$_3$). ^{13}C{^{1}H} NMR (THF-d_8): δ 121.1 (q, $J_{C–F}$ = 318 Hz, CF$_3$), 76.8 (s, O*C*(CH$_3$)$_3$), 68.5 (s, O*C*H$_2$CH$_2$), 33.2 (s, OC(*C*H$_3$)$_3$), 26.6 (s, OCH$_2$*C*H$_2$). Anal. Calcd for C$_{21}$H$_{43}$F$_6$O$_8$SZr: C, 41.77; H, 7.18. Found: C, 41.49; H, 6.77.

Synthesis of *fac*-[Sn(μ-O^{t}Bu)$_3$Zr(O^{t}Bu)$_3$], 12

Cis-ZrCl$_4$(THF)$_2$ (0.19 g, 0.50 mmol) in THF (20 mL), pre-cooled to –78 °C, was treated drop-wise with a full equivalent of [NaSn(O^{t}Bu)$_3$]$_2$ (0.36 g, 0.50 mmol) in THF (20 mL). The solution was allowed to slowly warm to room temperature and then stirred overnight. The solvent was removed *in vacuo*, and the solid residue was extracted into hexanes. Rectangular, colorless crystals precipitated out of the hexane solution upon storage at –10 °C for several days. Yield: 88 % (0.28 g, 0.43 mmol).

Mp: subl. (220 °C, 1 atm). ^{1}H NMR (C$_6$D$_6$): δ 1.53 (s, 27H, μ-OC(CH_3)$_3$), 1.47 (s, 27H, OC(CH_3)$_3$). ^{13}C{^{1}H} NMR (C$_6$D$_6$): δ 76.0 (s, μ-O*C*(CH$_3$)$_3$), 73.9 (s, O*C*(CH$_3$)$_3$),

34.9 (s, μ-OC(CH$_3$)$_3$, $J_{Sn–C}$ = 28.1 Hz), 34.0 (s, OC(CH$_3$)$_3$). Anal. Calcd for $C_{24}H_{54}O_6SnZr$: C, 44.44; H, 8.39. Found: C, 44.10; H, 8.20.

Synthesis of *fac*-[Sn(μ-O^{t}Bu)$_3$Hf(O^{t}Bu)$_3$], 13

To a cold (–78 °C) solution of *cis*-$HfCl_4(THF)_2$ (0.50 g, 1.10 mmol) in THF (30 mL) was added drop-wise a solution of [NaSn(O^{t}Bu)$_3$]$_2$ (1.55 g, 2.15 mmol) in THF (20 mL). The reaction mixture was then allowed to slowly warm to room temperature and finally stirred overnight. The precipitated NaCl was removed with a medium porosity frit. The solvent was removed in vacuo, and the solid residue was extracted into hexanes. Crystallization from hexanes at –10 °C afforded rectangular colorless crystals. Yield: 87 % (1.37 g, 1.86 mmol).

Mp: subl. (226 °C, 1 atm). ^{1}H NMR (C_6D_6): δ 1.56 (s, 27H, μ-OC(CH_3)$_3$), 1.47 (s, 27H, OC(CH_3)$_3$). ^{13}C{^{1}H} NMR (C_6D_6): δ 75.9 (s, μ-OC(CH$_3$)$_3$), 74.2 (s, OC(CH$_3$)$_3$), 34.5 (s, μ-OC(CH$_3$)$_3$, $J_{Sn–C}$ = 27.8 Hz), 34.3 (s, OC(CH$_3$)$_3$). Anal. Calcd for $C_{24}H_{54}O_6SnHf$: C, 39.17; H, 7.40. Found: C, 38.71; H, 7.23.

Synthesis of *fac*-[Ge(μ-^{t}BuO)$_3$Zr(O^{t}Bu)$_3$], 14

[Na(O^{t}Bu)$_3$Ge]$_2$ (0.58 g, 0.93 mmol) was dissolved in 20 mL of THF, and added drop-wise to a pre-cooled (–78 °C) solution of *cis*-$ZrCl_4(THF)_2$ (0.35 g, 0.93 mmol) in THF (20 ml). The reaction mixture was then allowed to slowly warm to room temperature and finally stirred overnight. The solvent was removed under vacuum and the solid residue was extracted into hexanes. Colorless, rectangular crystals, suitable for X-ray diffraction were obtained after the solution had been stored for a few days at –10 °C. Yield: 75 % (0.42 g, 0.70 mmol).

Mp: subl. (216 °C, 1 atm). ^{1}H NMR (C_6D_6): δ 1.49 (s, 27H, μ-OC(CH_3)$_3$), 1.49 (s, 27H, OC(CH_3)$_3$). ^{13}C{^{1}H} NMR (C_6D_6): δ 76.2 (s, μ-O*C*(CH_3)$_3$), 74.9 (s, OC(*C*H_3)$_3$), 34.0 (s, μ-O*C*(CH_3)$_3$), 33.2 (s, OC(*C*H_3)$_3$). Anal. Calcd for $C_{24}H_{54}O_6GeZr$: C, 47.84; H, 9.03. Found: C, 47.66; H, 8.96.

Synthesis of *fac*-[Ge(μ-O^{t}Bu)$_3$Hf(O^{t}Bu)$_3$], 15

A solution of [Na(O^{t}Bu)$_3$Ge]$_2$ (0.81 g, 1.29 mmol) in THF (20 mL) was added drop-wise to a pre-cooled (–78 °C) solution of *cis*-$HfCl_4(THF)_2$ (0.60 g, 1.29 mmol) in THF (20 ml). The reaction mixture was then allowed to slowly warm to room temperature and finally stirred overnight. The solvent was removed under vacuum and the solid residue was extracted into hexanes. Colorless, rectangular crystals, suitable for X-ray diffraction were obtained after the solution had been stored for a few days at –10 °C. Yield: 61 % (0.54 g, 0.78 mmol).

Mp: subl. (216 °C, 1 atm). ^{1}H NMR (C_6D_6): δ 1.52 (s, 27H, μ-OC(CH_3)$_3$), 1.49 (s, 27H, OC(CH_3)$_3$). ^{13}C{^{1}H} NMR (C_6D_6): δ 76.2 (s, μ-O*C*(CH_3)$_3$), 75.3 (s, OC(*C*H_3)$_3$), 34.3 (s, μ-O*C*(CH_3)$_3$), 33.2 (s, OC(*C*H_3)$_3$). Anal. Calcd for $C_{24}H_{54}O_6GeHf$: C, 41.79; H, 7.89. Found: C, 41.49; H, 7.49.

Synthesis of *fac*-[Pb(μ-O^{t}Bu)$_3$Zr(O^{t}Bu)$_3$], 16

A solution of [Na(O^{t}Bu)$_3$Pb]$_2$ (1.00 g, 1.11 mmol) in THF (20 mL) was added drop-wise to a pre-cooled (–78 °C) solution of *cis*-$ZrCl_4(THF)_2$ (0.42 g, 1.11 mmol) in THF (20 mL). The mixture was allowed to warm to room temperature and then was stirred for 16 h. The precipitated salt was removed by filtration. Concentration and storage at –10 °C afforded colorless, hexagonal crystals. Yield: 67 % (0.55 g, 0.75 mmol).

Mp: subl. (220 °C, 1 atm). ^{1}H NMR (C_6D_6): δ 1.59 (s, 27H, μ-OC(CH_3)$_3$), 1.42 (s, 27H, OC(CH_3)$_3$). ^{13}C{^{1}H} NMR (C_6D_6): δ 75.4 (s, μ-OC(CH$_3$)$_3$), 72.6 (s, OC(CH$_3$)$_3$), 35.5 (s, μ-OC(CH$_3$)$_3$, $J_{Pb–C}$ = 28.9 Hz), 34.2 (s, OC(CH$_3$)$_3$). Anal. Calcd for $C_{24}H_{54}O_6PbZr$: C, 39.11; H, 7.38. Found: C, 38.90; H, 7.34.

Synthesis of *fac*-[Pb(μ-O^{t}Bu)$_3$Hf(O^{t}Bu)$_3$], 17

A solution of [Na(O^{t}Bu)$_3$Pb]$_2$ (1.00 g, 1.11 mmol) in THF (20 mL) was added drop-wise to a pre-cooled (–78 °C) solution of *cis*-$HfCl_4(THF)_2$ (0.52 g, 1.12 mmol) in THF (20 mL). The mixture was allowed to warm to room temperature and it was stirred for 16 h. The precipitated salt was removed by filtration. Concentration and storage at –10 °C afforded colorless hexagonal crystals. Yield: 71 % (0.65 g, 0.79 mmol).

Mp: subl. (220 °C, 1 atm). ^{1}H NMR (C_6D_6): δ 1.60 (s, 27H, μ-OC(CH_3)$_3$), 1.42 (s, 27H, OC(CH_3)$_3$). ^{13}C{^{1}H} NMR (C_6D_6): δ 75.5 (s, μ-OC(CH$_3$)$_3$), 73.0 (s, OC(CH$_3$)$_3$), 35.5 (s, μ-OC(CH$_3$)$_3$, $J_{Pb–C}$ = 29.0 Hz), 34.5 (s, OC(CH$_3$)$_3$). Anal. Calcd for $C_{24}H_{54}O_6PbHf$: C, 34.97; H, 6.60. Found: C, 34.50; H, 6.55.

Results and Discussion

1. Synthesis and Spectroscopic Analysis of *fac*-{[Zr(O^{t}Bu)$_3$(THF)$_3$](SnCl$_3$)}, 6

The synthesis of compound **6** was achieved by treating *cis*-$ZrCl_4(THF)_2$ with one half-equivalent of dimeric sodium tri(*tert*-butoxy)stannate, $[Na(O^tBu)_3Sn]_2$ (Scheme 3).

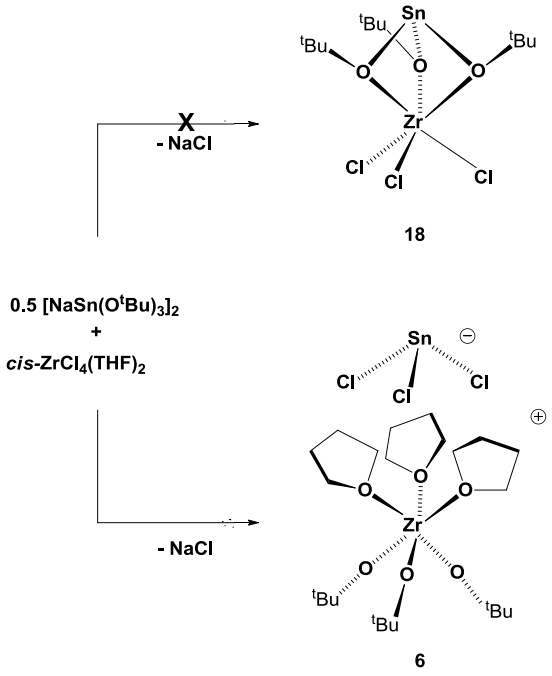

Scheme 3. Synthesis of compound **6**.

Compound **6** was obtained serendipitously; it was not the originally targeted compound. The target of this synthesis was the heteronuclear zirconium trichloro-tri(*tert*-butoxy)stannate, Sn(μ-O^{t}Bu)$_3$ZrCl$_3$, **18** (Scheme 3). Instead of **18**, the ionic compound, **6**, was formed by transfer of *tert*-butoxy groups from the stannate ligand to zirconium. Ionic **6** was found to be soluble in THF, but insoluble in hydrocarbon solvents. The formation of **6** arises from the abstraction of a chloride ion from Zr(O^{t}Bu)$_3$Cl by Lewis-acidic $SnCl_2$

to yield $Zr(O^tBu)_3^+$ and $SnCl_3^-$ (Scheme 4). Solvation of the unsaturated cationic $Zr(O^tBu)_3^+$ by THF molecules affords the contact ion pair **6**.

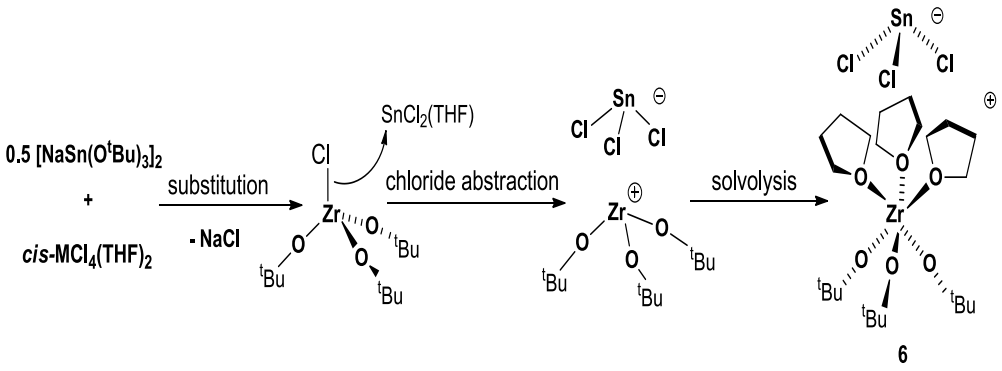

Scheme 4. Schematics for the formation of **6**.

The ^{1}HNMR spectrum of **6** (Figure 9) supports the C_3 symmetric structure of this compound. The spectrum was obtained in THF-d_8 and three signals were observed for the different protons found in the compound. On the basis of integrations, the spectrum revealed that the *ter*t-butoxy groups and the THF groups were present in a 1:1 ratio (*i.e.* 12:12:27). The methyl protons on the three different *tert*-butoxy groups were found to be equivalent, and they appeared as a sharp singlet at 1.27 ppm. The different methylene protons on the coordinated THF molecules were observed as triplets at 3.62 ppm and 1.77 ppm, respectively. The $^{13}C\{^1H\}$ NMR spectrum is in accordance with the structure observed, with singlet peaks for the methylene carbons of the coordinated THF molecule and two singlets for the quaternary and methyl carbons of the *tert*-butoxy groups.

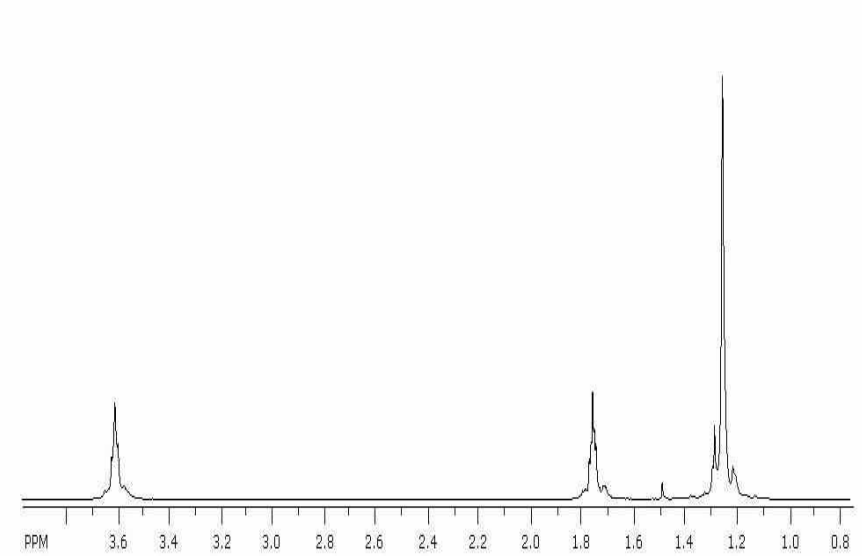

Figure 9. ^{1}H NMR Spectrum of **6**.

2. Solid-state Structure of *fac*-{Zr(O^{t}Bu)$_3$(THF)$_3$](SnCl$_3$)}, 7

Compound **6** crystallizes in the trigonal crystal system with three molecules in the unit cell. Supplemental crystallographic data are given in Tables 2 and 3. The molecules are located on 3-fold axes of space group *R*3. As mentioned before, the structural motif is composed of the cation, $Zr(O^tBu)_3(THF)_3^+$, and the anion, $SnCl_3^-$ (Figure 10). The geometry about the zirconium center of the cation is that of a distorted octahedron. In this compound, the THF molecules adopt a propeller-like conformation, thus making the cation chiral. Thus, the crystals are (i) chiral due to the homochirality of the cation and (ii) polar due to the general arrangement of the contact ion pairs, which all face the same direction. The molecule adopts a facial conformation with the three *tert*-butoxy groups occupying one face, and the three THF molecules occupying the other face. The preferred facial arrangement is dictated by the π-character of the ligands, with the less π-donating THF molecules favoring a trans coordination relative to the stronger π-donor alkoxides.

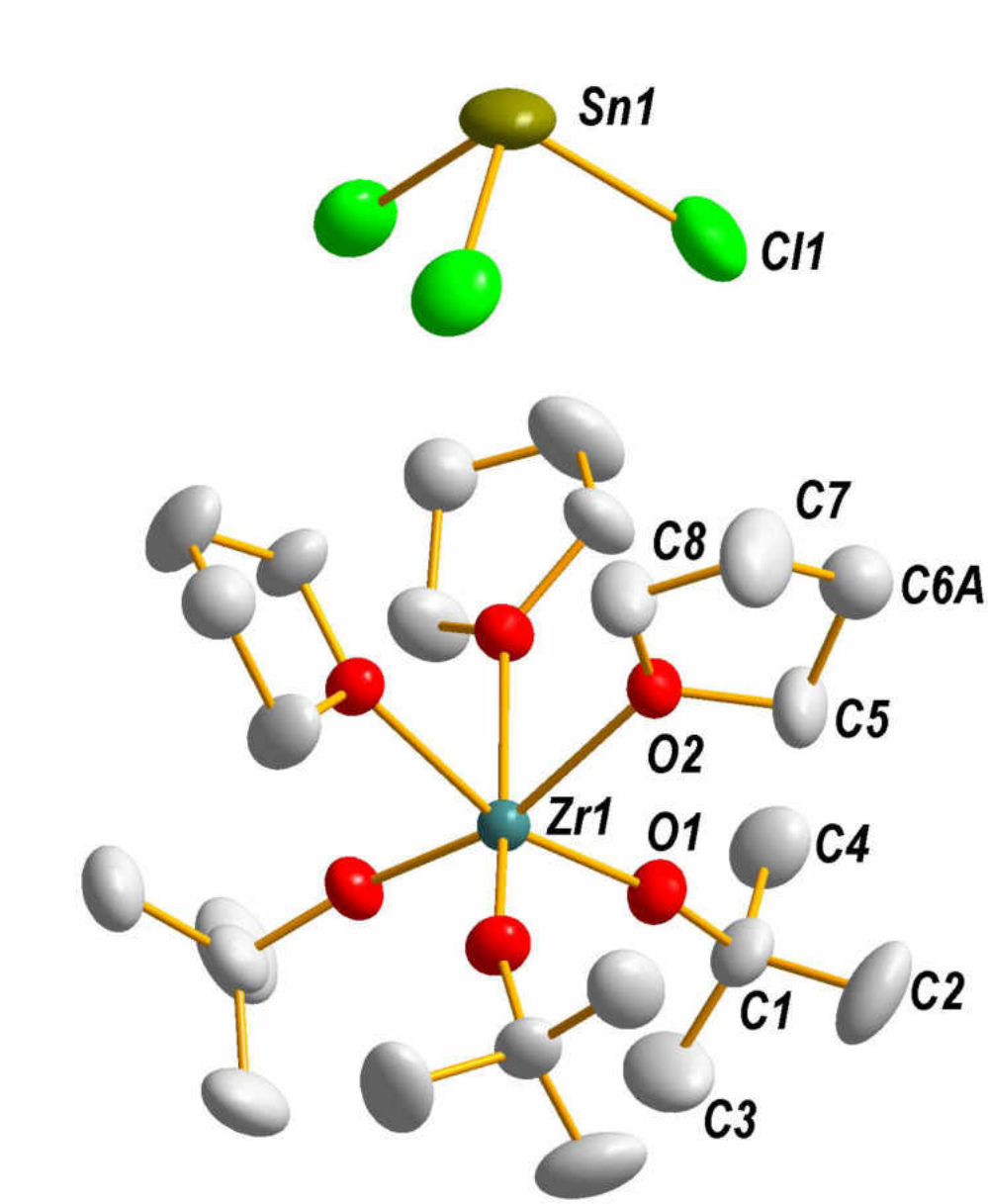

Figure 10. Solid-state structure and partial labeling scheme of **6**. With the exception of carbon (35%) all atoms are drawn at the 50% probability level.

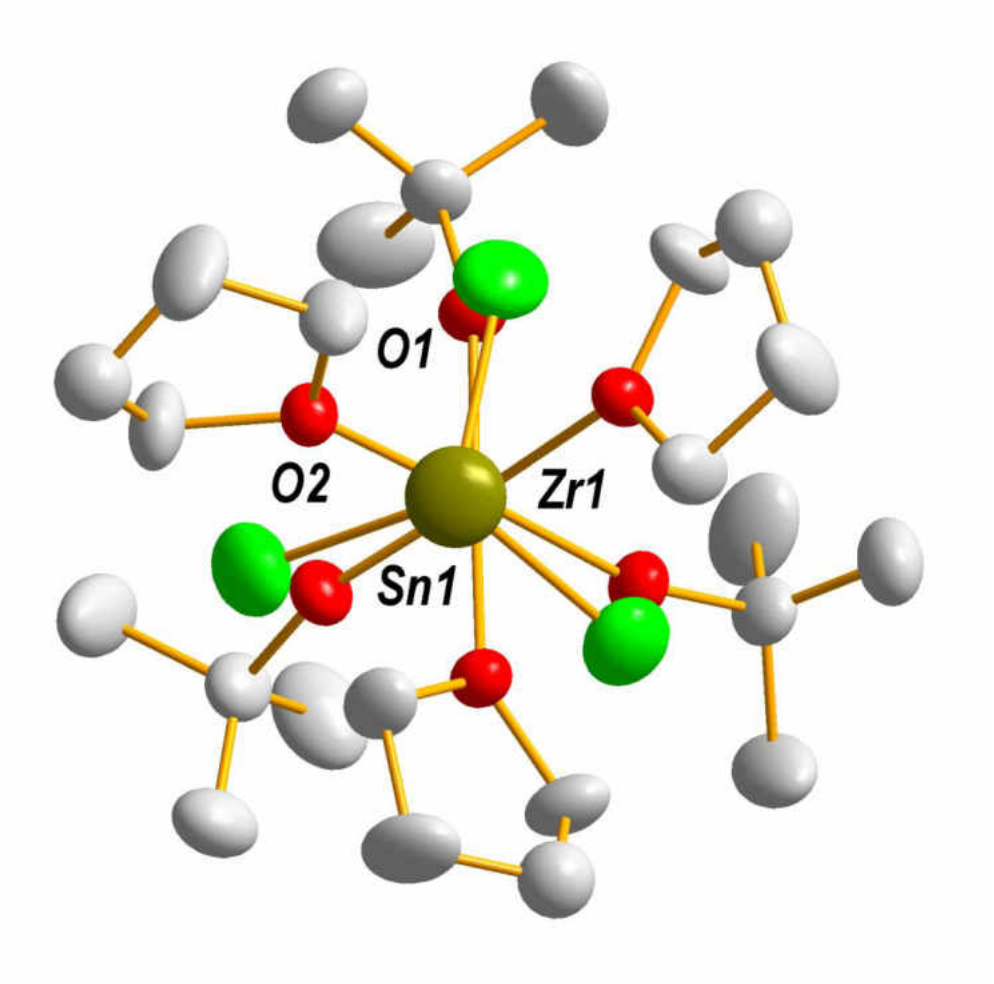

Figure 11. Solid-state structure of **6** showing the arrangement of the chlorines in the spaces between the THF molecules, thereby minimizing steric repulsion.

The $SnCl_3^-$ anion sits atop the $Zr(O^tBu)_3(THF)_3^+$ cation, and to minimize steric repulsion the chlorines of the $SnCl_3^-$ anion sit in the spaces between the THF molecules (Figure 11). The closest distance of approach between the anion and the cation is observed in the interaction of the α-methylene protons of the THF molecules and the chlorine atoms of the trichlorostannate, and this distance is 2.80 Å. This interaction arises due to the interionic coulombic forces in the compound.

The angles between the *tert*-butoxide groups are 102.35°(6): this is much larger than that expected for an octahedral geometry (90°), thereby creating a flat $Zr(O^tBu)_3$ pyramid. On the other hand, the angles between the THF molecules (79.02°(6)) are much smaller than expected, thereby creating a steeper $Zr(THF)_3$ pyramid.

The zirconium–alkoxide bond lengths are shorter than the sum of the covalent radii of zirconium and oxygen. These short Zr–O bond lengths together with the near linearity of the Zr–O–^{t}Bu bond angle (164(15)°) indicate the presence of π-interactions between zirconium and oxygen. The Zr–O (alkoxide) bond (1.9232(16) Å) is comparable to the terminal zirconium–alkoxide bonds (average Zr–O = 1.952(4) Å) in $K_2Zr_2(O^tBu)_{10}$[65] and the Zr–O bonds (Zr–O = 1.889(7) Å) in tetrahedral $Zr(O^tBu)_3Si(SiMe_3)_3$.[66] The Zr–O(THF) bonds (2.3272(15) Å) are much longer than the Zr−O^{t}Bu bonds, indicative of a much weaker bonding interaction. Compared to other Zr–O(THF) bonds, for example in $Cp_2Zr(O^tBu)(THF)(BPh_4)$ (Zr–O(THF) = 2.200(4) Å)[67] and $ZrCl_4$[2-(benzo[d]thiazol-2-yl)-6-methylphenol](THF) (Zr–O (THF) = 2.214(14) Å),[68] the Zr–THF bonds in **6** are considerably longer.

The $SnCl_3^-$ unit in **6** has identical bond lengths [2.466(16) Å] and bond angles (93.91(3) Å), which is due to symmetry constraints. These metric parameters lie in the range observed for the $SnCl_3^-$ unit in $[SnTi_2(O^iPr)_9][SnCl_3]$, which has non-equivalent Sn–Cl (2.329–2.488 Å) bond lengths and angles (93.1–99.4°).[69]

Table 2. Crystal data for compound **6**

Molecular formula	$C_{24}H_{51}Cl_3O_6SnZr$
fw	751.91 g/mol
Crystal system	trigonal
Space-group	*R*3 (146)
a, Å	14.7142(9)
b,Å	14.7142(9)
c,Å	13.8699(16)
α, deg	90
β, deg	90
γ, deg	120
V, Å^3	2600.6(4)
Z	3
F(000)	1152
ρ(calc), g cm^{-3}	1.440
λ, Å	0.710 73
temp, K	173
μ, mm^{-1}	1.282
$R(F)^a$	0.0227
$R_W(F^2)^b$	0.0589

[a] $R = \sum||F_o| - |F_c|| / |F|_o$. [b] $R_w = \{[\sum w(F_o^2 - F_c^2)] / [\sum w(F_o^2)^2]\}^{1/2}$; $w = 1/[\sigma^2(F_o)^2 + (xP)^2 + yP]$, where $P = (F_o^2 + 2F_c^2)/3$.

Table 3. Selected bond lengths (Å) and angles (°) for **6**

Bond Lengths			
Zr1–O1	1.9232(15)	Sn1–Cl1	2.4644(10)
Zr1–O1'	1.9232(15)	Sn1–Cl1$^{'}$	2.4644(10)
Zr1–O1$^{''}$	1.9232(15)	Sn1–Cl1$^{''}$	2.4644(10)
Zr1–O2	2.3272(15)	O1–C1	1.430(3)
Zr1–O2$^{'}$	2.3272(15)	O2–C5	1.455(3)
Zr1–O2$^{''}$	2.3272(15)		
Bond Angles			
O1–Zr1–O1	102.35(6)	O1$^{''}$–Zr1–O2$^{''}$	163.11(6)
O1$^{'}$–Zr1–O1$^{''}$	102.35(6)	O1$^{'}$–Zr1–O2	163.11(6)
O1–Zr1–O1$^{''}$	102.35(6)	O2$^{'}$–Zr1–O2	79.02(6)
O1–Zr1–O2	163.11(6)	O2$^{''}$–Zr1–O2$^{'}$	79.02(6)
O1$^{'}$–Zr1–O2	89.05(7)	O2$^{''}$–Zr1–O2	79.02(6)
O1–Zr1–O2$^{''}$	89.05(7)	Cl1$^{'''}$–Sn1–Cl$^{''}$	93.91(3)
O1$^{''}$–Zr1–O2$^{'}$	89.05(7)	Cl1$^{'''}$–Sn1–Cl1	93.91(3)
O1–Zr1–O2$^{'}$	87.06(6)	Cl1$^{''}$–Sn1–Cl1	93.91(3)
O1$^{'}$–Zr1–O2$^{''}$	87.06(6)	C1–O1–Zr1	164.00(15)
O1$^{''}$–Zr1–O2	87.06(6)		

3. Synthesis and Spectroscopic Analysis of *fac*-{[Hf(O^{t}Bu)$_3$(THF)$_3$](SnCl$_3$)}, 7

Compound **7**, the analogue of **6**, was synthesized by treating *cis*-$HfCl_4(THF)_2$ with one half-equivalent of dimeric sodium tri(*tert*-butoxy)stannate, $[Na(O^tBu)_3Sn]_2$ (Scheme 5).

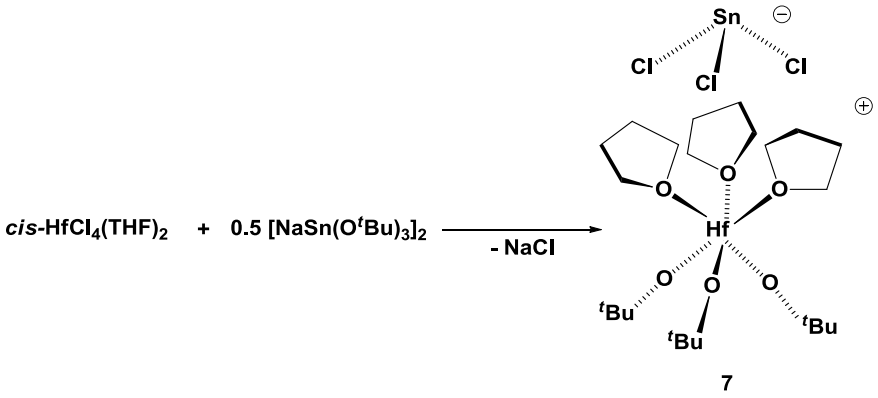

Scheme 5. Synthesis of compound **7**.

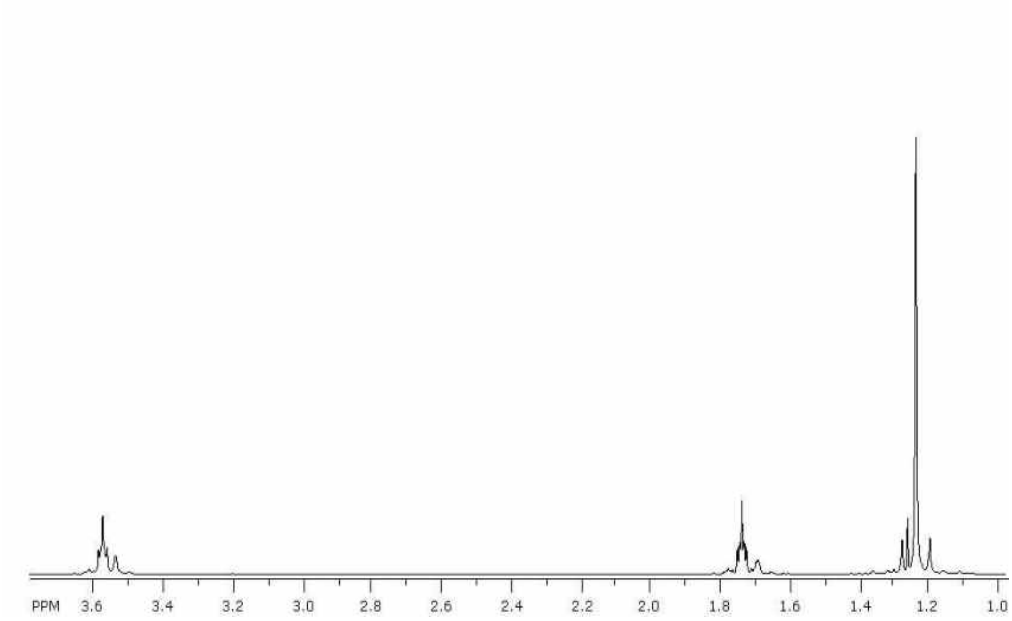

Figure 12. ^{1}H NMR spectrum of **7**.

The ^{1}H NMR spectrum of isomorphous **7** in THF-d_8 is similar to that of **6** (Figure 12), with three signals at 3.62, 1.77 and 1.27 ppm corresponding to the two groups of methylene protons of coordinated THF molecules and the methyl protons of the *tert*-butoxy groups respectively. Four signals were observed in the $^{13}C\{^{1}H\}$ NMR spectrum, with the peaks at 68.4 and 26.5 ppm assigned to the THF methylene carbons, while those at 75.2 and 33.4 ppm were assigned to quaternary and methyl *tert*-butoxy carbons, respectively.

4. Solid-State Structure of *fac*-Hf(O^{t}Bu)$_3$(THF)$_3$](SnCl$_3$)}, 7

The solid-state structure of **7** is shown in Figure 13. Compound **7** crystallizes in the trigonal crystal system with space group *R*3 and three molecules in the unit cell. Additional crystallographic data for this compound are given in Tables 4 and 5.

Similar to **6**, the molecules lie on three-fold rotation axes. The geometry about hafnium in the Hf(O^{t}Bu)$_3$(THF)$_3^+$ cation is that of a distorted octahedron. The molecule is chiral due to chirality of the cation, and the crystals obtained were polar due to the unidirectional placement of the cations and anions in the unit cell. The Hf−O (alkoxide) bonds (1.920(4) Å) and the Hf−O (THF) bonds (2.301(4) Å) in **7** are shorter than those in **6**, a phenomenon common to analogous zirconium and hafnium compounds. The Hf−O (alkoxide) bonds are comparable to those in [Hf(O^{t}Bu)$_2$(OCMe$_2$CH$_2$OMe)$_2$][70] (Hf−O^{t}Bu = 1.932(3)) and the terminal alkoxide bonds in [Hf$_2$(μ-O^{t}Bu)$_2$(O^{t}Bu)$_4$(C$_{36}$H$_{50}$O$_2$N$_2$)][71] (Hf−O^{t}Bu = 1.925(5) Å).

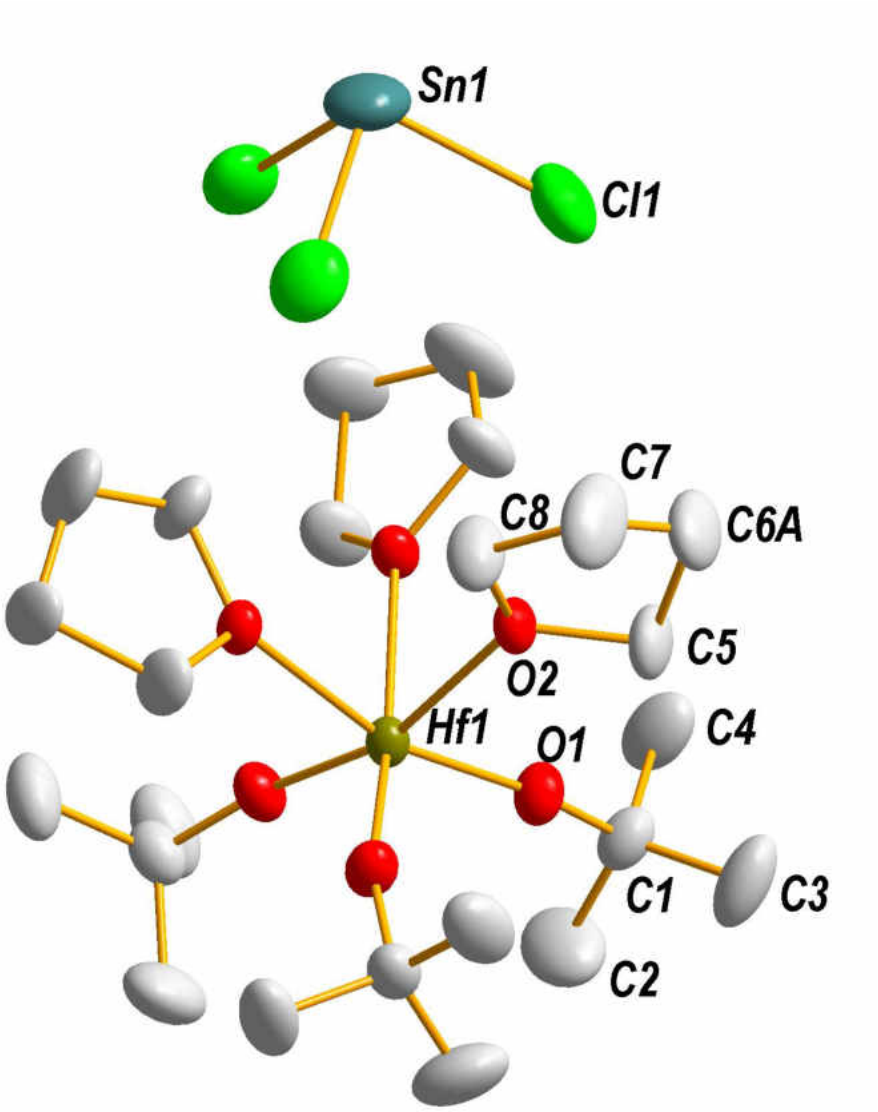

Figure 13. Solid-state structure and partial labeling scheme of **7**. With the exception of carbon (35%) all atoms are drawn at the 50% probability level.

Table 4. Crystal data for compound **7**

Molecular formula	$C_{24}H_{51}Cl_3O_6HfSn$
fw	839.18
Crystal system	trigonal
Space-group	*R*3(146)
a, Å	14.6870(16)
b,Å	14.6870(16)
c,Å	13.854(3)
α, deg	90
β, deg	90
γ, deg	120
V, Å^3	2588.0(7)
Z	3
F(000)	1248
ρ(calc), g cm^{-3}	1.615
λ, Å	0.710 73
temp, K	173
μ, mm^{-1}	3.993
$R(F)^a$	0.0333
$R_W(F^2)^b$	0.0815

[a] $R = \sum|F_o - F_c| \quad |F|_o$. [b] $R_w = \{[\quad w(F_o^2 - F_c^2)] / [\sum w(F_o^2)^2]\}^{1/2}$; $w = 1/[\sigma^2(F_o)^2 + (xP)^2 + yP]$, where $P = (F_o^2 + 2F_c^2)/3$.

Table 5. Selected bond lengths (Å) and angles (°) for **7**

Bond Lengths			
Hf1–O1	1.920(4)	O1–C1	1.410(9)
Hf1–O2	2.301(4)	O2–C5	1.451(8)
Sn1–Cl1	2.469(3)		
Bond Angles			
O1'–Hf1–O1	101.96(18)	O1'–Hf1–O2''	89.5(2)
O1'–Hf1–O1''	101.96(18)	O1''–Hf1–O2''	163.49(15)
O1–Hf1–O1''	101.96(18)	O2–Hf1–O2''	79.16(16)
O1–Hf1–O2	163.49(15)	O2''–Hf1–O2'	79.16(16)
O1'–Hf1–O2	87.01(18)	Cl1'–Sn1–Cl1	93.88(7)
O1''–Hf1–O2	89.5(2)	Cl1''–Sn1–Cl1	93.88(7)
O1–Hf1–O2'	89.5(2)	Cl1'–Sn1–Cl1''	93.88(7)
O1–Hf1–O2''	87.01(18)	C1–O1–Hf1	163.7(4)

5. Synthesis and Spectroscopic Analysis of $[ZrCl_2(O^tBu)_2(THF)_2]$, 8

In the synthesis of **6** from *cis*-$ZrCl_4(THF)_2$ and one half equivalent of dimeric sodium tri(*tert*-butoxy)stannate, $[Na(O^tBu)_3Sn]_2$, it was observed that, whenever there was a deficiency in the quantity of sodium tri(*tert*-butoxy)stannate used, a new compound, **8**, was obtained as the major product of the reaction. Based on the composition of **8**, the compound was then synthesized stoichiometrically from *cis*-$ZrCl_4(THF)_2$ and 1/3 equivalent of dimeric sodium tri(*tert*-butoxy)stannate, $[Na(O^tBu)_3Sn]_2$ (Scheme 6).

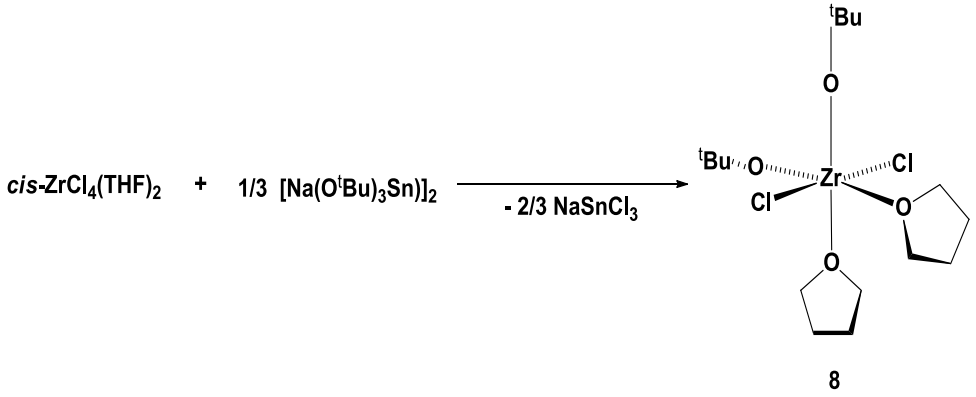

Scheme 6. Synthesis of compound **8**.

Compound **8** has ideal C_2 symmetry, and this is observed in its ^1H NMR spectrum which reveals the presence of one set of *tert*-butoxy groups and one type of THF molecules (Figure 14). The protons of the *tert*-butoxy group are observed as a singlet at 1.31 ppm. The methylene protons on the THF ligands appear as triplets at 3.62 and 1.77 ppm. The $^{13}C\{^1H\}$ NMR spectrum is in accordance, with singlet peaks at 68.4 and 26.6 ppm corresponding to the methylene carbons of the THF ligands, and singlets at 78.9 and

32.3 ppm attributed, respectively, to the quartenary and methyl carbons of the *tert*-butoxy groups.

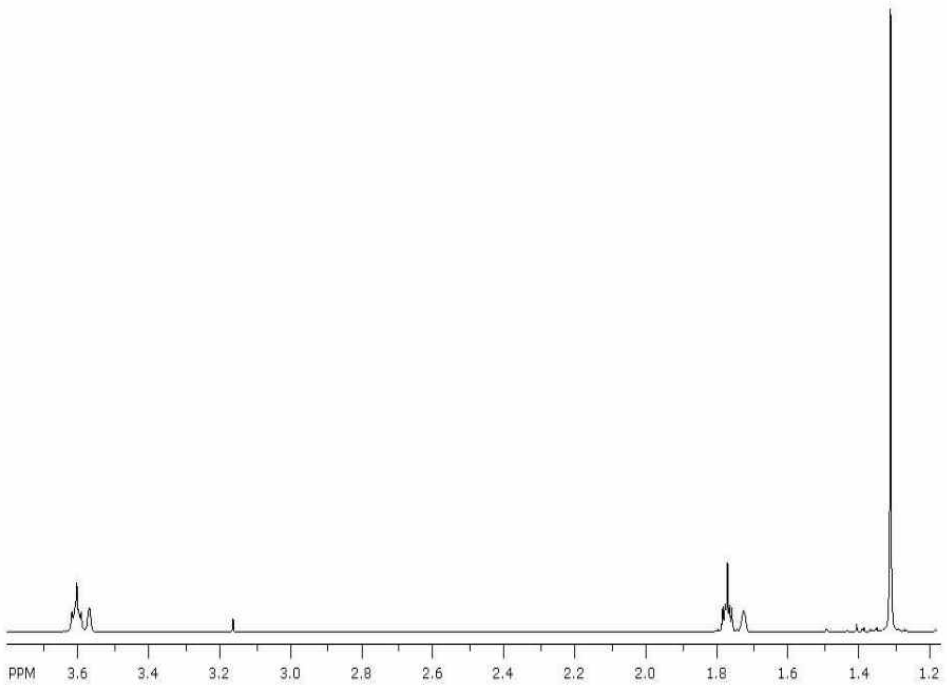

Figure 14. ^{1}H NMR spectrum of **8**.

6. Solid-State Structure of $[ZrCl_2(O^tBu)_2(THF)_2]$, 8

The solid-state structure of **8** is shown in Figure 15. Additional structural data are given in Tables 6 and 7. The molecule crystallizes in the monoclinic crystal system with space group $P2_1/n$ and four molecules in the unit cell. The geometry about the zirconium metal center is that of a distorted octahedron with angles enclosed by the alkoxides (O1–Zr1–O2 = 103.36(7)^o), the THF molecules (O3–Zr1–O4 = 76.98(6)^o) and the chloride ligands (Cl1–Zr1–Cl2 = 163.15(2)^o) all deviating from the expected 90^o and 180^o,

respectively. The ligands are arranged such that the *tert*-butoxides are trans to the THF molecules, and the chloride ligands are *trans* to each other. The adopted geometry has been observed for a range of compounds with the general formula $MCl_2(OR)_2(THF)_2$ (where OR = siloxide, aryloxide or boroxide).[72–74] This preferred placement of ligands around the zirconium metal center can be rationalized in terms of the π-donor strengths of the ligands, with the strongest π-donor alkoxides being trans to the weakest π-donor THF molecules, and the intermediary chloride ligands being trans to each other. The extensive double-bond character of the zirconium alkoxide bonds is observed in the length of the bonds, which are 1.8960(16) Å (Zr1–O1) and 1.9044(15) Å (Zr1–O2) long and the angles of the Zr–O–C bonds (Zr1–O1–C10 = 171.34(16)^o and Zr1–O2–C2 = 167.51(17)^o), which are close to linearity. The zirconium–THF bonds are much weaker, being 2.3184(15) and 2.3125(15) Å long. They are also longer than those in related compounds such as $Cl_3Zr[N(SiMe_3)PCl_2N(SiMe_3)]\cdot THF$[75] (Zr–O = 2.2651(12) Å) and $\{[ZrCl_3(THF)_2]_2C_6H_{10}O_2\}$[76] (average Zr–O(THF) = 2.259(5) Å). The average zirconium/chloride bond length in compound **8** is 2.4953(6) Å, and this average bond length is similar to that in $[(Ph_3SiO)_2ZrCl_2(THF)_2](PhMe)_2$[77] (Zr–Cl = 2.4683(9) Å), but significantly longer than that in the less sterically demanding $[ZrCl_3(THF)]_2(\mu\text{-}Cl)_2]$[77] (average terminal Zr–Cl = 2.3602(9) Å).

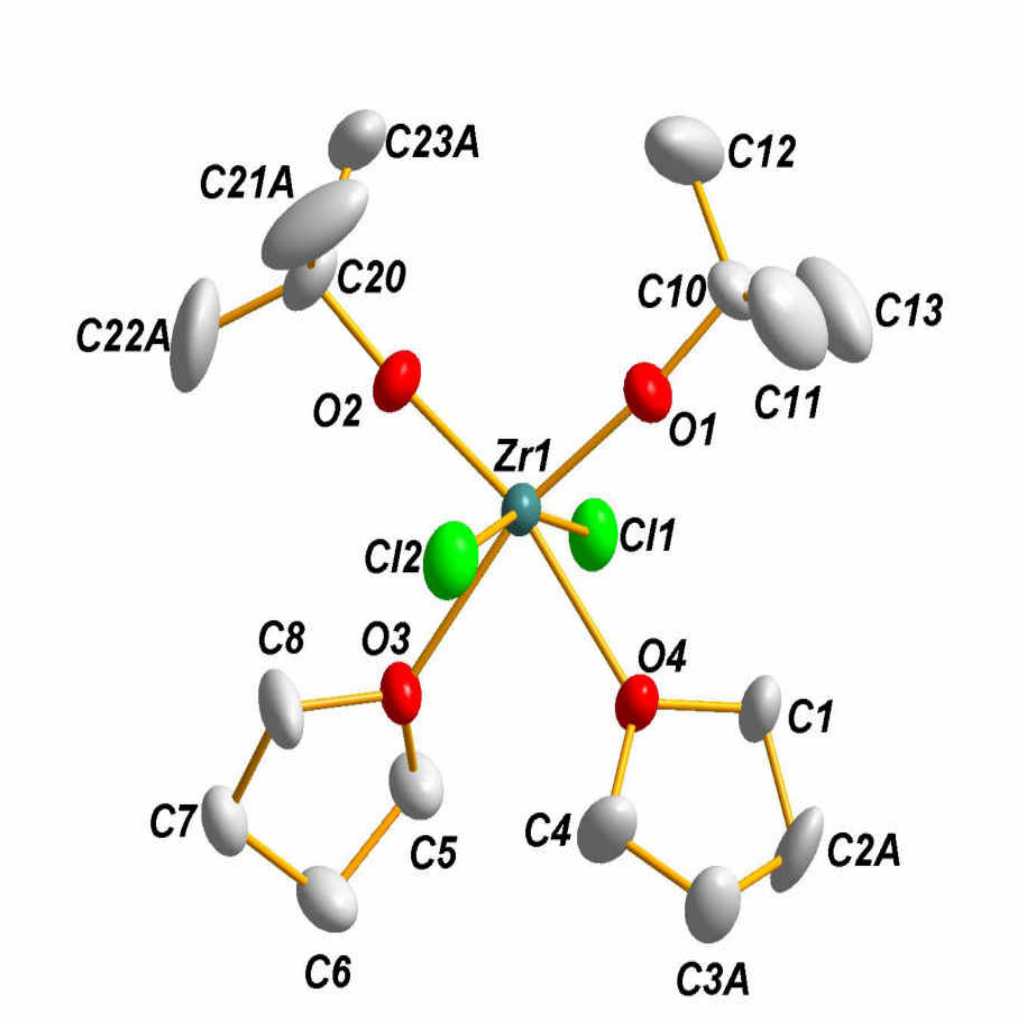

Figure 15. Solid-state structure and labeling scheme of **8**. With the exception of carbon (35%) all atoms are drawn at the 50% probability level.

Table 6. Crystal data for compound **8**

Molecular formula	$C_{16}H_{34}Cl_2O_4Zr$
fw	452.55
Crystal system	monoclinic
Space-group	$P2_1/n$(No. 14)
a, Å	12.2463(13)
b,Å	10.5873(11)
c,Å	17.2373(18)
α, deg	90
β, deg	91.977(2)
γ, deg	90
V, Å^3	2243.2(4)
Z	4
F(000)	944
ρ(calc), g cm^{-3}	1.340
λ, Å	0.71073
temp, K	173
μ, mm^{-1}	0.742
$R(F)^a$	0.0336
$R_W(F^2)^b$	0.0975

[a] $R = \sum||F_o| - |F_c|| / |F|_o$. [b] $R_w = \{[\sum w(F_o^2 - F_c^2)] / [\sum w(F_o^2)^2]\}^{1/2}$; $w = 1/[\sigma^2(F_o)^2 + (xP)^2 + yP]$, where $P = (F_o^2 + 2F_c^2)/3$.

Table 7. Selected bond lengths (Å) and angles (°) for **8**

Bond Lengths			
Zr1–O1	1.8960(16)	O1–C10	1.418(3)
Zr1–O2	1.9044(15)	O4–C40	1.450(3)
Zr1–O3	2.3184(15)	C10–C11	1.520(4)
Zr1–O4	2.3125(15)	O3–C5	1.448(3)
Zr1–Cl1	2.4936(6)	O4–C1	1.456(3)
Zr1–Cl2	2.4969(6)	C2A–C3A	1.527(10)
Bond Angles			
O1–Zr1–O2	103.36(7)	O2–Zr1–Cl2	92.77(5)
O1–Zr1–O3	166.16(6)	O3–Zr1–Cl1	82.55(4)
O1–Zr1–O4	89.60(6)	O3–Zr1–Cl2	84.78(4)
O2–Zr1–O3	90.25(6)	O4–Zr1–Cl1	84.12(4)
O4–Zr1–O3	76.98(6)	O4–Zr1–Cl2	82.24(4)
O1–Zr1–Cl1	92.88(5)	Cl1–Zr1–Cl2	163.15(2)
O1–Zr1–Cl2	96.85(5)	C10–O1–Zr1	171.34(16)
O2–Zr1–Cl1	98.33(5)	C20–O2–Zr1	167.51(17)

7. Synthesis and Spectroscopic Analysis of $[HfCl_2(O^tBu)_2(THF)_2]$, 9

Compound **9**, the hafnium analogue of **8**, was synthesized in a similar manner by treating *cis*-$HfCl_4(THF)_2$ with 1/3 equivalent of dimeric sodium tri(*tert*-butoxy)stannate, $[Na(O^tBu)_3Sn]_2$ (Scheme 7).

Characterization of **9** by NMR spectroscopy gives spectra identical to those of **8**. The ^{1}H NMR spectrum of **9** is shown in Figure 16. The spectrum shows peaks for coordinated THF and *tert*-butoxy ligands. The methylene protons on the coordinated THF molecules were observed as triplets at 3.62 and 1.77 ppm, respectively. The protons on the *tert*-butoxy groups appeared as a singlet at 1.30 ppm.

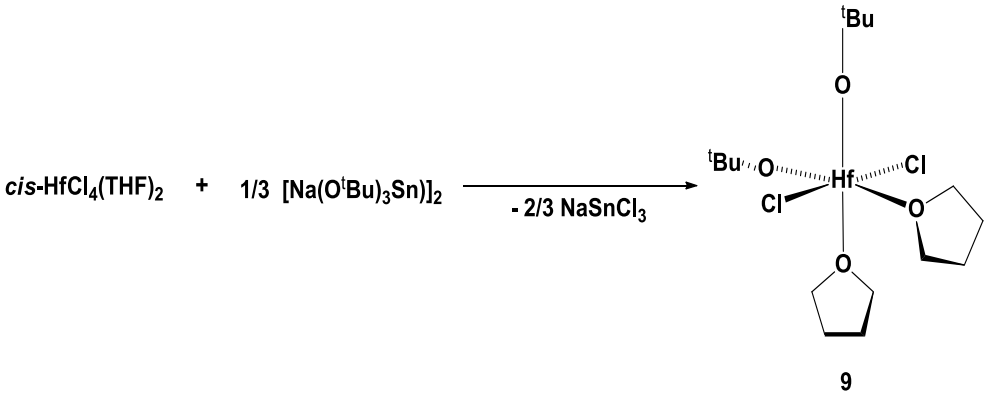

Scheme 7. Synthesis of compound **9**.

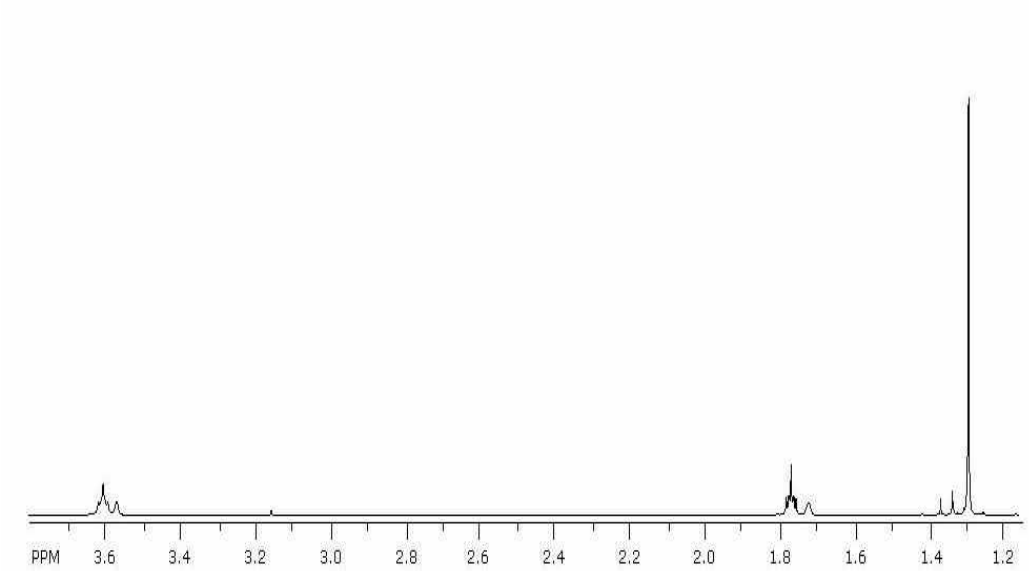

Figure 16. ^{1}H NMR spectrum of **9**.

8. Solid-state Structure of $[HfCl_2(O^tBu)_2(THF)_2]$, 9

The solid-state structure of **9** is shown in Figure 17. The compound crystallizes in the monoclinic crystal system with space group $P2_1/n$. Crystal parameters and selected bond lengths and angles are listed in Table 8 and 9, respectively.

The structure of **9** is analogous to that of **8** with the same arrangement of ligands around the hafnium center. The geometry about hafnium is that of a distorted octahedron. The Hf–O^{t}Bu bonds [1.904(4) Å and 1.894(4) Å] and the Hf–O(THF) [(2.293(4) Å and 2.285(4) Å] are slightly shorter than those in **8**, a characteristic which is due to the lanthanide contraction.

Compared to other hafnium *ter*t-butoxy containing compound, the Hf–O^{t}Bu bonds in **9** are shorter than those in $Hf(O^tBu)_2(C_8H_{12}O_2N)_2$[78] (Hf–O^{t}Bu = 1.9298(26) and 1.9393(28) Å) and $Hf(O^tBu)_2(C_5H_{11}O_2)_2$[79] (Hf–O^{t}Bu = 1.9320(32) and 1.9316(36) Å).

The Hf−O(THF) bonds (2.4704(12)) in complex **9** are longer than those in the less sterically encumbered hafnium pentachloride tetrahydrofuran anion in $[Na{\cdot}18\text{-crown-}6][HfCl_5(THF)^-]$[80] (average Hf–THF = 2.21(1) and Hf−Cl = 2.415(3)) and in the dimeric chlorosiloxane complex $[Cl_2HfOSiO^tBu_2(THF)_2]_2$[81] (average Hf–THF = 2.294(3) and average Hf–Cl = 2.461(13)), while the Hf–Cl bonds (2.4699(11)Å) in **9** are comparable to those in the above compounds.

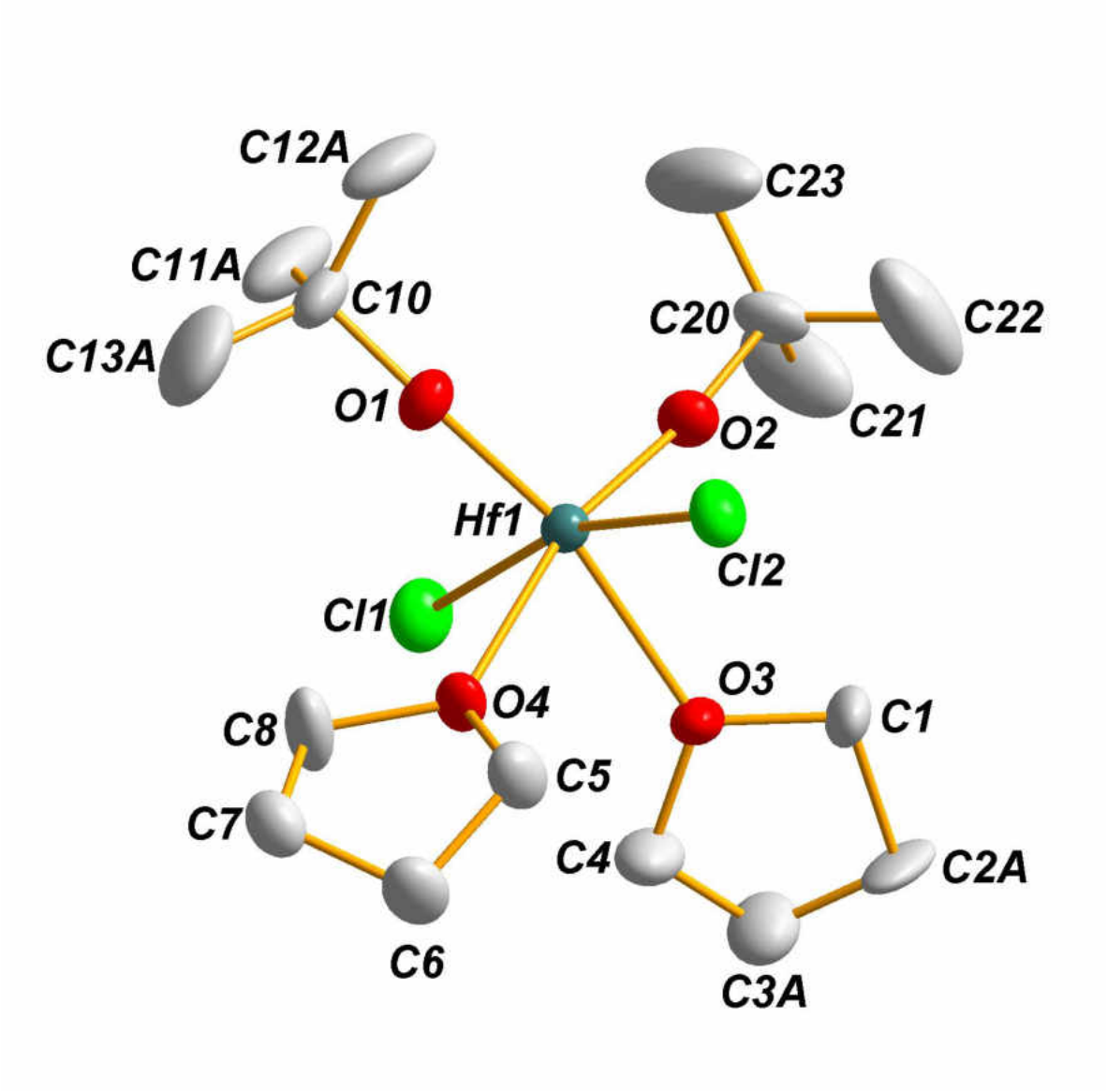

Figure 17. Solid-state structure and labeling scheme of **9**. With the exception of carbon (35%) all atoms are drawn at the 50% probability level

Table 8. Crystal data for compound **9**

Molecular formula	$C_{16}H_{34}Cl_2HfO_4$
fw	539.82
Crystal system	monoclinic
Space-group	$P2_1/n$
a, Å	12.2463(13)
b,Å	10.5873(11)
c,Å	17.2373(18)
α, deg	90
β, deg	92.164(2)
γ, deg	90
V, Å^3	2233.3(4)
Z	4
F(000)	1072
ρ(calc), g cm^{-3}	1.606
λ, Å	0.710 73
temp, K	173
μ, mm^{-1}	4.924
$R(F)^a$	0.0291
$R_W(F^2)^b$	0.0737

[a] $R = \sum|F_o - F_c| \quad |F|_o$. [b] $R_w = \{[\quad w(F_o^2 - F_c^2)] / [\sum w(F_o^2)^2]\}^{1/2}$; $w = 1/[\sigma^2(F_o)^2 + (xP)^2 + yP]$, where $P = (F_o^2 + 2F_c^2)/3$

Table 9. Selected bond lengths (Å) and angles (°) for **9**

Bond Lengths			
Hf1−O1	1.904(4)	Hf1−Cl1	2.4704(12)
Hf1−O2	1.894(4)	Hf1−Cl2	2.4699(11)
Hf1−O3	2.293(4)	O1−C10	1.414(6)
Hf1−O4	2.285(4)	O2−C20	1.416(7)
Bond Angles			
O1−Hf1−O2	104.23(17)	O1−Hf1−Cl2	97.88(12)
O1−Hf1−O3	166.46(16)	O2−Hf1−Cl1	96.62(11)
O1−Hf1−O4	90.20(16)	O2−Hf1−Cl2	92.66(11)
O2−Hf1−O3	89.06(16)	O3−Hf1−Cl1	82.77(9)
O2−Hf1−O4	165.39(16)	O3−Hf1−Cl2	83.84(9)
O3−Hf1−O4	76.65(14)	O4−Hf1−Cl1	84.75(9)
O1−Hf1−Cl1	92.97(12)	O4−Hf1−Cl2	82.91(9)
Cl2−Hf1−Cl1	163.55(4)	C20−O2−Hf1	170.2(4)
C10−O1−Hf1	166.6(4)		

9. Synthesis and Spectroscopic Analysis of $[Ti(O^tBu)_2(OTf)_2(THF)_2]$, 10

Attempts at synthesizing titanium analogues of compounds **6**–**9**, by treating *cis*-$TiCl_4(THF)_2$ with dimeric sodium tri(*tert*-butoxy)stannate, $[Na(O^tBu)_3Sn]_2$, did not yield clean products. The formations of many different products dissimilar from the

expected ones were observed by NMR spectroscopy. The only identifiable product, *trans*-[Sn(O^{t}Bu)Cl]$_2$, was confirmed by X-ray crystallography. To circumvent this problem, we thought that the titanium analogue of **6** and **7**, *fac*-{[Ti(O^{t}Bu)$_3$(THF)$_3$](SnCl$_3$)}, could be accessed via the reaction of Ti(O^{t}Bu)$_3$Cl with SnCl$_2$ in THF. However, this attempt failed to yield the desired product. The failure of titanium to react in a manner similar to that of zirconium and hafnium was attributed to its much smaller size.

Chlorotri(*tert*-butoxy)titanium, Ti(O^{t}Bu)$_3$Cl, however, reacted with silver triflate to afford compound **10** (Scheme 8). Complex **10** was initially believed to be the triflate anologue of **6** and **7**, based on its NMR spectra. However, the solid-state structure of **10** revealed it to be a ditriflate instead of the expected monotriflate. Compound **10** was found to be soluble in THF, but insoluble in hydrocarbon solvents.

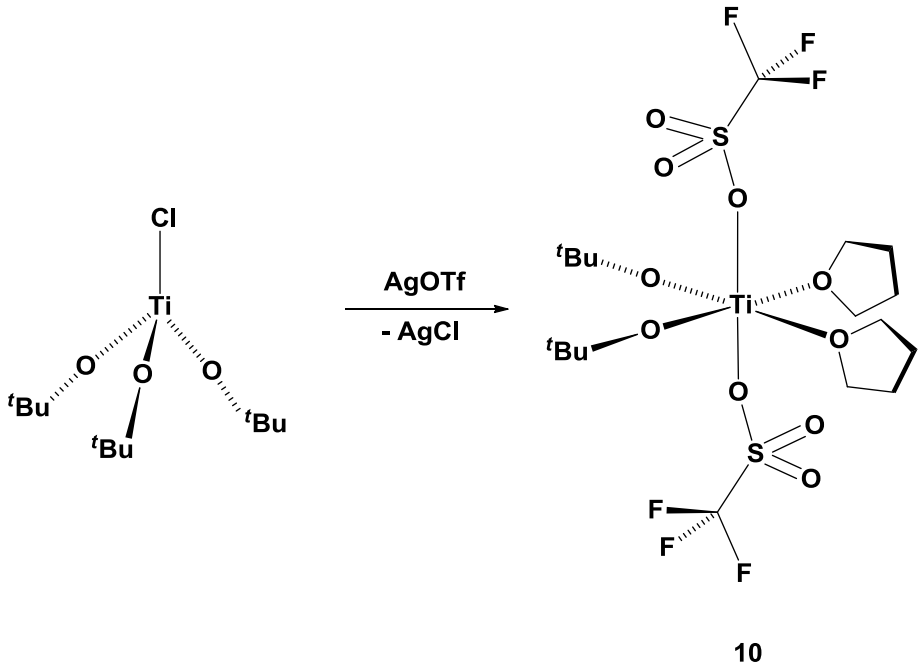

10

Scheme 8. Synthesis of compound **10**.

Although $Ti(O^tBu)_3Cl$ and AgOTf were combined in a 1:1 ratio, the isolated product was a ditriflate complex. The product obtained was not believed to have arisen from a simple metathesis reaction. Instead, compound **10** was thought to have come from the disproportionation of the initially expected product, $[Ti(O^tBu)_3(THF)_3(OTf)]$, into $[Ti(O^tBu)_2(THF)_2(OTf)_2]$, **10**, and $Ti(O^tBu)_4$.

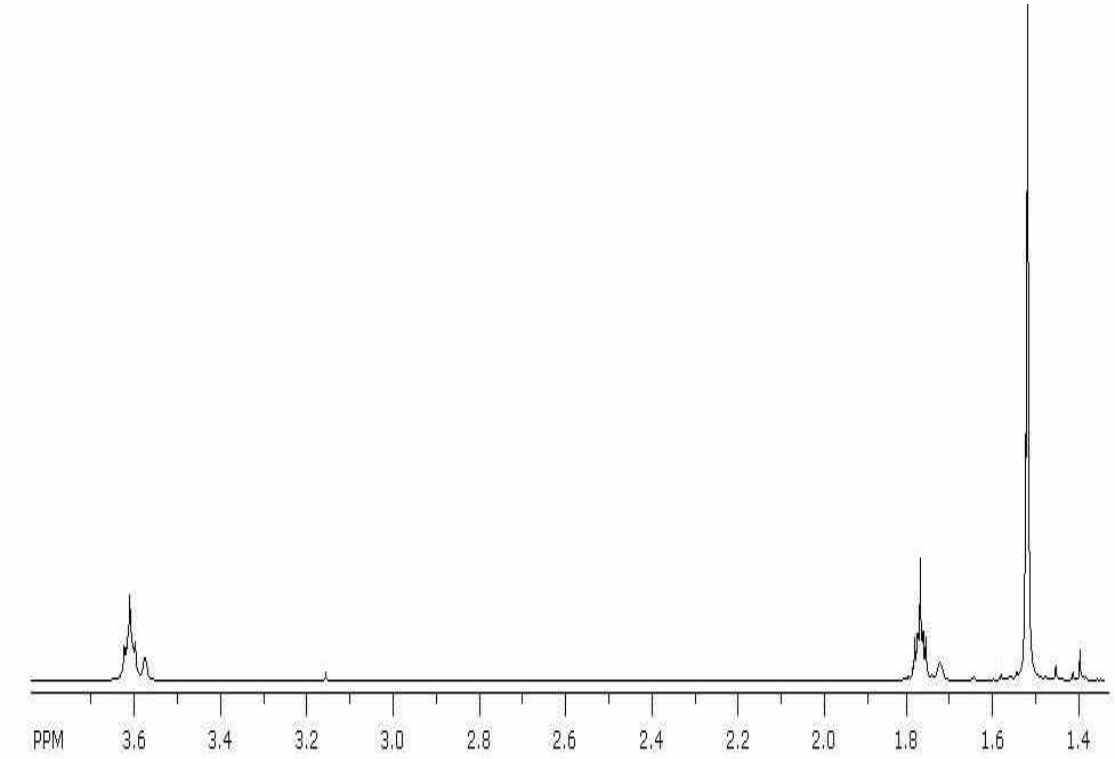

Figure 18. ^{1}H NMR spectrum of **10**.

The ^{1}H NMR spectrum of **10** obtained in THF-d_8 reveals three signals in addition to that of the deuterated THF (Figure 18). Compound **10** is C_2 symmetric, and so the two THF and two alkoxy groups are equivalent. The signals observed at 3.62 and 1.77 ppm in the ^{1}H NMR spectrum were attributed to the methylene protons of the coordinated THF molecules, while the signal at 1.52 ppm was assigned to the protons of the *tert*-butoxy

group. The $^{13}C\{^{1}H\}$ NMR spectrum showed five peaks at 120.8, 96.1, 68.3, 31.4, and 26.4 ppm. The singlet peaks at 68.3 and 26.4 were assigned to the methylene carbons on the THF molecules. The peaks for the *tert*-butoxy group were attributed to the singlets at 96.1 ppm (quaternary carbon) and 31.4 ppm (methyl carbon). The last peak at 120.8 ppm (average), observed as a quartet was assigned to the carbon atom of the trifluoromethyl unit of the triflate. Because ^{19}F has a spin of ½, the three fluorine atoms split the signal of the carbon atom into a quartet.

10. Solid-state Structure of $[Ti(O^tBu)_2(OTf)_2(THF)_2]$, 10

Compound **10** crystallized in the trigonal crystal system with space group *P*3*c*1 and 6 molecules in the unit cell. Supplemental crystallographic data for this compound are listed in Tables 10 and 11.

The geometry about titanium is that of a distorted octahedron, with the *tert*-butoxy groups being trans to the THF molecules and the triflate groups being trans to each other (Figure 19). This arrangement of ligands is similar to that in **8** and **9**, the only difference being the replacement of the chloride ligands by triflate ligands.

In the unit cell of **10**, the molecules sit on a site with crystallographic two-fold symmetry. This renders the *tert*-butoxy, THF, and triflate groups equivalent. The Ti−O^{t}Bu bond (1.7421(17) Å) is similar to that in $[Ti(C_5H_8NOS_2)_3(O^tBu)]$[82] (1.742(2) Å), but slightly longer than those in $[Ti(C_5H_9NOS)_2(O^tBu)_2]$[83] (1.79(10) Å) and $[(O^tBu)_3TiMn(CO)_5]$[59] (average Ti−O^{t}Bu = 1.756(4) Å). The Ti−O^{t}Bu bond length and the Ti−O−C bond angle (174.37(17) Å) indicate the presence of π-bonding. The Ti−O(THF) bonds are much weaker, and they are 2.1905(17) Å long. The Ti−OTf bonds

(2.0325(17) Å) are also longer than the alkoxide bonds. Compared to other Ti−OTf bonds, those in **10** are shorter than that in [Cp*Ti(OTf)][84] (2.107(2) Å), but slightly longer than those in {[Ti($C_{34}H_{28}O_4$)($OTf)_2$]·2$CDCl_3$}[85] (1.9923(12) Å).

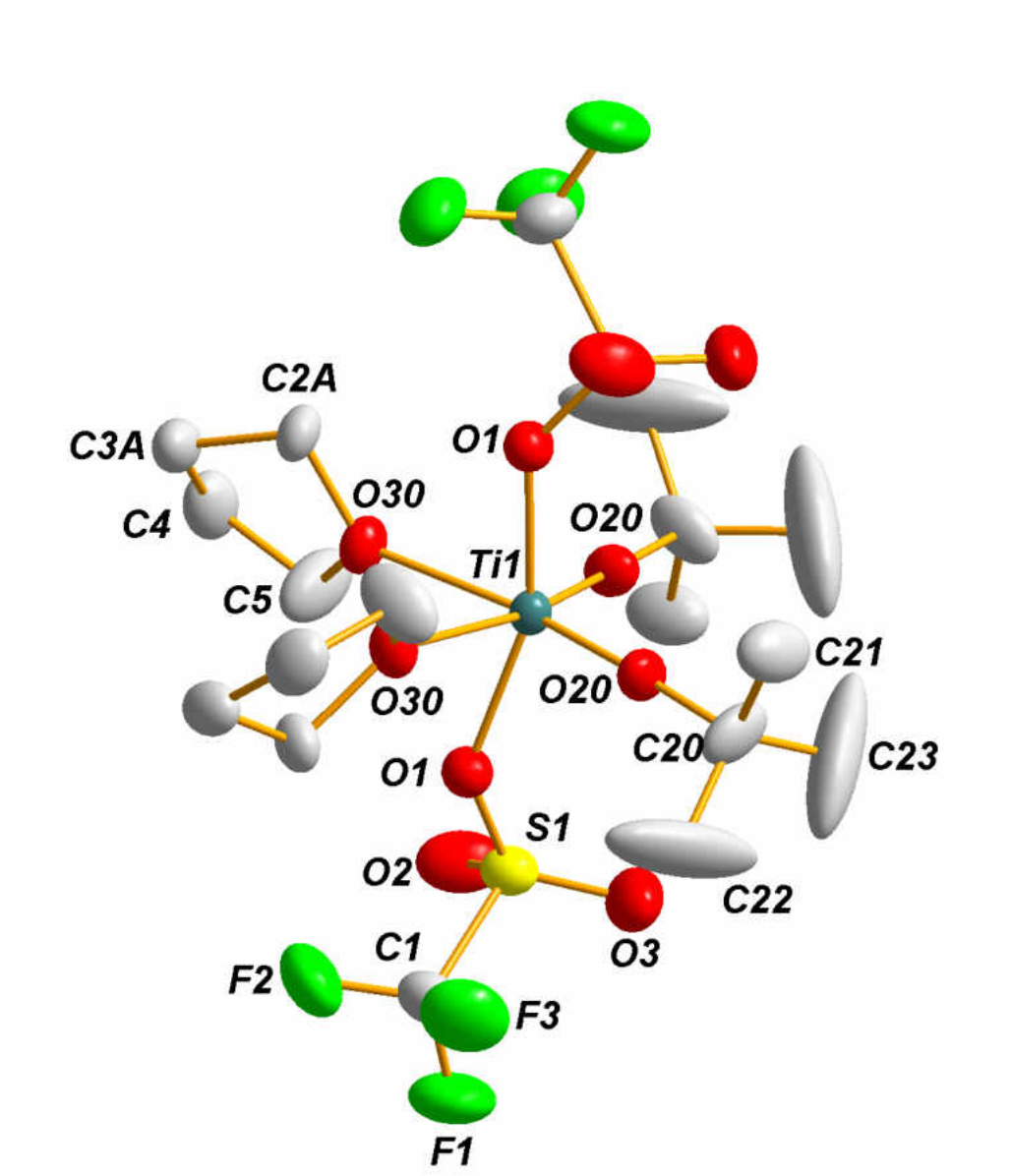

Figure 19. Solid-state structure and labeling scheme of **10**. With the exception of carbon (35%) all atoms are drawn at the 50% probability level.

Table 10. Crystal data for compound **10**

Molecular formula	$C_{18}H_{34}F_6O_{10}S_2Ti$
Formula weight	636.47 g/mol
Crystal system	trigonal
Space-group	*P*3*c*1 (No. 165)
a, Å	16.6042(8)
b,Å	16.6042(8)
c,Å	17.7297(17)
α, deg	90
β, deg	90
γ, deg	120
V, Å^3	4233.19(5)
Z	6
F(000)	1980
ρ(calc), g cm^{-3}	1.498
λ, Å	0.71073
temp, K	173
μ, mm^{-1}	0.537
$R(F)^a$	0.0510
$R_W(F^2)^b$	0.1484

[a] $R = \sum|F_o - F_c| \quad |F|_o$. [b] $R_w = \{[\quad w(F_o^2 - F_c^2)] / [\sum w(F_o^2)^2]\}^{1/2}$; $w = 1/[\sigma^2(F_o)^2 + (xP)^2 + yP]$, where $P = (F_o^2 + 2F_c^2)/3$.

Table 11. Selected bond lengths (Å) and angles (°) for **10**

Bond Lengths			
Ti1−O20	1.7421(17)	F1−C1	1.332(4)
Ti1−O30	2.1905(17)	F2−C1	1.314(4)
Ti1−O1	2.0325(17)	F3−C1	1.328(4)
S1−O1	1.4832(18)	O20−C20	1.411(3)
S1−O2	1.426(2)	O30−C2A	1.495(5)
S1−O3	1.421(2)	O30−C5	1.440(3)
S1−C1	1.816(3)		
Bond Angles			
O1−Ti1−O30	82.21(7)	F3−C1−F1	108.1(3)
O1−Ti1−O1'	159.28(10)	F2−C1−F3	107.7(3)
O20−Ti1−O1	96.63(8)	S1−O1−Ti1	138.35(11)
O20−Ti1−O30	89.93(7)	O2−S1−O1	112.82(13)
O20'−Ti1−O20	103.08(12)	O3−S1−O1	113.78(13)
O30−Ti1−O30'	77.07(9)	O3−S1−O2	118.83(17)
F2−C1−F1	108.4(3))	C20−O20−Ti1	174.37(17)

11. Synthesis and Spectroscopic Analysis of *fac*-[Zr(O^{t}Bu)$_3$(OTf)(THF)$_2$], 11

THF being a weak donor, the M←THF bonds in **6** and **7** are not very strong. Hence, it should be possible to derivatize the compounds by replacing the THF molecules with stronger nucleophiles. Attempts at converting **6** to CpZr(O^{t}Bu)$_3$ by treating it with NaCp gave CpSnCl (isolated and confirmed by X-ray crystallography),[86,87] among other products. Trials with 15-crown-5 also gave a known compound, {[(15-crown-5)$_2$Sn](SnCl$_3$)$_2$}.[88,89] Treatment with $NaBH_4$ resulted in the reduction of tin to elemental tin. It was thus observed in all the cases that instead of the nucleophiles interacting with the cationic group 4 unit {Zr(O^{t}Bu)$_3$}$^+$, it preferentially reacted with the trichlorostannate, {SnCl$_3$}$^-$. To eliminate the interference of the trichlorostannate, we sought to replace this counter ion with a triflate anion. Hence, compound **11** was obtained by treating **6** with silver triflate in THF at room temperature (Scheme 9).

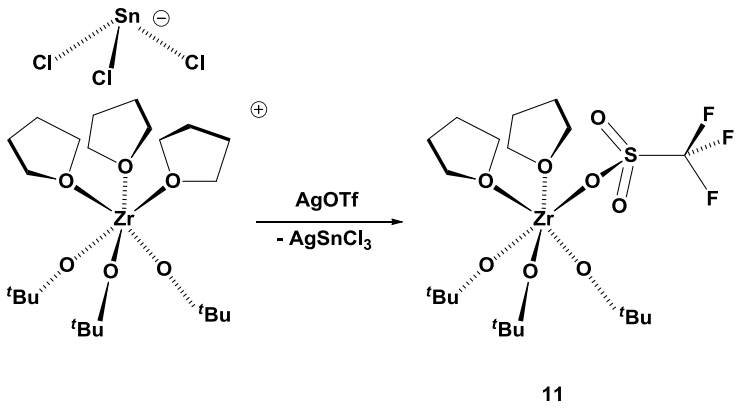

Scheme 9. Synthesis of compound **11**.

Characterization of **11** by ^{1}H NMR spectroscopy revealed a sharp singlet peak for the *tert*-butoxy groups at 1.30 ppm (Figure 20). The methylene protons of the THF ligands were observed as very broad peaks. The ^{13}C{^{1}H) NMR spectrum showed a singlet

peak each for the quaternary and primary carbons of the *tert*-butoxy group, and two singlet peaks for the methylene carbons of the THF ligands (Figure 21). The triflate was observed as a quartet at 121.1 ppm ($^1J_{C–F}$ = 318 Hz). From NMR spectroscopy, it can be inferred that the *tert*-butoxy groups and the THF ligands are equivalent, but this differs from the solid state structure of **11**, which revealed that the molecule was a contact ion pair in the solid state, thereby rendering these groups inequivalent. This suggested the possibility of a fast triflate exchange in solution. To determine this, we added excess AgOTf to a sample of **11**, in hopes of seeing two different signals for the triflate in the ^{13}C NMR spectrum. However, the results obtained did not support the hypothesis of a slow exchange.

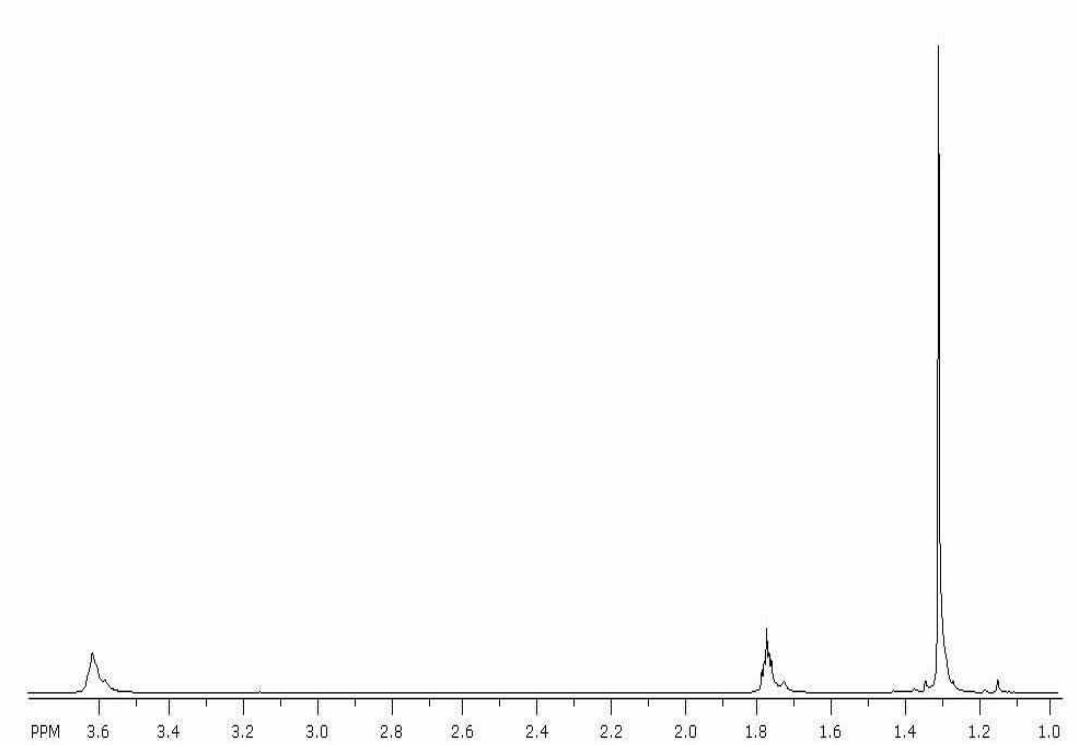

Figure 20. ^{1}H NMR spectrum of **11**.

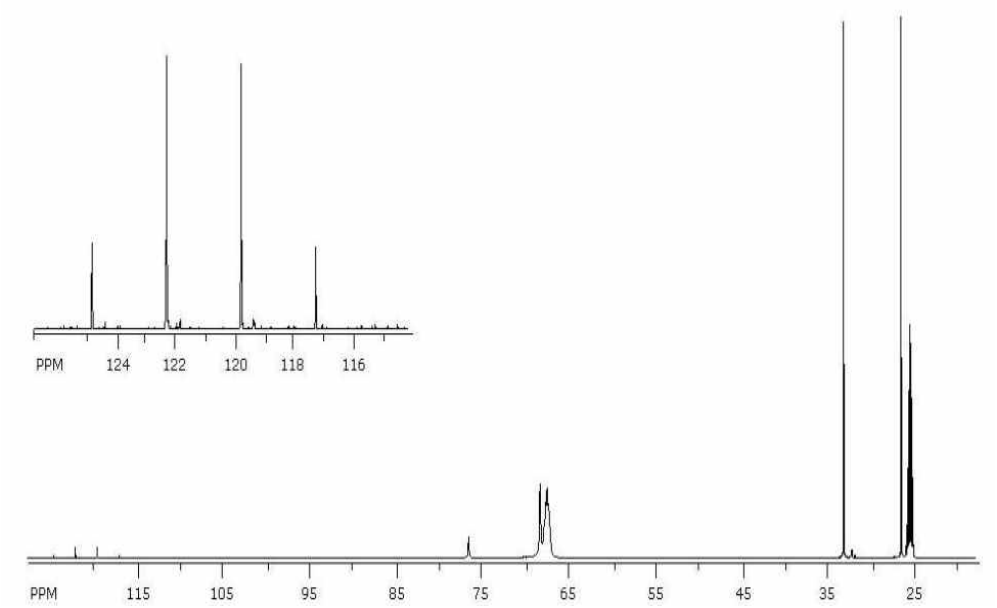

Figure 21. $^{113}C\{^{1}H\}$ NMR spectrum of **11**. Also shown is an inset of the 125–116 ppm region.

12. Solid-state Structure of *fac*-[Zr(O^{t}Bu)$_3$(OTf)(THF)$_2$], 11

The solid state structure of **11** is shown in Figure 22. The compound crystallizes in the orthorhombic crystal system with space group $P2_12_12_1$. Crystal parameters and selected bond lengths and angles are listed in Tables 12 and 13, respectively.

Similar to the previous compounds, the geometry about zirconium is that of a distorted octahedron. The Zr(O^{t}Bu)$_3$ unit in **11** is very similar to that in **6**, with analogous Zr–O^{t}Bu bond lengths. However, the angle enclosed by the Zr–O^{t}Bu bonds in **11** is smaller than that in **6**. Another difference between **6** and **11** is the small asymmetry in the lengths of the Zr–O^{t}Bu bonds in **11**. Those opposite the THF molecules (1.9160(16) Å) are slightly shorter than the one opposite the triflate ion (1.9326(16) Å).

The Zr–THF bonds (2.3180(16) and 2.3241(16) Å) in **11** are longer than the Zr–O^{t}Bu bonds, but comparable to that in the previous compounds. The Zr–OTf bond (2.2371(17)) is also longer than the Zr–O^{t}Bu bonds. Compared to the Zr–OTf bonds in

related compounds, that in **11** is similar to that in $\{[Zr(C_{31}H_{51}N_6Si_2)(OTf)]\cdot C_7H_8\}$[90] (2.286(2) Å), but longer than those in $[(Cp^*)_2Zr(OTf)_2]$[91] (2.146(2) Å, 2.153(2) Å) and $[(C_5H_3{}^tBu_2)_2Zr(SH)(OTf)]$[92] (2.199(3) Å).

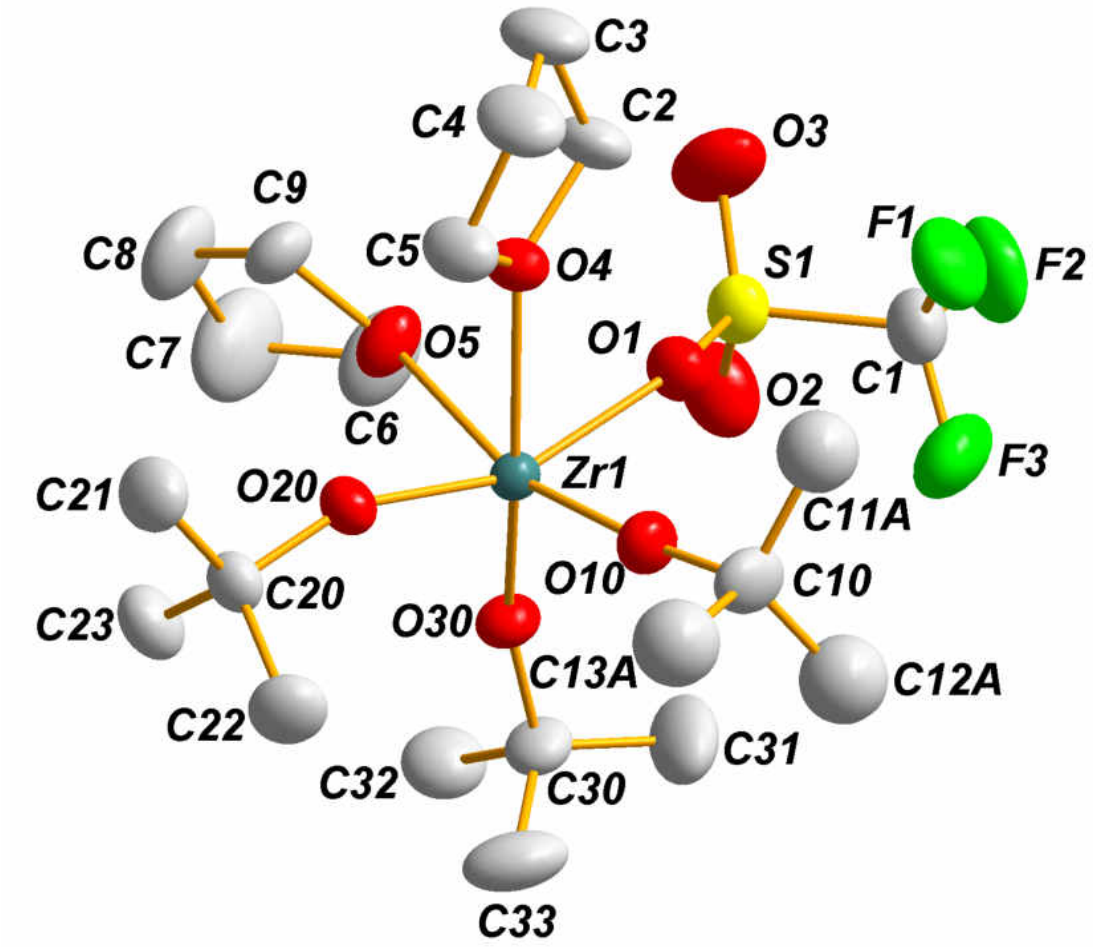

Figure 22. Solid-state structure and labeling scheme of **11**. With the exception of carbon (35%) all atoms are drawn at the 50% probability level.

Table 12. Crystal data for compound **11**

Molecular formula	$C_{21}H_{43}F_3O_8SZr$
fw	603.83
Crystal system	orthorhombic
Space-group	$P2_12_12_1$
a, Å	9.2782(9)
b,Å	17.4312(17)
c,Å	18.1017(18)
α, deg	90
β, deg	90
γ, deg	90
V, Å^3	2927.6(5)
Z	4
F(000)	1264
ρ(calc), g cm^{-3}	1.370
λ, Å	0.710 73
temp, K	173
μ, mm^{-1}	0.503
$R(F)^a$	0.0306
$R_W(F^2)^b$	0.0867

[a] $R = \sum|F_o - F_c| \quad |F|_o$. [b] $R_w = \{[\quad w(F_o^2 - F_c^2)] / [\sum w(F_o^2)^2]\}^{1/2}$; $w = 1/[\sigma^2(F_o)^2 + (xP)^2 + yP]$, where $P = (F_o^2 + 2F_c^2)/3$.

Table 13. Selected bond lengths (Å) and angles (°) for **11**

Bond Lengths			
Zr1−O10	1.9150(17)	O30−C30	1.422(3)
Zr1−O20	1.9326(16)	S1−O1	1.4671(18)
Zr1−O30	1.9170(16)	S1−O2	1.420(2)
Zr1−O1	2.2371(17)	S1−O3	1.425(2)
Zr1−O4	2.3241(16)	C1−S1	1.805(3)
Zr1−O5	2.3180(16)	C1−F1	1.344(4)
O10−C10	1.404(3)	C1−F2	1.336(4)
O20−C20	1.415(3)	C1−F3	1.324(4)
Bond Angles			
O10−Zr1−O20	101.27(7)	O1−Zr1−O5	78.34(7)
O10−Zr1−O30	102.29(8)	O5−Zr1−O4	77.55(7)
O10−Zr1−O1	90.37(7)	C10−O10−Zr1	175.05(18)
O10−Zr1−O4	89.89(7)	C20−O20−Zr1	155.34(14)
O10−Zr1−O5	164.44(8)	C30−O30−Zr1	159.97(17)
O20−Zr1−O30	101.53(7)	S1−O1−Zr1	153.93(12)
O20−Zr1−O1	160.02(7)	O2−S1−O1	113.98(12)
O20−Zr1−O4	84.82(6)	O1−S1−C1	100.65(13)
O20−Zr1−O5	86.87(7)	O2−S1−C1	103.86(15)
O30−Zr1−O1	91.63(7)	O3−S1−C1	103.80(17)
O30−Zr1−O4	164.72(7)	O3−S1−O1	113.69(13)
O30−Zr1−O5	88.84(7)	O2−S1−O3	118.01(16)
O1−Zr1−O4	78.96(6)	F3−C1−F1	107.2(3)
F2−C1−F1	107.5(2)	F3−C1−F2	108.4(3)

13. Synthesis and Spectroscopic Analysis of *fac*-[Sn(μ-O^{t}Bu)$_3$Zr(O^{t}Bu)$_3$], 12

The synthesis of **12** was achieved by treating *cis*-$ZrCl_4(THF)_2$ with one full equivalent of dimeric sodium tri(*tert*-butoxy)stannate, $[Na(O^tBu)_3Sn]_2$ (Scheme 10). Heterobimetallic **12** is made up of three terminal alkoxides that coordinate the zirconium metal on one face, and the other face is chelated by one unit of the ligand. So, it is observed from the formation of **12** that one unit of the ligand $\{Sn(O^tBu)_3\}$ can be transferred to the zirconium metal center only when the Lewis acidity of the metal center is sufficiently reduced, as in **6.** Compound **12** was found to be soluble in THF and hydrocarbon solvents. Crystalline **12** sublimed at 220 ^oC (1 atm). A literature search showed that compound **12** had previously been synthesized from $Zr(O^tBu)_4$ and $Sn(O^tBu)_2$ in diethyl ether.[56]

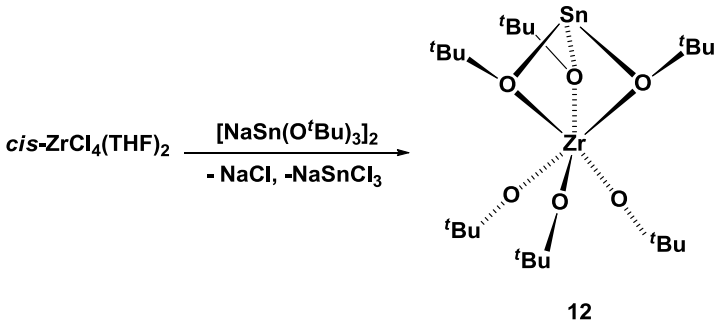

Scheme 10. Synthesis of compound **12**.

Characterization of **12** by ^1H NMR spectroscopy revealed the presence of two sharp singlets at 1.53 and 1.47 ppm in addition to the signal for deuterated benzene (Figure 23). The peak at 1.53 ppm is assigned to the methyl protons of the bridging *tert*-butoxy group. That at 1.47 ppm is attributed to the methyl protons of the terminal *tert*-butoxy group. The $^{13}C\{^1H\}$ NMR spectrum showed four peaks at 34.0, 34.9, 73.9 and

76.0 ppm (Figure 24). The signals at 34.0 and 73.9 ppm are attributed to the respectively to the primary and quaternary carbons of the terminal alkoxy groups, respectively. The signal at 34.9 ppm showed coupling to the tin atom and was therefore, assigned to the methyl carbons of the bridging alkoxides. Finally, the signal at 76.0 ppm was attributed to the quaternary carbons of the bridging alkoxides.

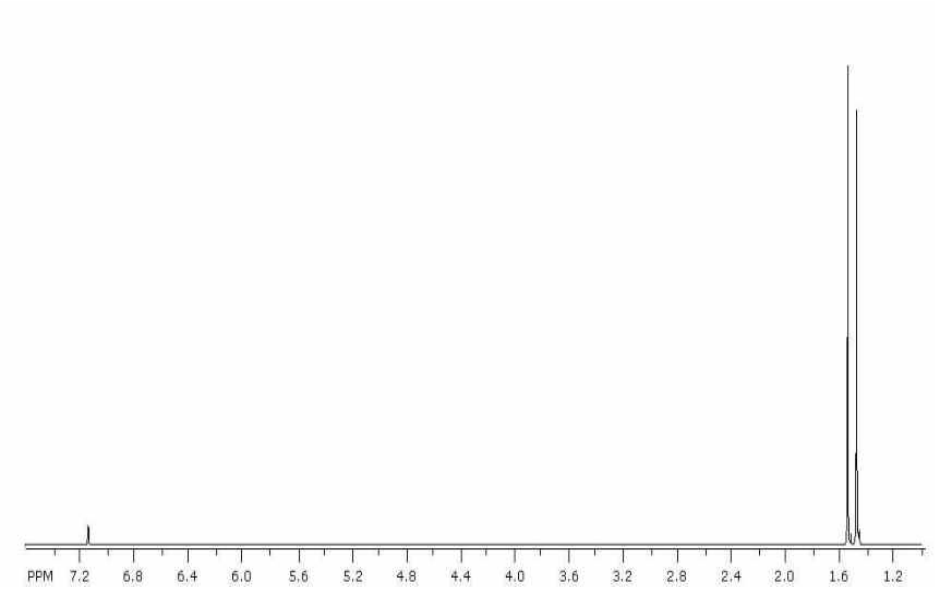

Figure 23. ^{1}H NMR spectrum of **12**.

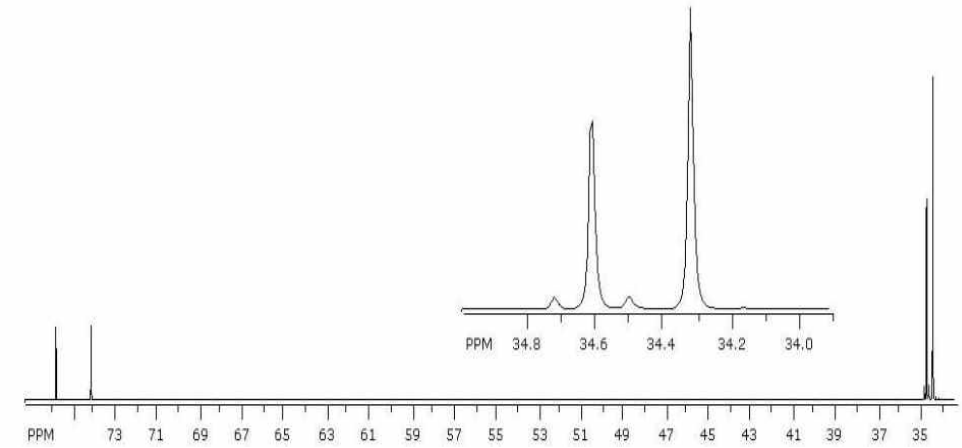

Figure 24. ^{13}C{^{1}H} NMR spectrum of **12**. Also shown is an inset of the 35−34 ppm region.

14. Solid-state Structure of *fac*-[Sn(μ-O^{t}Bu)$_3$Zr(O^{t}Bu)$_3$], 12

Crystals of **12** grown from THF did not diffract well. Single crystals, which diffracted better and from which the structure of **12** was obtained, were grown from hexane. Although the synthesis of **12** had been previously reported and the stoichiometry of the compound had been properly formulated based on NMR spectroscopy and elemental analysis data, attempts to obtain an X-ray structure by the authors were thwarted by the disorder of the Sn atom. In solving the structure of **12**, we faced the same problems arising from the disorder of tin. However, we were able to solve and refine to acceptable *R*-values the single-crystal X-ray data of complex **12**. The structure of **12** is shown in Figure 25. Supplemental crystallographic data are given in Tables 14 and 15.

Complex **12** crystallizes in the trigonal crystal system with space group *P*3*m*1 and three molecules in the unit cell. The molecules are C_3-symmetric and they lie on special sites with 3*m* symmetry (Figure 25). There is a three-fold axis of rotation that goes through the zirconium and tin metal centers and makes the terminal alkoxides equivalent and the bridging alkoxides equivalent. There is also a plane of symmetry that runs through each *tert*-butoxy group (Figure 26).

The geometry about zirconium is that of a distorted octahedron. The deviation from octahedral geometry in **12** is very large. This is caused by the constraint on the zirconium-bridging alkoxide angles arising from the facial chelation of the zirconium metal center by tri-*tert*-butoxy stannate. This leads to O^{t}Bu–Zr–O^{t}Bu angles that are 68.5(3)^o rather than the expected 90^o. The Zr(O^{t}Bu)$_3$ pyramid in **12** is similar to those in **6** and **11**, with almost identical bonds (Zr–O^{t}Bu = 1.930(5) Å). The Zr–μ-O^{t}Bu (2.309(8) Å) bonds are much longer the terminal *tert*-butoxide bonds.

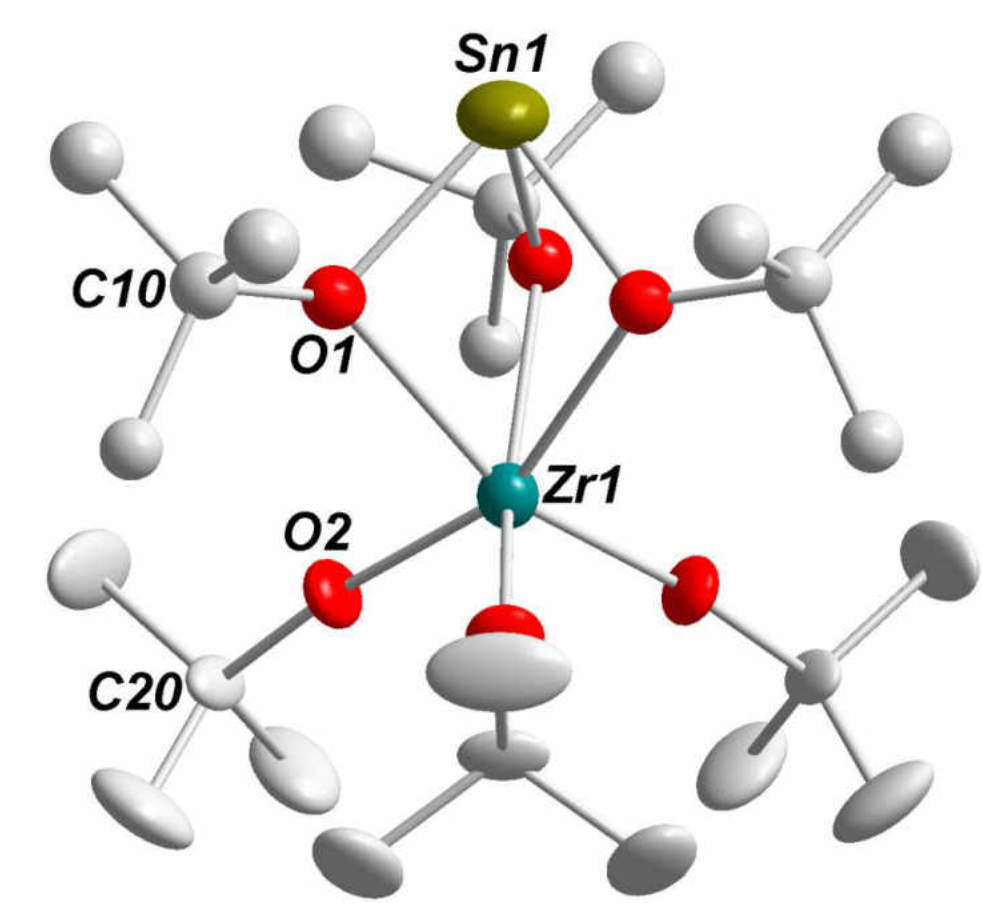

Figure 25. Solid-state structure and partial labeling scheme of **12**. With the exception of carbon (35%) all atoms are drawn at the 50% probability level.

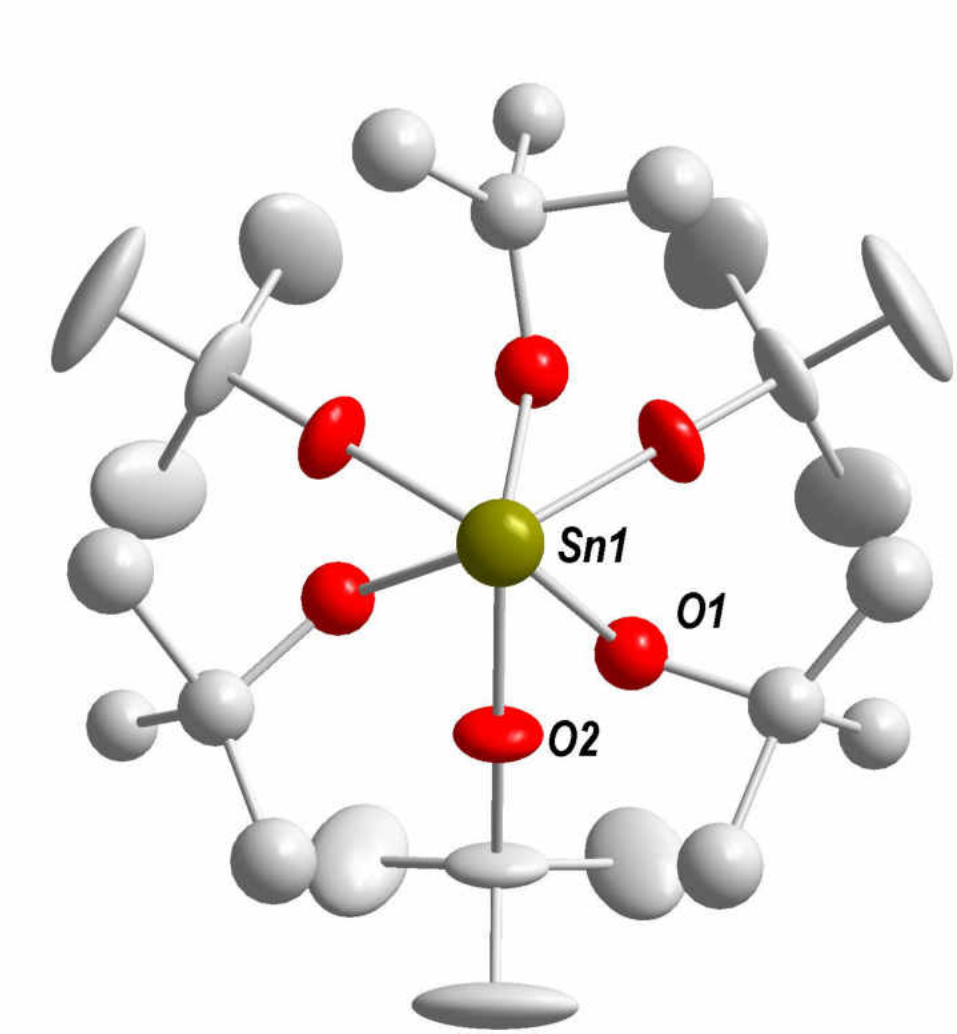

Figure 26. Top view of **12** showing C_3 symmetry of the compound.

Table 14. Crystal data for compound **12**

Molecular formula	$C_{24}H_{54}O_6SnZr$
fw	648.58
Crystal system	trigonal
Space-group	*P*3*m*1(156)
a, Å	17.1304(12)
b,Å	17.1304(12)
*c,*Å	9.4890(14)
α, deg	90
β, deg	90
γ, deg	120
V, Å^3	2411.5(4)
Z	3
F(000)	1008
ρ(calc), g cm^{-3}	1.340
λ, Å	0.710 73
temp, K	173
μ, mm^{-1}	1.130
$R(F)^a$	0.0519
$R_W(F^2)^b$	0.1400

[a] $R = \sum|F_o - F_c| \quad |F|_o$. [b] $R_w = \{[\quad w(F_o^2 - F_c^2)] / [\sum w(F_o^2)^2]\}^{1/2}$; $w = 1/[\sigma^2(F_o)^2 + (xP)^2 + yP]$, where $P = (F_o^2 + 2F_c^2)/3$.

Table 15. Selected bond lengths (Å) and angles (°) for **12**

Bond Lengths			
Zr1−O1	2.309(8)	Sn1−O1	2.082(8)
Zr1−O1'	2.309(8)	Sn1−O1'	2.082(8)
Zr1−O1''	2.309(8)	Sn1−O1''	2.082(8)
Zr1−O2	1.948(6)	O1−C1	1.427(17)
Zr1−O2'	1.948(6)	O2−C2	1.426(16)
Zr1−O2'	1.948(6)		
Bond Angles			
O1'−Zr1−O1	68.5(3)	O2'−Zr1−O1	159.8(7)
O1''−Zr1−O1	68.5(3)	O2''−Zr1−O1'	159.8(7)
O1'−Zr1−O1''	68.5(3)	O1'−Sn1−O1	77.2(3)
O2−Zr1−O1	93.4(3)	O1''−Sn1−O1	77.2(3)
O2−Zr1−O1'	93.4(3)	O1''−Sn1−O1'	77.2(3)
O2'−Zr1−O1'	93.4(3)	C20−O2−Zr1	173.2(6)
O2''−Zr1−O1	93.4(3)	C10−O1−Zr1	136.4(7)

15. Synthesis and Spectroscopic Analysis of *fac*-[Sn(μ-O^{t}Bu)$_3$Hf(O^{t}Bu)$_3$], 13

Complex **13**, the hafnium analogue of **12**, was synthesized in a similar manner by treating *cis*-$HfCl_4(THF)_2$ with a full equivalent of dimeric sodium tri(*tert*-butoxy)stannate, $[Na(O^tBu)_3Sn]_2$ (Scheme 11).

The ^{1}H NMR spectrum of **13** is very similar to that of **12** with two sharp singlet peaks for the bridging and terminal *tert*-butoxy groups (Figure 27). The ^{13}C NMR spectrum is also in accordance with the observed structure, with four carbon signals for the bridging and terminal alkoxides. The methyl carbon of the bridging *tert*-butoxy group shows coupling to tin ($^3J_{Sn-C}$ = 28 Hz).

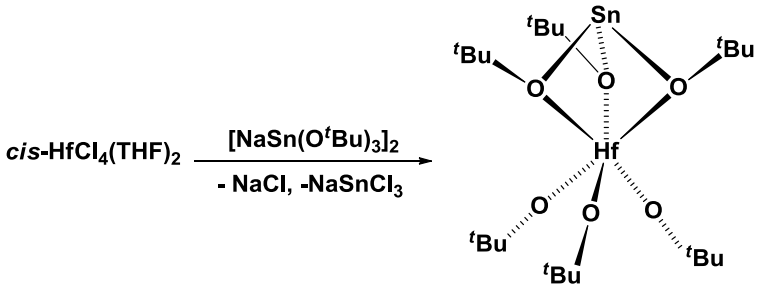

Scheme 11. Synthesis of compound **12**.

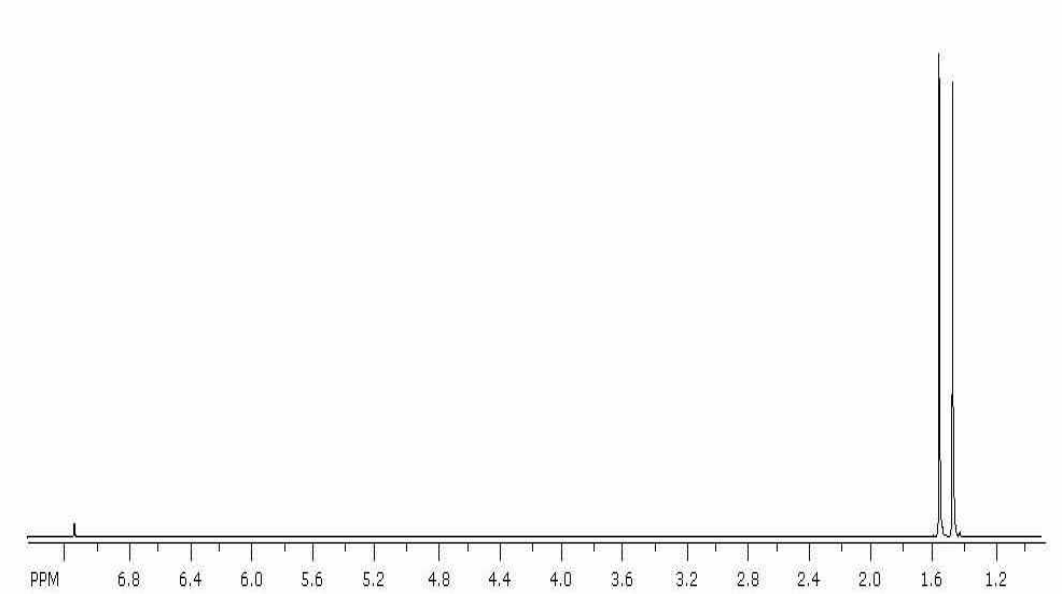

Figure 27. ^{1}H NMR spectrum of **13**.

16. Solid-state Structure of *fac*-[Sn(μ-O^{t}Bu)$_3$Hf(O^{t}Bu)$_3$], 13

X-ray quality crystals of **13** were grown from hexanes. Similar to **12**, the compound crystallized in the trigonal crystal system with space group *P*3*m*1 and three molecules in the unit cell. The solid state structure of **13** is given in Figure 28. Supplemental crystallographic data are listed in Tables 16 and 17.

Aspects of the structure similar to that of **12** already discussed shall not be repeated. The geometry about hafnium is that of a highly-distorted octahedron, caused by the facial chelation of hafnium by the Sn(O^{t}Bu)$_3$ unit. Compared to **12**, the bridging Hf–μ-O^{t}Bu (2.242(13) Å) and terminal Hf–O^{t}Bu (1.941(13) Å) bonds in **13** are slightly shorter.

The structure of **13** is similar to that of *fac*-{[C$_4$H$_2$N(2,5-CH$_2$NMe$_2$)$_2$]Hf(O^{t}Bu)$_3$}, in which the tridentate pincer pyrrolyl ligand chelates the hafnium center in a facial fashion, forming a highly distorted octahedron.[93] The Hf(O^{t}Bu)$_3$ pyramids in both compounds are similar, with the terminal Hf–O^{t}Bu (1.925(3), 1.931(3), 1.946(3) Å) bonds in the pyrrolyl complex being similar to those in **13**. The angles enclosed by the *tert*-butoxide ligands in the compound (99.18(12)^o) are also very close to those in **13** (99.3(8)^o).

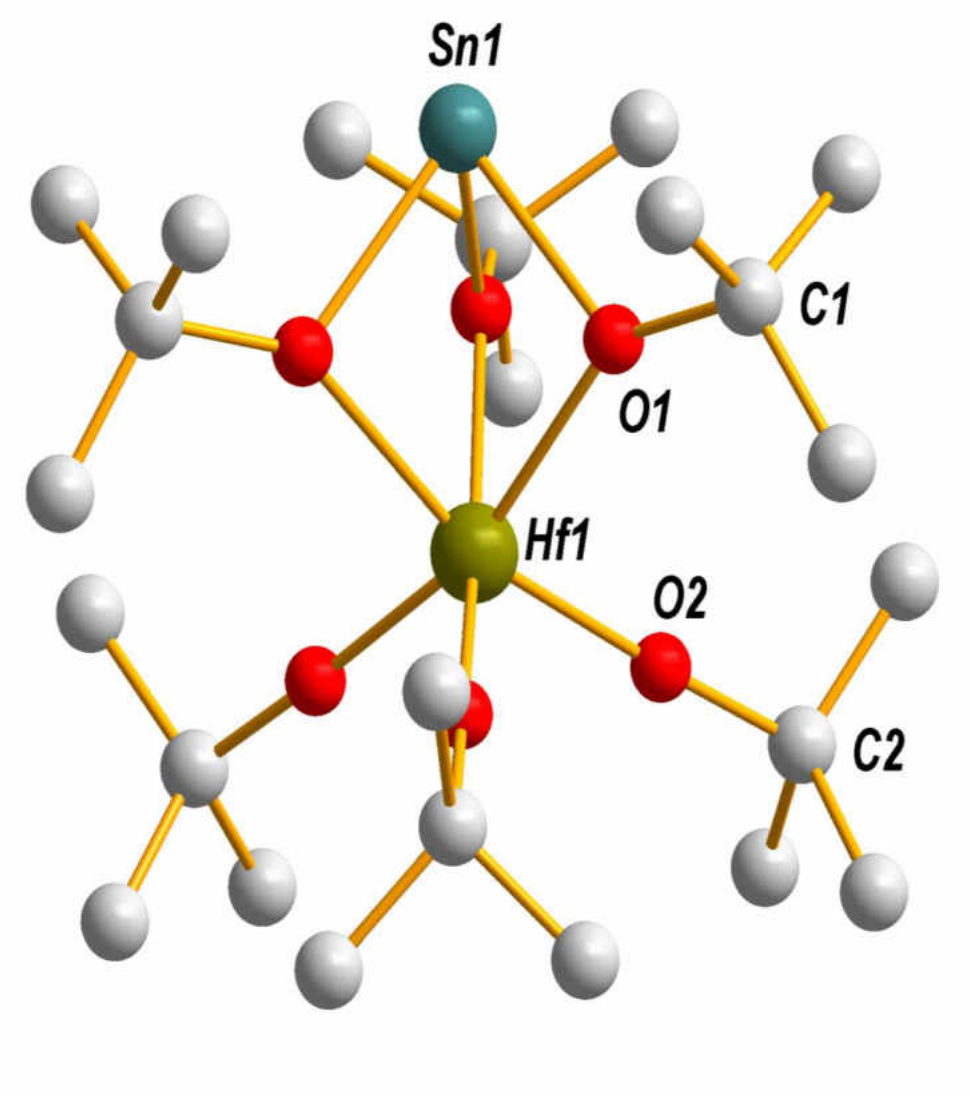

Figure 28. Ball and stick representation of **13**.

Table 16. Crystal data for compound **13**

Molecular formula	$C_{24}H_{54}HfO_6Sn$
fw	735.85 g/mol
Crystal system	trigonal
Space-group	*P*3*m*1
a, Å	17.091(10)
b,Å	17.091(10)
c,Å	9.4768(11)
α, deg	90
β, deg	90
γ, deg	120
V, Å^3	2397.3(3)
Z	3
F(000)	1104
ρ(calc), g cm^{-3}	1.529
λ, Å	0.710 73
temp, K	173
μ, mm^{-1}	4.056
$R(F)^a$	0.0694
$R_W(F^2)^b$	0.1902

[a] $R = \sum|F_o - F_c| \quad |F|_o$. [b] $R_w = \{[\quad w(F_o^2 - F_c^2)] / [\sum w(F_o^2)^2]\}^{1/2}$; $w = 1/[\sigma^2(F_o)^2 + (xP)^2 + yP]$, where $P = (F_o^2 + 2F_c^2)/3$.

Table 17. Selected bond lengths (Å) and angles (°) for **13**

Bond Lengths			
Hf1−O1	2.242(13)	Sn1−O1	2.107(14)
Hf1−O1'	2.242(13)	Sn1−O1'	2.107(14)
Hf1−O1''	2.242(13)	Sn1−O1''	2.107(14)
Hf1−O2	1.941(13)	O1−C1	1.427(17)
Hf1−O2'	1.941(13)	O2−C2	1.426(16)
Hf1−O2'	1.941(13)		
Bond Angles			
O1'−Hf1−O1	69.9(6)	O2'−Hf1−O1	159.8(7)
O1''−Hf1−O1	69.9(6)	O2''−Hf1−O1'	159.8(7)
O1'−Hf1−O1''	69.9(6)	O1'−Sn1−O1	75.1(6)
O2−Hf1−O1	93.7(5)	O1''−Sn1−O1	75.1(6)
O2−Hf1−O1'	93.7(5)	O1''−Sn1−O1'	75.1(6)
O2'−Hf1−O1'	93.7(5)	C2−O2−Hf1	172.8(16)
O2''−Hf1−O1	93.7(5)	C1−O1−Hf1	143.2(12)

17. Synthesis and Spectroscopic Analysis of *fac*-{[Ge(μ-O^{t}Bu)$_3$Zr(O^{t}Bu)$_3$]}, 14 and *fac*-{[Ge(μ-^{t}BuO)$_3$Hf(O^{t}Bu)$_3$]}, 15

In contrast to the reactions of *cis*-$MCl_4(THF)_2$, M = Zr or Hf, with one half-equivalent of sodium tri(*tert*-butoxy)stannate to furnish complexes **6** and **7**, respectively, the interaction of these Group 4 tetrachlorides with one half equivalent of sodium tri(*tert*-butoxy)germanate did not yield the germanium analogues of **6** and **7**. The difference in

reactivity is due to the lower Lewis-acidity of germanium dichloride, which apparently does not form trichlorogermanate as readily as tin did formed trichlorostannate.

Homologous products akin to **12** and **13** were isolated when *cis*-$MCl_4(THF)_2$, M = Zr or Hf, was treated with one equivalent of sodium tri(*tert*-butoxy)germanate. For zirconium and hafnium, we were able to isolate compounds **14** and **15**, respectively, as shown in Scheme 12. The compounds sublime and are soluble in hydrocarbon solvents, from which they crystallized (hexane).

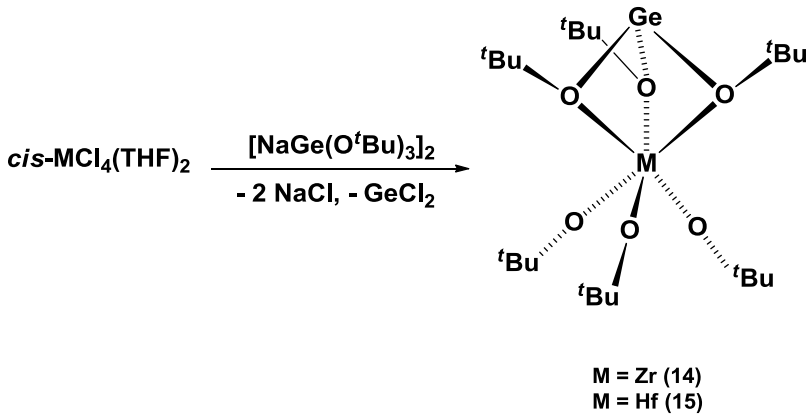

Scheme 12. Synthesis of compounds **14** and **15**.

Analysis of the compounds by ^{1}H NMR spectroscopy gave spectra similar to those of **12** and **13**. Two sharp singlet peaks, attributed to the protons of the bridging and terminal *tert*-butoxy groups, were observed in each spectrum (Figures 29 and 30). The $^{13}C\{^1H\}$ NMR spectra were in accordance with the observed structures with four peaks in addition to those of the deuterated solvents.

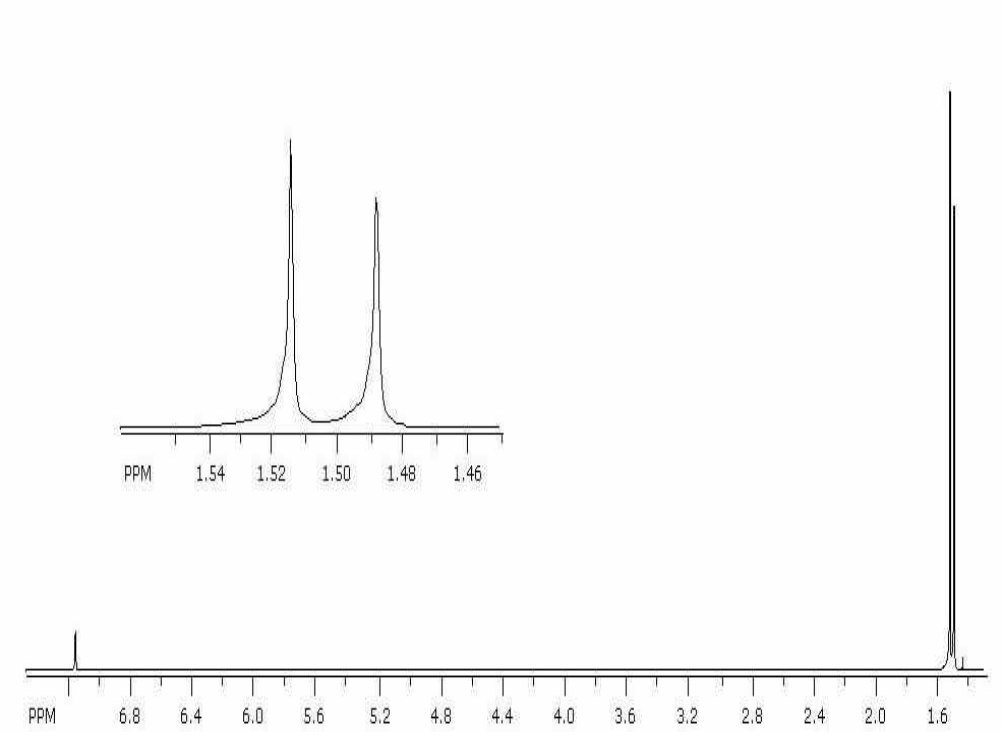

Figure 29. ^{1}H NMR spectrum of **14**. Also shown is an inset of the 1.54−1.46 ppm region.

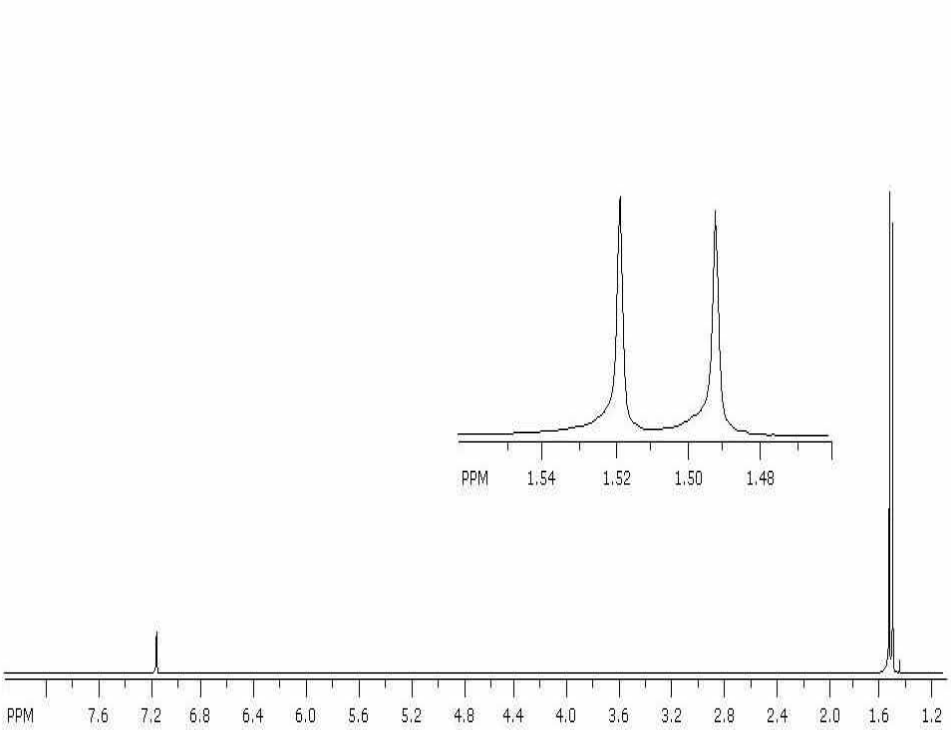

Figure 30. ^{1}H NMR spectrum of **15**. Also shown is an inset of the 1.54−1.48 ppm region.

18. Solid-state Structure of *fac*-{[Ge(μ-O^{t}Bu)$_3$Hf(O^{t}Bu)$_3$]}, 15

X-ray quality crystals of **14** and **15** were grown from hexane solutions. Although data sets were collected on both compounds, due to the disorder in the position of the germanium atom in both compounds, at present, only the structure of **15** has been solved and refined to an acceptable *R*-value.

The solid state structure of **15** is shown in Figure 31. The structure obtained for **15** is analogous to those of **12** and **13**. The only difference between **13** and **15** is the germanium that replaces tin in **15**. Similar to the previous homologues, the tri(*tert*-butoxy)germanate chelates one face of the octahedral coordinated hafnium, intrinsically causing large geometrical deviations, which results in O^{t}Bu−Ge−O^{t}Bu (77.2(3)^o) and O^{t}Bu−Hf−O^{t}Bu (68.5(3)^o) angles that are smaller than those in **13** (O^{t}Bu−Sn−O^{t}Bu = 75.1(6)^o and O^{t}Bu−Hf−O^{t}Bu = 69.9(6)^o). The bridging Hf−O^{t}Bu bonds (2.309(8) Å) are longer than those in **13** (2.242(13) Å) and the Hf(O^{t}Bu)$_3$ pyramid in both **13** and **15** are almost isometrical. The terminal Hf−O^{t}Bu bonds (1.987(11) Å) in **15** are similar to those in **13** (1.941(13) Å). The angles enclosed by these bonds in both **13** (O^{t}Bu−Hf−O^{t}Bu = 99.3(8)^o) and **15** (O^{t}Bu−Hf−O^{t}Bu = 98.8(3)^o) are also very close to each other.

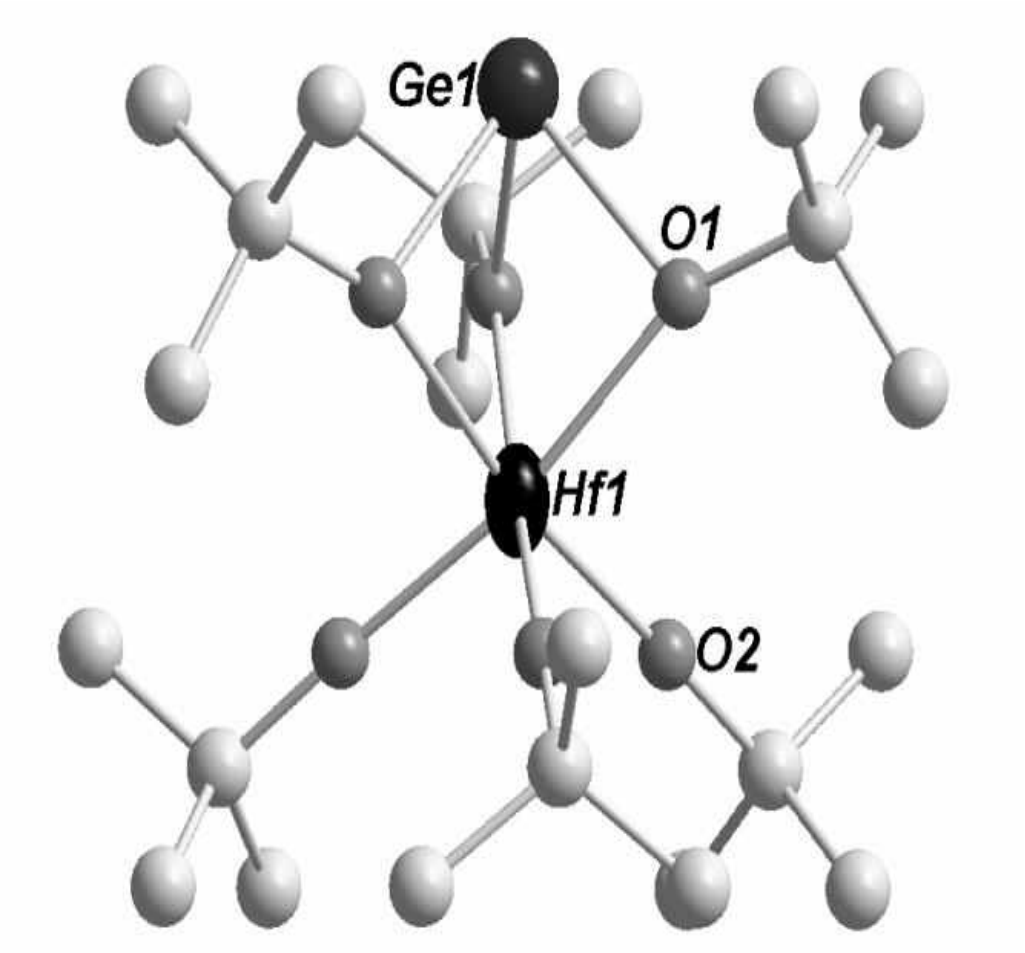

Figure 31. Ball and stick representation of **15**.

19. Synthesis and Spectroscopic Analysis of *fac*-[Pb(μ-O^{t}Bu)$_3$Zr(O^{t}Bu)$_3$], 16, and *fac*-[Pb(μ-O^{t}Bu)$_3$Hf(O^{t}Bu)$_3$], 17

To complete our studies of group 4/Group 14 *tert*-butoxides, we investigated the interaction of the group 4 metal chlorides with tri(*tert*-butoxy)plumbate, the lead analogue of the two previous ligands. Similar to germanium, but in contrast to tin, the reaction between *cis*-$MCl_4(THF)_2$ M = Zr or Hf, and one half-equivalent of tri(*tert*-butoxy)plumbate did not yield analogues of **6** and **7**. The similarity in reactivity of the plumbate ligand to the germanate ligand, but in contrasting behavior to the stannate ligand can again be explained by the lower Lewis acidity of $PbCl_2$.

Akin to germanium and tin, *cis*-$MCl_4(THF)_2$, M = Zr or Hf, reacts with one equivalent of tri(*tert*-butoxy)plumbate to furnish sublimable **16** and **17**, homologues of **12**, **13**, **14**, and **15** (Scheme 13). Compound **16** had previously been reported by Caulton and coworkers, while complex **17** is a new compound. Caulton *et al*. synthesized the compound **16** by mixing Pb(O^{t}Bu)$_2$ and Zr(O^{t}Bu)$_4$ in ether.[56]

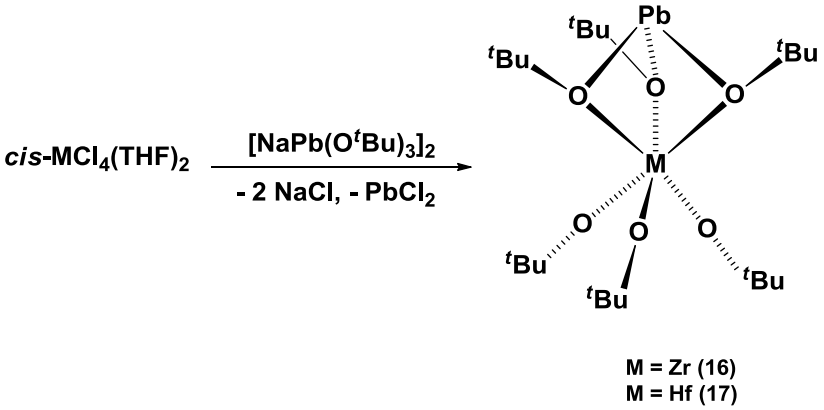

Scheme 13. Syntheses of compounds **16** and **17**.

NMR spectra obtained for the compounds were characteristic for these double alkoxide complexes with two sharp singlets in the ^{1}H NMR spectrum and four peaks in

the $^{13}C\{^{1}H\}$ NMR spectrum. Similar to that of the tin compounds, the signals for the bridging methyl carbon atoms showed coupling to lead (which has one isotope with nuclear spin ½, ^{207}Pb).

X-ray quality crystals of **16** and **17** were grown from THF solutions. Data collection was done on both crystals and they suffered the same crystallographic problems observed in the previous homologues. The crystals were merohedrally twinned and showed disorder of the group 14 element. The collected data have not yet been solved and refined.

Summary and Conclusion

The interaction of Group 14 alkoxometallates with group 4 metal tetrachlorides has been studied. The products obtained from this reactions show that these molecules are not good chelating ligands for group 4 metals, as these highly Lewis acidic metals degraded these ligands through *tert*-butoxide abstractions.

Tri(*tert*-butoxy)stannate acted as a selective alkoxylating agent, forming monomeric group 4 metal *tert*-butoxide/chloride species, a feat which is normally difficult to achieve, since alkoxide ligands have a high propensity to bridge more than one metal center. Neutral species such as $[MCl_2(O^tBu)_2(THF)_2]$ were synthesized with 1/3 equivalent of the dimeric ligand. Interaction of 1/2 equivalent of the dimeric ligand with one equivalent of the metal tetrachlorides afforded the ionic species *fac*-$\{[M(O^tBu)_3(THF)_3](SnCl_3)\}$, in which the trichlorostannate anion is weakly coordinating.

These ionic compounds are believed to have been formed by the abstraction of a chloride ion from $M(O^tBu)_3Cl$ by $SnCl_2$. Interference by the trichlorostannate unit in *fac*-$\{[Zr(O^tBu)_3(THF)_3](SnCl_3)\}$ caused us to replace it with the triflate anion, thereby yielding *fac*-$\{Zr(O^tBu)_3(THF)_2(OTf)\}$, in which the triflate was coordinated to the metal in the solid state. One unit of the ligand was ultimately transferred to the group 4 metal centers only when its Lewis acidity had been sufficiently attenuated, as in *fac*-$\{M(O^tBu)_3(THF)_3](SnCl_3)\}$, thereby yielding the neutral complexes *fac*-$[Sn(O^tBu)_3 M(O^tBu)_3]$.

In contrast, tri(*tert*-butoxy)germanate and plumbate did not form the cationic *tert*-butoxide complexes *fac*-$\{[M(O^tBu)_3(THF)_3](SnCl_3)\}$. The reason for this difference in reactivity was attributed to the lower Lewis acidity of the dichlorides of germanium and lead. Similar to the stannate ligand, the germanate and plumbate ligands did form sublimable complexes of the type *fac*-$[Sn(O^tBu)_3M(O^tBu)_3]$ (where M = Zr or Hf and E = Ge or Pb), although the yields of these reactions were somewhat lower.

CHAPTER II

INTERACTION OF η^5-$CpZrCl_3$·dme WITH GROUP 14 ALKOXOMETALATES, $[NaE(O^tBu)_3]_2$ (E = Ge, Sn or Pb)

Introduction

Metal complexes of the cyclopentadienyl ligand have been reported for basically all metals of the periodic table.[94–96] The Cp ligand's ability to act as both a donor and acceptor, combined with its pentahapto chelation of metal centers, usually produces very robust complexes. The stability imparted by the Cp ligand to its metal complexes has made these compounds indispensable in processes, such as catalysis and various organic transformations.[97–102] In main group chemistry, σ- and π-bound cyclopentadienyl ligands may act as leaving groups.[103] Therefore, Cp main group metal complexes are usually used as precursors or synthons for the syntheses of Cp metal complexes of transition, lanthanide, actinide, or other main group metals.

Mono-, bis-, tris-, and even tetrakis-(cyclopentadienyl) complexes have been reported for the group 4 metals.[104] The most popular among them are the bis(cyclopentadienyl) complexes of the group 4 metallocenes, which have been widely used as industrial catalysts for the polymerization of olefins.[105–110] The mono-Cp or half-sandwich Group 4 complexes have fewer applications compared to those of the bent metallocenes, and they are mainly used as precursors to mixed half-sandwiched

compounds.[104] Among transition metal Cp complexes, Group 4 metal Cp compounds are among the most stable, being rivaled in stability only by those of the group 8 metals.[111] The Zr–Cp bonds in zirconocenes have been found to survive acidic work up in the syntheses of chiral *ansa*-metallocenes and halide exchange in the presence of strong Lewis acids such as BBr_3.[112,113] However, like all metal-carbon bonds, group 4 metal Cp bonds are not stable to hydrolysis. Generally the Cp anion in these compounds is displaced under protic conditions, while aprotic displacements are rarely encountered.[114–117] Moreover, Cp–M bond cleavage is mainly reported for titanium, as can be observed in the comproportionation of $(\eta^5\text{-Cp})_2TiCl_2$ with $TiCl_4$ to give $(\eta^5\text{-Cp})TiCl_3$.[118]

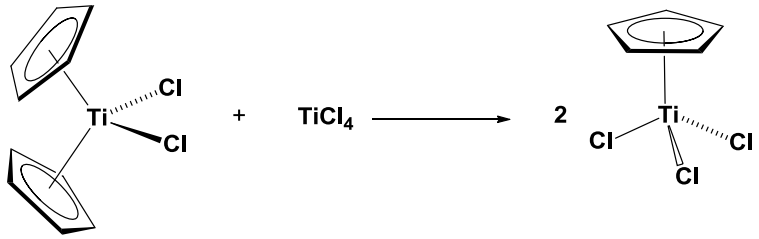

Scheme 14. Synthesis of $(\eta^5\text{-Cp})TiCl_3$

Our goal was to synthesize mixed-ligand sandwich complexes from η^5-$CpZrCl_3 \cdot dme$ and the group 14 alkoxometallates, $[NaE(O^tBu)_3]_2$ (where E = Ge, Sn or Pb). Instead of the targeted compounds, we observed displacement of the Cp ligand and substitution reactions that differed from those envisaged.

Experimental

Description of Techniques and Chemicals Used

General Procedures

All experiments were performed under an atmosphere of argon, using standard Schlenk techniques. Solvents were dried and freed of molecular oxygen by distillation under an atmosphere of nitrogen from sodium- or potassium-benzophenone ketyl immediately before use. NMR spectra were recorded on a Bruker AVANCE-500 NMR spectrometer at 25 °C. The ^{1}H, $^{13}C\{^{1}H\}$ NMR spectra are referenced relative to (i) C_6D_5H (7.16 ppm) and C_6D_6 (128.39 ppm) (ii) $O(CDHCD_2)_2$ (3.58 ppm), $O(CD_2CDH)_2$ (1.73 ppm), $O(CD_2CD_2)_2$ (67.57 ppm), and $O(CD_2CD_2)_2$ (25.37 ppm), respectively. Melting points were obtained on a Mel-Temp apparatus; they are uncorrected. Midwest Microanalytical Services, Indianapolis, Indiana and Columbia Analytical Services, Tucson, Arizona, performed the elemental analyses. The reagents $CpZrCl_3$ and NaO^tBu were purchased from Strem and Aldrich, respectively, while $CpZrCl_3 \cdot dme$,[119] and $[NaE(O^tBu)_3]_2$ (where E = Ge[53], Sn[58] or Pb[53]) were prepared according to published procedures.

Synthesis of $\{[(O^tBu)_2ClZr(\mu\text{-}ClSnCp)(\mu\text{-}O^tBu)_2ZrCl(O^tBu)_2]\cdot C_6D_6\}$, 19

A two-neck 100 mL flask was charged with $CpZrCl_3 \cdot dme$ (1.28 g, 3.62 mmol) and $[NaSn(O^tBu)_3]_2$ (1.31 g, 1.81 mmol) in a glove box. The flask was cooled to –78 °C and 40 mL of CH_2Cl_2 was then added. The resultant mixture was stirred overnight while it warmed to room temperature. The solvent was removed *in vacuo* and the product was extracted into a $CHCl_3/C_6D_6$ mixture. Concentration and crystallization at –20 °C

afforded colorless crystals, which where shown to be CpSnCl. Then, from the supernatant, large hexagonal crystals of the above product were obtained. Yield: 84 % (1.51 g, 1.53 mmol).

Mp: 102 °C. ^{1}H NMR (THF-d_8): δ 7.29 (s, C_6D_5H), 5.94 (s, 5H, Cp), 1.27 (s, 54H, OC(CH_3)$_3$). ^{13}C{^{1}H} NMR (THF-d_8): δ 128.60 (t, J = 48 Hz, C_6D_6), 111.6 (s, C_5H_5), 75.6 (s, OC(CH$_3$)$_3$), 33.2 (s, OC(CH$_3$)$_3$). Anal. Calcd for $C_{35}H_{59}D_6Cl_3O_6SnZr_2$: C, 42.23; H, 7.18. Found: C, 41.87; H, 6.47.

Synthesis of {(THF)·NaCp·NaCp·NaSn(O^{t}Bu)$_3$]$_2$·THF}, 20

To a solution of NaO^{t}Bu (1.02 g, 10.5 mmol) in 10 mL of THF was added drop-wise a solution of CpSnCl (0.77 g, 3.50 mmol) in 15 mL of THF at room temperature. The reaction mixture was stirred for 6 h, upon which it became cloudy and slightly pinkish. Filtration, concentration and storage at –4 °C afforded colorless rectangular crystals. Yield: 89 % (1.61 g, 1.56 mmol).

Mp: 228–230 °C. ^{1}H NMR (C_6D_6): δ 6.59 (s, 10H, C_5H_5), δ 3.57 (t, $^{3}J_{HH}$ = 13 Hz, 8H, OCH_2CH$_2$), δ 1.42 (t, $^{3}J_{HH}$ = 13 Hz, 8H, OCH_2CH$_2$), δ 1.32 (s, 54H, OC(CH_3)$_3$). ^{13}C{^{1}H} NMR (C_6D_6): 105.6 (s, C_5H_5), 70.4 (s, OC(CH$_3$)$_3$), 68.2 (s, OCH$_2$CH$_2$), 35.9 (s, OC(CH$_3$)$_3$), 26.2 (s, OCH$_2$$CH_2$). Anal. Calcd for $C_{41}H_{78}Na_4O_{7.75}Sn_2$: C, 48.06; H, 7.61. Found: C, 47.69; H, 7.25.

Synthesis of *fac*-[Ge(μ-O^{t}Bu)$_3$ZrCl(O^{t}Bu)$_2$], 21

A solution of [NaGe(O^{t}Bu)$_3$]$_2$ (0.62 g, 0.99 mmol) in CH_2Cl_2 (20 mL) was added drop-wise to a pre-cooled (–78 °C) solution of CpZrCl$_3$·dme (0.70 g, 1.98 mmol) in 20 mL of CH_2Cl_2. The reaction mixture was stirred at –78 °C for 2 h and at room temperature for a further 4 h. Filtration yielded a faintly-yellow solution. Concentration and storage of the

solution at –20 °C for several days afforded colorless crystals. Yield: 63 % (0.35 g, 0.62 mmol).

Mp: 212–214 °C. ^{1}H NMR (THF-d_8): δ 1.50 (s, 18H, μ-OC(CH_3)$_3$), 1.48 (s, 9H, μ-OC(CH_3)$_3$), 1.39 (s, 18H, OC(CH_3)$_3$). ^{13}C{^{1}H} NMR (THF-d_8): δ 79.1 (s, μ-O*C*(CH$_3$)$_3$), 77.4 (s, μ-O*C*(CH$_3$)$_3$), 77.0 (s, OC(*C*H$_3$)$_3$), 33.0 (s, μ-O*C*(CH$_3$)$_3$), 32.9 (s, μ-O*C*(CH$_3$)$_3$), 32.7 (s, OC(*C*H$_3$)$_3$). Anal. Calcd for $C_{20}H_{45}ClGeO_5Zr$: C, 42.53; H, 8.03. Found: C, 42.23; H, 7.89.

Synthesis of CpZr(O^{t}Bu)$_3$, 22

$CpZrCl_3$·dme (1.00 g, 2.83 mmol) and [NaPb(O^{t}Bu)$_3$]$_2$ (1.27 g, 1.42 mmol) were combined in 25 mL of CH_2Cl_2 in a two-neck 100 mL flask. The resultant mixture was stirred at –78 °C for 2 h and then allowed to warm to room temperature where it was stirred for 4 h. The beige colored precipitate (a mixture of $PbCl_2$ and NaCl) was removed by filtration over a celite pad on a medium porosity frit to give a light-yellow solution. Removal of the solvent *in vacuo* gave a yellowish, oily residue, which turned red when exposed to air. Distillation (80–83 °C, 0.75 mmHg) of this residue gave a colorless liquid that solidified upon storage at –4 °C. Yield: 80 % (0.85 g, 2.26 mmol).

Mp: 32 °C. ^{1}H NMR (C_6D_6): δ 6.34 (s, 5H, C_5H_5), 1.24 (s, 27H, OC(CH_3)$_3$). ^{13}C{^{1}H} NMR (C_6D_6): δ 111.3 (*s, C*$_5$H$_5$), 75.8 (s, O*C*(CH$_3$)$_3$), 33.1 (s, O*C*(CH$_3$)$_3$).

Results and Discussion

1. Synthesis and Spectroscopic Analysis of {[Zr(O^{t}Bu)$_3$Cl]$_2$.CpSnCl}, 19

The syntheses of the mixed ligand half-sandwich compound **23** was attempted by mixing equimolar amounts of $CpZrCl_3 \cdot dme$ and $[NaSn(O^tBu)_3]_2$ (Scheme 15). By having an alkoxide and a Cp ligand (both of which are good σ/π donors), the aim was to create a metal center with good olefin polymerization properties. Interestingly, instead of compound **23**, complex **19** was obtained as the major product of the reaction. An initial crop of crystals obtained was exclusively composed of CpSnCl and this was confirmed by NMR spectroscopy and X-crystallography. From the supernatant, we obtained compound **19**, whose structure and composition was also confirmed by X-ray crystallography. We observed that the Cp ligand had been transferred from the zirconium to tin. The transfer of the Cp ligand from zirconium to tin is very unusual because the opposite reaction usually occurs. As stated above, the non-protic displacement of the Cp ligand is uncommon for group 4 metal Cp compounds and in cases where it has been observed, titanium Cp compounds were involved. The Cp–Ti bond-dissociation energies are ~ 30 kcal/mol lower than those of the heavier group members, Zr and Hf. [120−123]

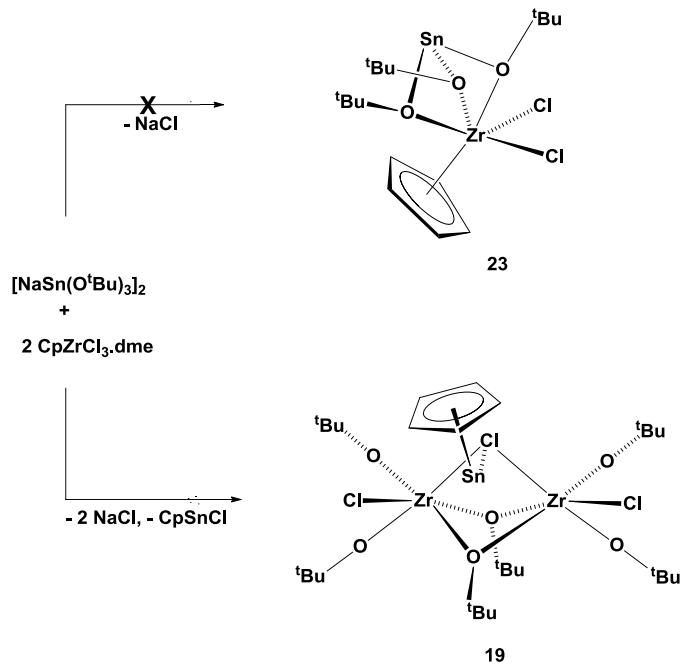

Scheme 15. Synthesis of compound **19**.

The non-protic loss of the Cp ligand from transition metals has been observed before, but it has been mostly reported for late transition metal complexes with labilized Cp rings like Cp_2Co and Cp_2Ni.[124] Cp ligand loss has also been observed in the conversion of the rhenium complex [η^5-CpRe(NO)(CH_3)PMe_3] to {[CpRe(NO)(CH_3)(PMe_3)$_4$]$^+$Cp$^-$}, but the Cp expulsion was only achieved under forceful conditions using high concentrations of PMe_3 (about 50% by volume) and heating at 50 ^oC for 17 days.[125] The formation of the trinuclear compound **19** can be explained using the hard-soft acid/base (HSAB) concept, with the hard alkoxides preferring the harder zirconium over the softer tin and the softer Cp ligand favoring the softer tin.[111]

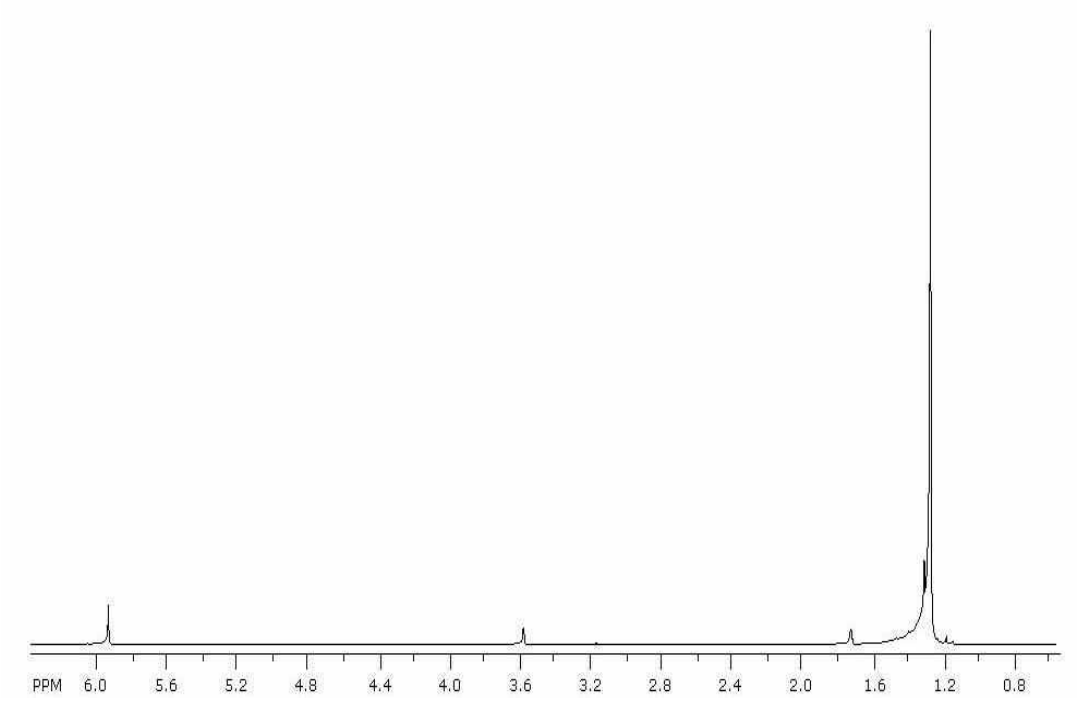

Figure 32. ^{1}H NMR spectrum of **19**.

The ^{1}H NMR spectrum of **19** in THF-d_8 revealed the presence of two peaks in a 5:54 ratio in addition to the solvent signals (Figure 32). The peak at 5.94 ppm was assigned to the Cp protons while that at 1.27 was attributed to the methyl protons of the *tert*-butoxy group. The ^{13}C NMR spectrum showed peaks at 111.6, 75.6 and 33.2 ppm, consistent with a compound having equivalent Cp and *tert*-butoxy protons, respectively (Figure 33). However, the evidence from NMR spectroscopy did not match the structure of the compound obtained by X-ray crystallography. This suggests that the solution structure is different from the solid-state structure, and that the compound dissociates in solution to give two species: either $CpSn^{+}$ and $[Zr_2(O^tBu)_6Cl_3]^{-}$ or CpSnCl and $[Zr_2(O^tBu)_6Cl_2]$.

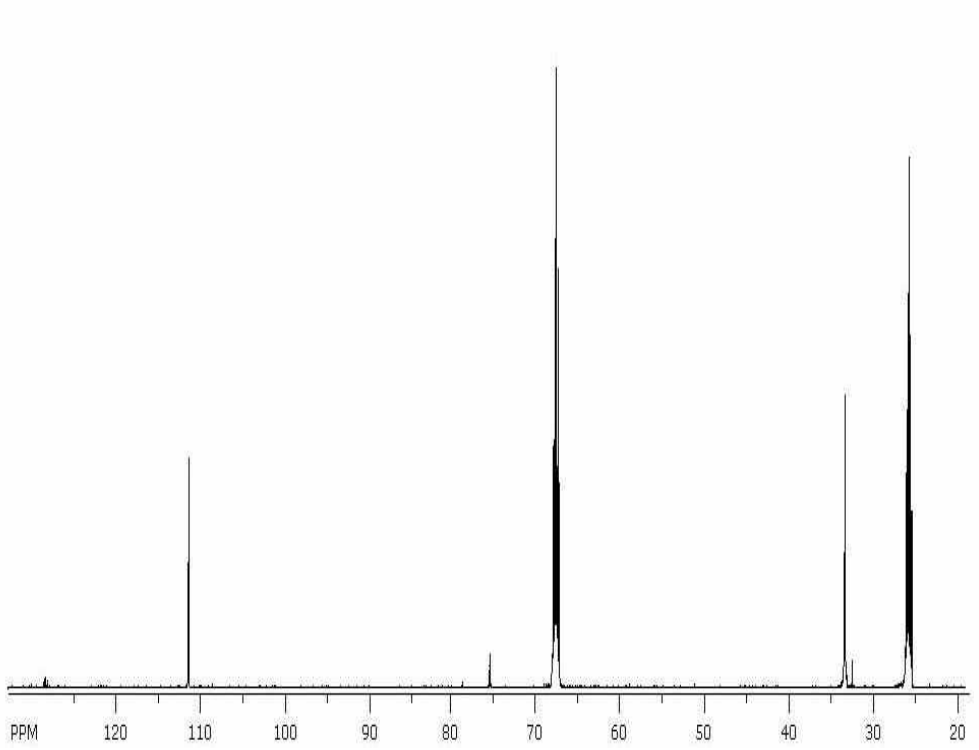

Figure 33. $^{13}C\{^{1}H\}$ NMR spectrum of **19**.

2. Solid-state Structure of {[Zr(O^{t}Bu)$_3$Cl]$_2$.CpSnCl}, 19

X-ray quality crystals of **19** were grown from a chloroform/deuterated benzene solvent mixture. The compound crystallized in the orthorhombic crystal system with space group *Pnma* and four molecules in the unit cell. Because the space group has eight general positions, it was evident that the molecule had crystallographic symmetry. Only a two-fold rotation axis and a mirror plane are possible for this space group, and as it turned out, the molecule has crystallographic symmetry *m*. Additional crystallographic data are given in Tables 18 and 19.

The structure of compound **19** is shown in Figure 34. The compound is composed of two zirconium ions and one tin ion, which are all connected by bridging alkoxides and a chloride. The compound can best be considered as consisting of $CpSn^{+}$ and

$[Zr_2(O^tBu)_6Cl_3]^-$. This formulation is based on the elongation of the Sn−Cl2 bond [2.8549(7) Å], which is longer than that in CpSnCl {where Sn−Cl = 2.679(5) Å} and the prevalence of the face-sharing bioctahedron, $Zr_2X_9^-$, in zirconium alkoxide chemistry. A structurally similar compound had previously been obtained from an equimolar mixture of CpSnCl and $KZr_2(O^iPr)_9$, or alternatively, from one-half equivalent of $\{ClSn[Zr_2(O^iPr)_9]\}_2$ and NaCp, but poor crystal quality resulted in a low-quality X-ray analysis with concomitant low precision bond parameters.[126]

In compound **19**, each zirconium atom is surrounded by two bridging and two terminal *tert*-butoxides and one terminal and one bridging chloride. The geometry about zirconium is that of a distorted octahedron. The terminal alkoxide bonds (1.9108(13) Å and 1.9053(13) Å) are much shorter than the bridging alkoxide bonds (2.2410(11) Å and 2.1642(11) Å). These bonds are comparable to the terminal (average Zr−O^{t}Bu = 1.972(2) Å) and bridging *tert*-butoxide units (average Zr−O^{t}Bu = 2.148(2) Å) in the dinuclear zirconium *tert*-butoxide, $[(O^tBu)_3Zr(\mu\text{-}O^tBu)_2(\mu\text{-}NCCH_3)Zr(O^tBu)_3]$.[127]

The Cp−Sn interactions are unsymmetrical; hence there are three sets of Sn−C bonds (2.462(3), 2.599(3), and 2.681(3) Å). The C–C distances of the Cp ring range from 1.342(6) to 1.395(6) Å and are indicative of delocalized π-bonds. This gives the CpSn moiety a much more regular appearance than that in the disordered Cp unit of CpSnCl.[86]

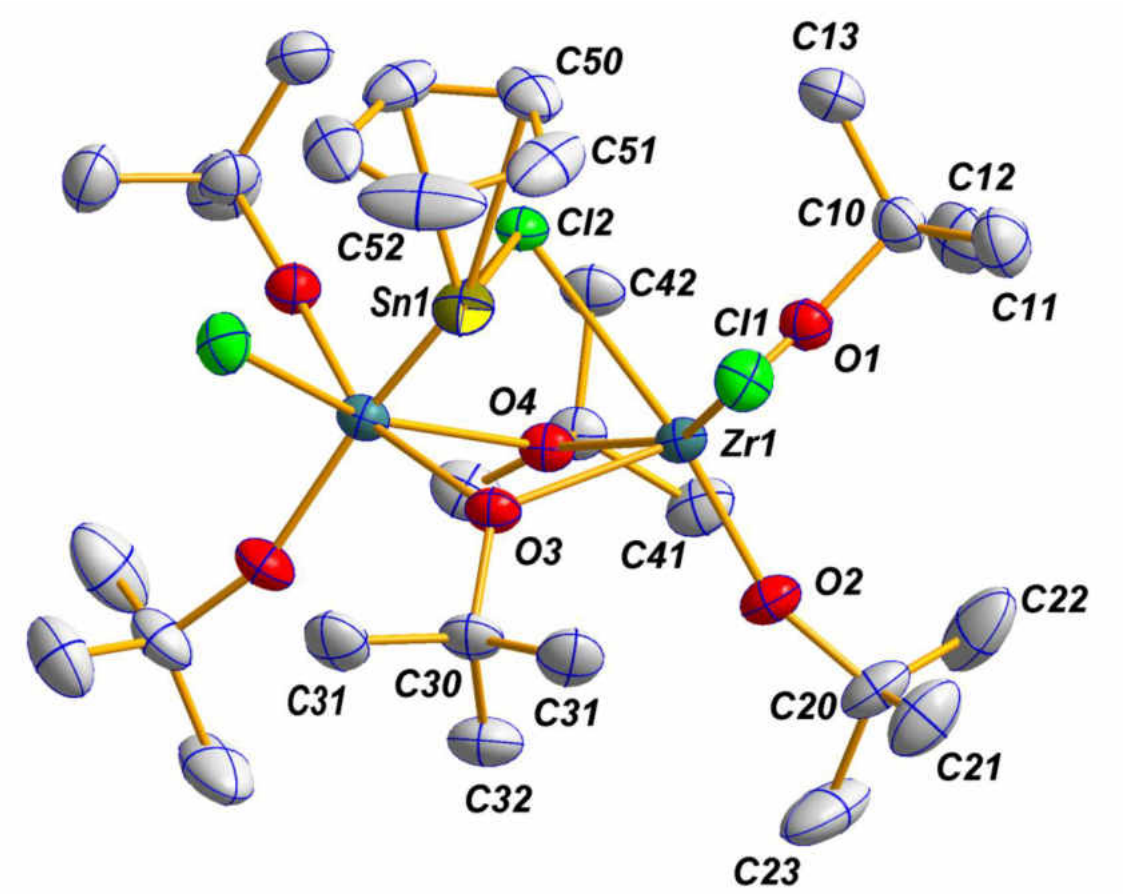

Figure 34. Solid-state structure and labeling scheme of **19**. With the exception of carbon (35%) all atoms are drawn at the 50% probability level.

Table 18. Crystal data for compound **19**

Molecular formula	$C_{35}H_{65}Cl_3O_6SnZr_2$
fw	989.35
Crystal system	orthorhombic
Space-group	*Pnma*(No. 62)
a, Å	20.1266(19)
b,Å	18.1626(17)
c,Å	12.1624(11)
α, deg	90
β, deg	90
γ, deg	90
V, Å^3	4446.0(7)
Z	4
F(000)	2016
ρ(calc), g cm^{-3}	1.478
λ, Å	0.710 73
temp, K	173
μ, mm^{-1}	1.235
$R(F)^a$	0.0285
$R_W(F^2)^b$	0.0783

[a] $R = \sum||F_o| - |F_c|| \; / \sum|F|_o$. [b] $R_w = \{[\sum w(F_o^2 - F_c^2)] / [\sum w(F_o^2)^2]\}^{1/2}$; $w = 1/[\sigma^2(F_o)^2 + (xP)^2 + yP]$, where $P = (F_o^2 + 2F_c^2)/3$.

Table 19. Selected bond lengths (Å) and angles (°) for **19**

Bond Lengths			
Zr1−O1	1.9108(13)	Sn1−Cl2	2.8549(7)
Zr1−O2	1.9053(13)	Sn1−C50	2.463(3)
Zr1−O3	2.2410(11)	Sn1−C51	2.601(3)
Zr1−O4	2.1642(11)	Sn1−C52	2.681(3)
Zr1−Cl1	2.5351(5)	C50−C51	1.331(6)
Zr1−Cl2	2.7691(5)	C51−C52	1.415(6)
Bond Angles			
O2−Zr1−O1	100.89(6)	O4−Zr1−Cl1	152.79(4)
O1−Zr1−O3	159.40(6)	O1−Zr1−Cl2	87.51(4)
O1−Zr1−O4	99.59(6)	O2−Zr1−Cl2	171.59(5)
O2−Zr1−O3	99.56(6)	O3−Zr1−Cl2	72.06(4)
O2−Zr1−O4	103.61(6)	O4−Zr1−Cl2	75.06(4)
O4−Zr1−O3	73.02(5)	C10−O1−Zr1	163.30(12)
Cl1−Zr1−Cl2	80.810(18)	C20−O2−Zr1	159.91(14)
O1−Zr1−Cl1	91.64(4)	C30−O3−Zr1	125.38(7)
O2−Zr1−Cl1	98.42(5)	C40−O4−Zr1	127.30(4)
O3−Zr1−Cl1	87.83(4)		

3. Synthesis and Spectroscopic Analysis of {(THF)·NaCp·NaCp·NaSn(O^{t}Bu)$_3$]$_2$ · THF}, 20

Treatment of the CpSnCl isolated from the formation of the trinuclear compound **19**, with NaO^{t}Bu did not lead to a straightforward substitution to give CpSnO^{t}Bu. ^{1}H NMR spectrum of the crude reaction mixture revealed a broad peak for the Cp ion, a strong sharp singlet peak for the *tert*-butoxy ligand, and two peaks for coordinated THF molecules (Figure 35). The composition of the compound was only determined from its structure obtained by X-ray crystallography. It was seen that the compound was an adduct of NaCp and NaSn(O^{t}Bu)$_3$. Based on its composition, we were also able to synthesize the compound by combining equimolar amounts of NaCp and NaSn(O^{t}Bu)$_3$ in THF (Scheme 16).

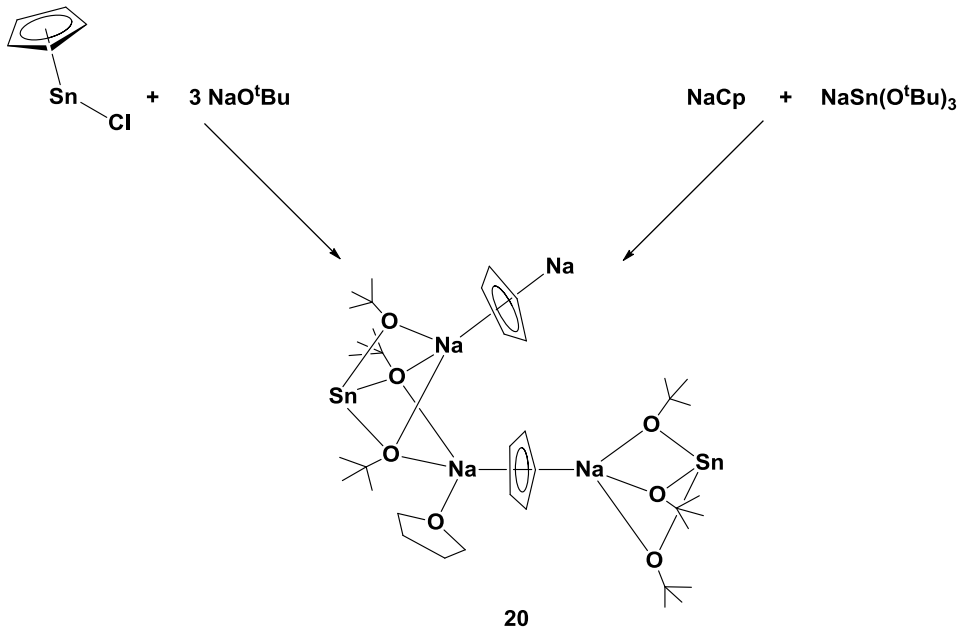

Scheme 16. Synthesis of compound **20**.

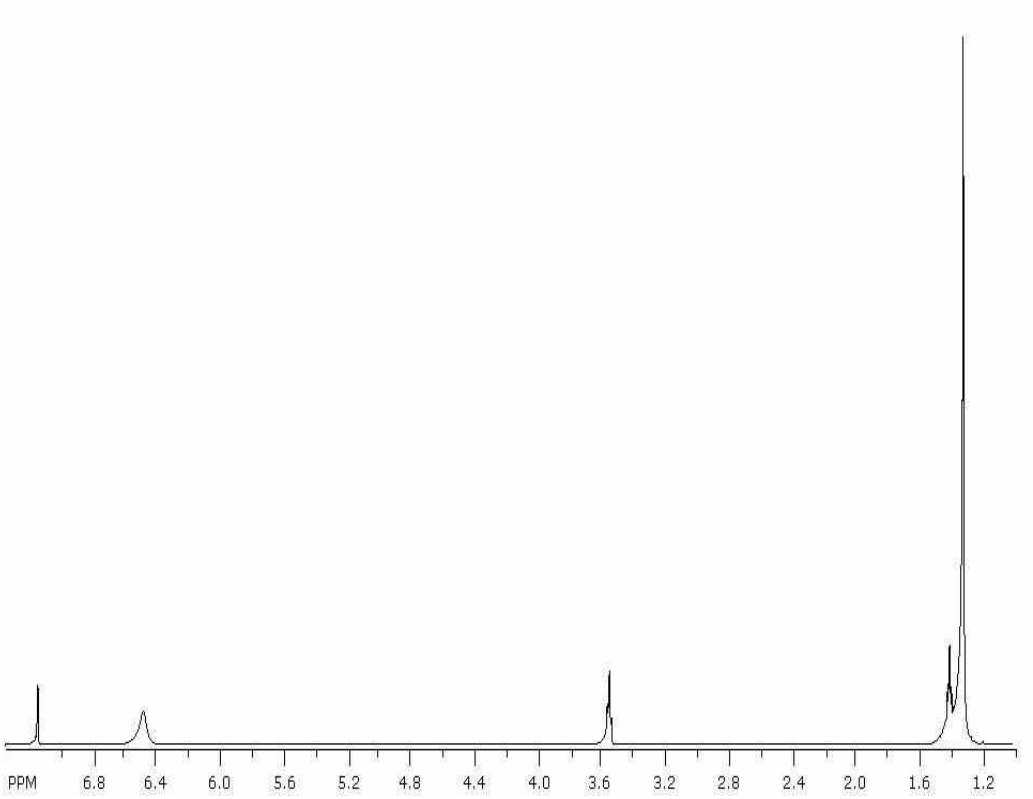

Figure 35. ^{1}H NMR spectrum of **20**.

4. Solid-state Structure of {(THF)·NaCp·NaCp·NaSn(O^{t}Bu)$_3$]$_2$·THF}, 20

Compound **20** crystallized in the triclinic crystal system, space group *P*-1, with two molecules in the unit cell. Additional crystallographic data are given in Tables 20 and 21.

As can be seen from Figure 36, compound **20** is a coordination polymer made up of repeating NaCp, NaSn(O^{t}Bu)$_3$, THF·NaCp, and NaSn(O^{t}Bu)$_3$ units. These four repeating units together with one THF molecule make up the asymmetric unit in this polymer. The repeating unit is made up four different crystallographic sodium ions and the structure was disordered due to the unusual composition of the asymmetric unit. The repeating units are arranged in a zigzag fashion in the polymer backbone, but are linear

through the Na−Cp−Na section. The repeating units are arranged such that the Cp rings are sandwiched between two sodium ions and they chelate them in a pentahapto fashion.

The four crystallographically different Na−Cp interactions are symmetrical, with equidistant Na−C bonds. These Na−C bonds [average = 2.708(10) Å] are slightly longer than those in NaCp [average = 2.649(9) Å], but shorter than those in CpNa(TMEDA) [average = 2.925(11) Å]. [128,129]

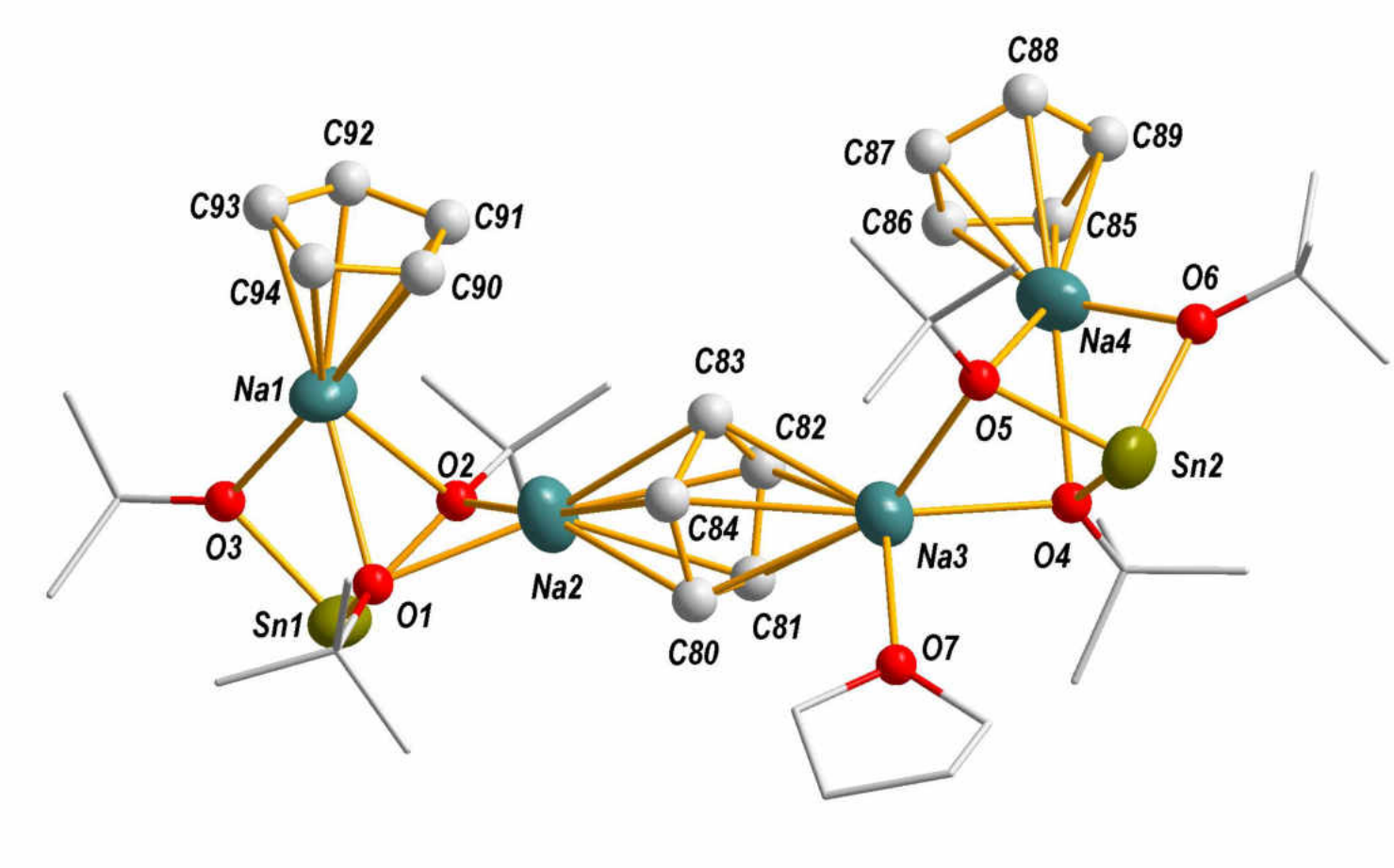

Figure 36. Solid-state structure and labeling scheme of **20**. With the exception of carbon (35%) all atoms are drawn at the 50% probability level.

Table 20. Crystal data for compound **20**

Molecular formula	$C_{42}H_{62}Na_4O_8Sn_2$
fw	1024.26
Crystal system	triclinic
Space-group	P -1 (2)
a, Å	13.968(2)
b, Å	14.558(2)
c, Å	16.226(2)
α, deg	102.481(2)
β, deg	105.016(2)
γ, deg	114.745(2)
V, Å^3	2688.8(7)
Z	2
F(000)	1044
ρ(calc), g cm^{-3}	1.265
λ, Å	0.710 73
temp, K	173
μ, mm^{-1}	1.002
$R(F)^a$	0.0542
$R_W(F^2)^b$	0.1636

[a] $R = \sum|F_o - F_c| \quad |F|_o$. [b] $R_w = \{[\quad w(F_o^2 - F_c^2)] / [\sum w(F_o^2)^2]\}^{1/2}$; $w = 1/[\sigma^2(F_o)^2 + (xP)^2 + yP]$, where $P = (F_o^2 + 2F_c^2)/3$.

Table 21. Selected bond lengths (Å) and angles (°) for **20**

Bond Lengths			
Na1−O1	2.514(4)	Na2−C(80−84)	2.710(9)
Na1−O2	2.568(4)	Na3−C(80−84)	2.727(10)
Na1−O3	2.206(4)	Na4−C(85−89)	2.714(13)
Na2−O1	2.333(4)	Sn1−O1	2.085(3)
Na2−O2	2.309(4)	Sn1−O2	2.084(3)
Na3−O4	2.370(4)	Sn1−O3	2.055(3)
Na3−O5	2.390(3)	Sn2−O4	2.077(3)
Na3−O7	2.446(7)	Sn2−O5	2.089(3)
Na1−C(90−94)	2.682(10)	Sn2−O6	2.044(6)
Bond Angles			
O2−Sn1−O1	76.66(12)	O3−Na1−O2	73.60(13)
O3−Sn1−O1	87.70(13)	O2−Na2−O1	67.69(12)
O3−Sn1−O2	87.95(13)	O4−Na3−O5	65.86(11)
O4−Sn2−O5	76.80(12)	O5−Na4−O4	62.86(11)
O6−Sn2−O4	88.52(18)	O6−Na4−O4	74.68(18)
O6−Sn2−O5	88.54(17)	O6−Na4−O5	76.87(17)
O1−Na1−O2	61.17(11)	O3−Na1−O1	74.54(12)

5. Synthesis and Spectroscopic Analysis of fac-[Ge(μ-O^{t}Bu)$_3$ZrCl(O^{t}Bu)$_2$], 21

Treatment of $CpZrCl_3$·dme with $[NaGe(O^tBu)_3]_2$, akin to the stannate reaction resulted in the displacement of the Cp ligand from zirconium, albeit with the formation of different products (Scheme 17). The ^{1}H NMR spectrum of the crude reaction mixture revealed a change in the chemical shift of the Cp proton, indicative of a change in the coordination environment of the Cp ligand. The new Cp compound observed was later confirmed to be Cp_2Ge, based on its ^{1}H and ^{13}C NMR spectroscopic data and the physical characteristics of this compound, all of which have been reported in the literature.[130]

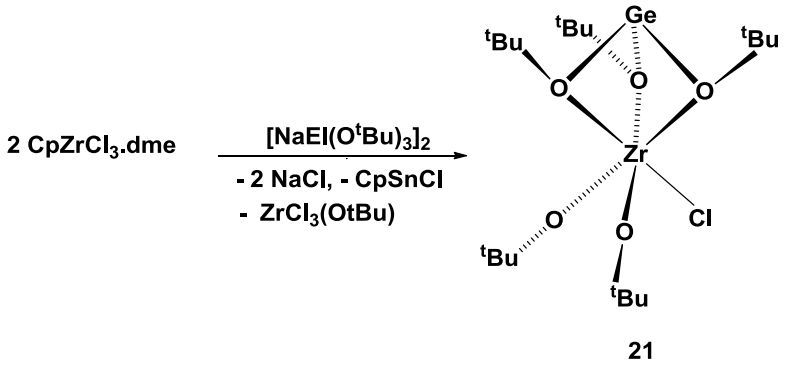

Scheme 17. Synthesis of compound **21**.

Compound **21** was the only product that was crystallized from the reaction mixture. Its structure was confirmed by X-ray crystallography. The ^{1}H NMR spectrum of the compound showed three sets of *tert*-butoxy protons in a 2:2:1 ratio, in accordance with the solid state structure. The terminal *tert*-butoxy protons were equivalent and their signals appeared at 1.39 ppm, while two of the bridging *tert*-butoxy groups were equivalent and the other different, and they were observed at 1.50 and 1.48 ppm, respectively.

6. Solid-state Structure of fac-[Ge(μ-O^{t}Bu)$_3$ZrCl(O^{t}Bu)$_2$], 21

Compound **21** crystallized in the monoclinic crystal system with space group $P2_1/n$ and four molecules in the unit cell. Additional crystallographic data for the compound are listed in Tables 22 and 23.

The structure of **21** is shown in Figure 37. The structure is similar to those of compounds **12**, **13**, and **15**, except for a chloride which replaced a terminal *tert*-butoxide. The presence of the chloride reduced the symmetry of this complex and unlike its counterparts which crystallized in the trigonal crystal system, **21** crystallized in the monoclinic crystal system. Similar to the previous complexes, compound **21** was highly disordered with the geometry around zirconium being that of a distorted octahedron, with the angles between the terminal *tert*-butoxide and bridging *tert*-butoxide all deviating from the expected 90 and 180°.

The terminal Zr−O^{t}Bu bonds (1.918(4) Å and 2.030(4) Å) are crystallographically inequivalent and they are similar to those observed in the previous compounds. The bridging Zr−O^{t}Bu bonds (92.113(4) Å, 2.143(6) Å, and 2.258(3) Å) are as expected, much longer than the terminal bonds. The Ge−O^{t}Bu bonds are also non-equivalent and range from 1.940(6) to 2.010(4) Å. The large variations observed in these bonds, which otherwise should not differ very much from each other, could be attributed to the disorder in the structure of the compound. The Zr−Cl bond is comparable to similar bonds in other compounds.[119,131]

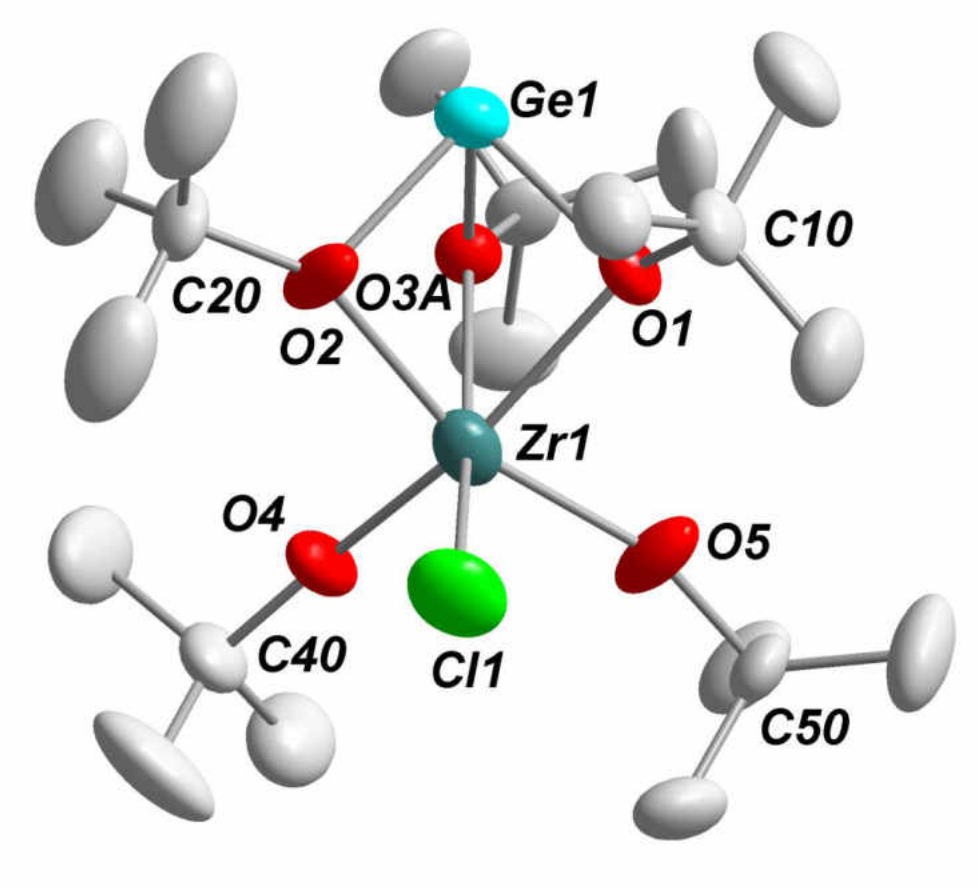

Figure 37. Solid-state structure and labeling scheme of **21**. With the exception of carbon (35%) all atoms are drawn at the 50% probability level.

Table 22. Crystal data for compound **21**

Molecular formula	$C_{20}H_{45}ClGeO_5Zr$
fw	564.82
Crystal system	monoclinic
Space-group	$P2_1/n$ (14)
a, Å	11.832(17)
b,Å	16.075(2)
c,Å	14.900 (2)
α, deg	90
β, deg	93.065(2)
γ, deg	90
V, Å^3	2829.8(7)
Z	4
F(000)	1176
ρ(calc), g cm^{-3}	1.326
λ, Å	0.710 73
temp, K	173
μ, mm^{-1}	1.548
$R(F)$[a]	0.0638
$R_W(F^2)$[b]	0.1937

[a] $R = \sum|F_o - F_c| \quad |F|_o$. [b] $R_w = \{[\quad w(F_o^2 - F_c^2)] / [\sum w(F_o^2)^2]\}^{1/2}$; $w = 1/[\sigma^2(F_o)^2 + (xP)^2 + yP]$, where $P = (F_o^2 + 2F_c^2)/3$.

Table 23. Selected bond lengths (Å) and angles (°) for **21**

Bond Lengths			
Zr1−O1	2.258(3)	Ge1−O2	1.994(4)
Zr1−O2	2.113(4)	Ge1−O3A	1.940(6)
Zr1−O3A	2.143(6)	O1−C10	1.429(6)
Zr1−O4	1.918(4)	O2−C20	1.397(6)
Zr1−O5	2.030(4)	O3A−C30	1.497(7)
Zr1−Cl1	2.4521(13)	O4−C40	1.398(6)
Ge1−O1	2.010(4)	O5−C50	1.398(6)
Bond Angles			
O1−Zr1−O2	77.05(17)	O2−Zr1−Cl1	92.62(13)
O1−Zr1−O3	70.4(18)	O3−Zr1−Cl1	158.9(17)
O1−Zr1−O4	166.53(15)	O4−Zr1−Cl1	98.22(13)
O1−Zr1−O5	84.85(19)	O2−Ge1−O1	85.78(16)
O2−Zr1−O3	69.9(2)	O3A−Ge1−O1	80.0(2)
O2−Zr1−O4	98.7(2)	O3A−Ge1−O2	76.6(2)
O2−Zr1−O5	161.2(2)	C40−O4−Zr1	174.0(4)
O3−Zr1−O4	96.2(21)	C50−O5−Zr1	162.3(4)
O3−Zr1−O5	99.4(21)	Ge1−O1−Zr1	85.28(12)
O4−Zr1−O5	97.8(2)	Ge1−O2−Zr1	89.70(15)
O1−Zr1−Cl1	94.75(10)	Ge1−O3−Zr1	90.3(28)

7. Synthesis and Spectroscopic Analysis of $CpZr(O^tBu)_3$, 22

The reaction between $CpZrCl_3 \cdot dme$ and $[NaPb(O^tBu)_3]_2$ in methylene chloride at ambient temperature, unlike those of the stannate and germanate, did not lead to the displacement of the Cp ligand from zirconium. Instead, a simple substitution of chloride and alkoxide ligands was observed with the precipitation of a beige solid, which was later shown to be a mixture of NaCl and $PbCl_2$ (Scheme 18).

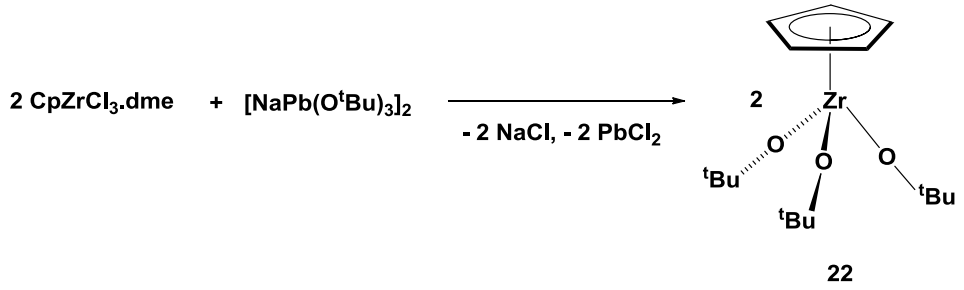

Scheme 18. Synthesis of compound **22**.

The synthesis of **22**, the product of the above reaction, had previously been reported, but the compound was obtained from the comproportionation of Cp_2Mg and $Zr(O^tBu)_4$ in benzene.[97] Although its synthesis had been reported, the state of matter or its mode of isolation was never reported. Compound **22** was obtained as a colorless oil, which was isolated by distillation at 80−83 °C and 0.75 mmHg. The oil hardened when stored at –4 °C and melted at 32 °C. Characterization of **22** by ^1H NMR spectroscopy in benzene revealed the presence of two peaks at 6.34 and 1.24 ppm in a 5:27 ratio, respectively (Figure 38). The peak at 6.34 ppm was assigned to the Cp protons and that at 1.24 ppm was attributed to the protons of the *tert*-butoxy group. The $^{13}C\{^1H\}$ NMR spectrum showed three peaks, with one singlet at 111.3 ppm for the Cp carbons and two

signals at 75.8 and 33.1 ppm for the quaternary and primary carbons of the *tert*-butoxy groups, respectively.

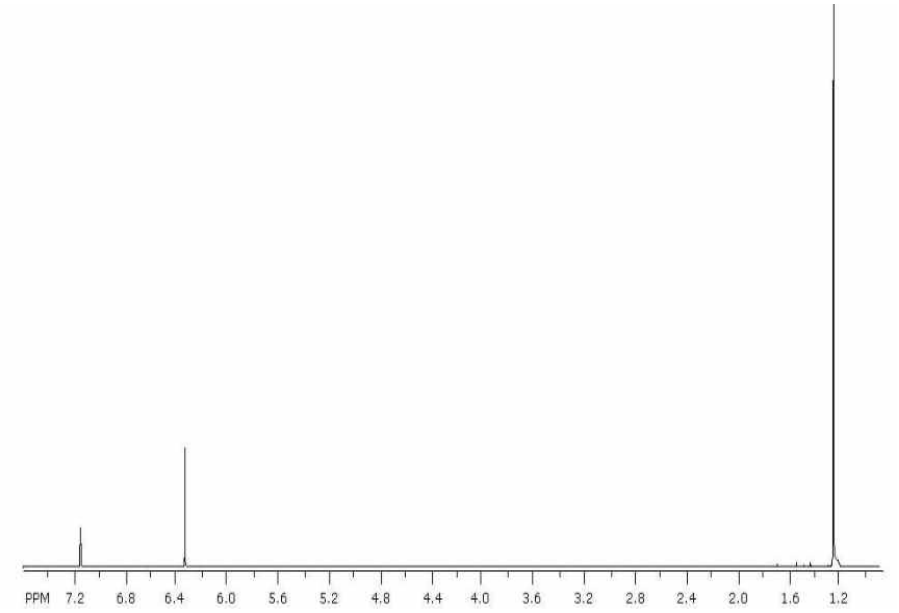

Figure 38. ^{1}H NMR spectrum of **22**.

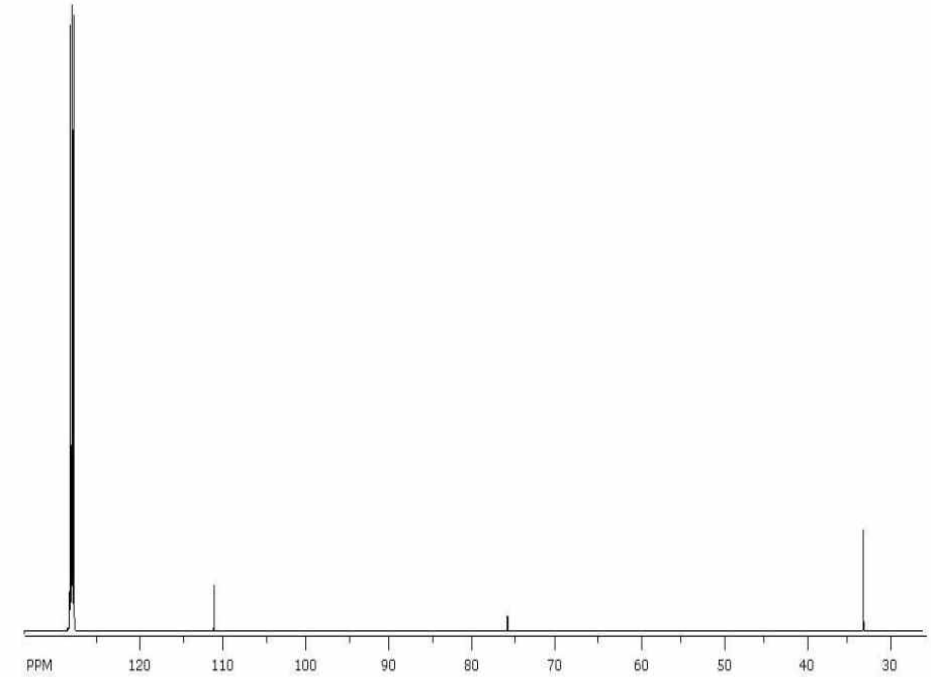

Figure 39. $^{13}C\{^{1}H\}$ NMR spectrum of **22**.

Summary and Conclusion

The interaction of $CpZrCl_3$·dme with group 14 alkoxometallates at ambient temperatures was investigated. The reactions, which all differed in their outcomes, were not those expected.

The reaction of $CpZrCl_3$·dme with sodium tri(*tert*-butoxy)stannate led to the isolation of the trinuclear complex $\{[Zr(O^tBu)_3Cl]_2 \cdot CpSnCl\}$ **19** instead of the expected simple substitution product $CpZrCl_2(O^tBu)_3Sn$ **23**. There was transfer of the Cp ligand from zirconium to tin, leading to the isolation of compound **19** and CpSnCl. This was rather suprising, since one would expect the Cp ligand, which is a good σ- and π-donor, to preferably form a compound with the electron deficient and more electropositive zirconium rather than tin. The CpSnCl isolated reacted with sodium *tert*-butoxide to give $NaSn(O^tBu)$ and NaCp, which co-crystallized as the coordination polymer, $\{(THF) \cdot NaCp \cdot NaCp \cdot NaSn(O^tBu)_3]_2 \cdot THF\}$ **20**. Sodium tri(*tert*-butoxy)germanate reacted analogously to the stannate, with the displacement of the Cp ligand from zirconium, but gave different products, *fac*-$[Ge(\mu\text{-}O^tBu)_3ZrCl(O^tBu)_2]$ **21**, Cp_2Ge and $ZrCl_3(O^tBu)$. Only the interaction with sodium tri(*tert*-butoxy)plumbate failed to dislodge the cyclopentadienyl ligand from zirconium, leading to a novel and almost quantitative synthesis of $CpZr(O^tBu)_3$ **22**. The reactions of the stannate and germanate show that $CpZrCl_3$ is not as inert as its extensive use as a catalyst and source material would suggest.

Since transition metal cyclopentadienide complexes are widely used in catalysis, where such facile, room-temperature degradations reported herein are clearly detrimental, a better understanding of these displacements is therefore highly desirable. The scope of

these reactions with early transition metal complexes, both with and without cyclopentadienide ligands is being explored.

CHAPTER III

CATALYTIC SYNTHESIS OF *TERT*-BUTOXIDES OF GROUP 4 (Ti, Zr and Hf) AND GROUP 5 (Nb) METALS USING TRI(*TERT*-BUTOXY)STANNATE

Introduction

Homometallic alkoxides of Group 4 and 5 metals have generally been synthesized using some of the methods described at the beginning of this dissertation: anodic oxidation of the respective metals in alcohol, alcoholysis of the amide, metathesis with alkali-metal alkoxides or a base (ammonia or pyridine), alcohol interchange and transesterification of metal alkoxides. These methods work best for the preparation of alkoxides of lower aliphatic alcohols. The preparations of tetra- and penta-*tert*-butoxides do not work as well due to the steric bulk of the *tert*-butyl group. There are not many suitable methods available for the synthesis of tetra- and penta-substituted *tert*-butoxides of group 4 and 5 metals. The above methods and their limitations are discussed below.

The anodic dissolution of metals in alcohol route has been employed for the commercial synthesis of alkoxides of Ti, Zr, Hf, Nb and Ta.[1] This method allows for the preparation of homoleptic alkoxides of the type $M(OR)_n$, n = 4 or 5, where R = Me, Et, ^{i}Pr, and ^{n}Bu. Although this method works for the synthesis of the above metal alkoxides, it cannot be used to obtain the corresponding *tert*-butoxides.

Alcohol interchange has been attempted for the synthesis of *tert*-butoxides of zirconium by Bradley and Mehrotra (eq 3.1).[133] They tried replacing the methoxy and

ethoxy groups of $Zr(OR)_4$ with *tert*-butoxides and observed that regardless the quantity of ^tBuOH used and the time of reflux, only three methoxy or ethoxy groups could be replaced. The final products were dimeric species, such as $[(O^tBu)_3Zr(OR)_2Zr(O^tBu)_3]$. The reaction presumably stopped after the third substitution due to steric reasons.

$$\mathbf{Zr(OR)_4 + 3\ ^tBuOH \xrightarrow[\text{excess}]{} Zr(O^tBu)_3(OR) + 3\ ROH} \quad (3.1)$$
R = Me, Et

Mehrotra *et al*. successfully synthesized tetra-*tert*-butoxides of Ti, Zr, Hf, Nb and Ta by the transesterification of the metal isopropoxides.[133–135] This was the first suitable method for the synthesis of the tetra- and penta-*tert*-butoxides of these metals. The success of this approach was attributed to the difference in boiling point between CH_3COO^iPr (89 °C) and CH_3COO^tBu (98 °C), which allowed for easy removal of the former by distillation (eq. 3.2). This method generally works well for the preparation of *tert*-butoxides of the group 4 and 5 metals.

$$\mathbf{Zr(^iPrO)_4{\cdot}^iPrOH + 4\ CH_3COO^tBu \longrightarrow Zr(O^tBu)_4 + {}^iPrOH + 4\ CH_3COO^iPr} \quad (3.2)$$

Metal amides have also been used for the synthesis of metal alkoxide complexes. Amides react with alcohols to yield a metal alkoxide and the corresponding amines. Group 4 and 5 metals usually form very stable complexes with amide ligands.[136] The valence orbitals of these metals are not completely filled and since amides are good σ- and π-donors, there is typically π-donation from the amido ligand to the metal center (Figure 40). This is usually reflected in the length of the M−N bond, which is shorter than the sum of the covalent radii of the two atoms that form the bond.

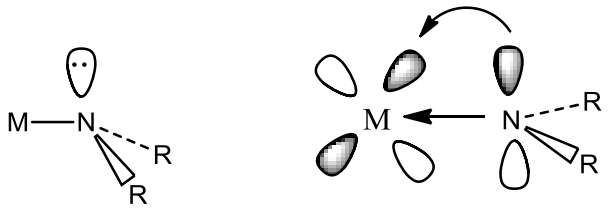

Figure 40. Ligand–metal π-bonding in metal amides (copied from reference 136).

The synthesis of tetra- and penta-substituted *tert*-butoxides of Group 4 and 5 metals from their corresponding diakylamides was reported by Thomas.[137] This technique provided quantitative amounts of the desired product and also produced gaseous by-products, which were easily eliminated. However, the strong π-bond formed between amides and most electropositive metals in higher oxidation state prevents their alcoholysis with ^{t}BuOH, which is a weak acid. Another limitation of the technique lies in the fact that the dialkylamides of these metals are not commercially available and so they have to be synthesized, which makes the process time consuming and expensive.[2] Hence, this method of synthesis is reserved for the laboratory synthesis of these compounds. Bis(trimethylsilyl)amides, which are weaker π-donors than the corresponding dialkylamides have been used to overcome the problems associated with the latter.[2] Unfortunately, the high prices of $LiN(SiMe_3)_2$ and $HN(SiMe_3)_2$, which are the starting materials for the synthesis of bis(trimethylsilyl)amides, confines this method to the laboratory.[2]

The reaction between a metal halide and an alcohol in the presence of a base is the most popular method for the synthesis of metal alkoxides of Group 4 and 5 metals.[1,2] The bases used are usually group 1 alkoxides, ammonia and pyridine. The easiest laboratory

method for the synthesis of titanium alkoxides is the reaction between titanium tetrahalide (preferably chloride) with the alkoxides of Li, Na, or K (eq. 3.3). This method also works for the syntheses of tertiary alkoxides of titanium. Unfortunately, the tertiary alkoxides of the other metals in these groups (Zr, Hf, Nb, and Ta) cannot be obtained because their alkoxides form stable heterobimetallic alkoxides with these alkali metals, ($NaZr(O^tBu)_5$, $LiNb(O^tBu)_6$, and $KZr(O^tBu)_5$).[138] The alkoxotitanates are very unstable, presumably due to the smaller size of titanium; hence, $Ti(O^tBu)_4$ is obtained in good yield. In the attempted synthesis of the alkoxides of the heavier metals, their alkoxometallates (heterobimetallic by-products) are very stable and volatile, such that the yields of the reactions are significantly reduced and separation of the product from these alkoxometallates by distillation is difficult.

$$\mathbf{TiCl_4 + 4\,MOR \longrightarrow Ti(OR)_4 + 4\,MCl} \qquad 3.3$$

M = Li, Na, K

To circumvent the problems associated with the direct alcoholysis of metal halides (formation of stable heterobimetallic alkoxides and the difficulty associated with the separation of the precipitated alkali-metal chlorides), these metal halides are treated with the corresponding alcohol in the presence of ammonia (eq. 3.4).[1,2]

$$\mathbf{MCl_4 + 4\,ROH + 4\,NH_3 \xrightarrow{benzene} M(OR)_4 + 4\,NH_4Cl\ (s)} \qquad 3.4$$

The above route is known as the ammonia method and it has the following advantages: i) the reaction is carried out in benzene and the precipitated NH_4Cl, which is crystalline in this solvent, is easily filtered off, ii) excess base is easily removed by evaporation, iii) unlike the alkali alkoxide method, no heterobimetallic side products are obtained, iv) heat needed to drive the reaction is produced by the neutralization of

liberated HCl with NH_3.[1,2] Pyridine has also been used as the base in the above synthesis. The limitations of this method are: i) the solvent of choice, benzene, is carcinogenic; hence, there is the need to explore other solvents, and ii) substitution of chlorides by *tert*-butoxides does not always go to completion. Bradley *et al.* had successfully synthesized $Zr(OR)_4$ (R = Et, ^{i}Pr, ^{s}Bu, and ^{n}Bu) from $(C_5H_6N)_2ZrCl_6$, by treating the latter with the corresponding alcohol in ammonia.[139] Attempts at repeating this reaction with *tert*-butanol stopped at the chloroalkoxide $ZrCl(O^tBu)_3 \cdot 2C_5H_5N$ (eq. 3.5). Mathur *et al.* recently observed the same phenomenon.[140] Their attempted synthesis of penta-*tert*-butoxy niobium from Nb_2Cl_{10} and *tert*-butanol in ammonia/pyridine stopped at the tetra substituted product, tetra-*tert*-butoxy-(pyridine)-niobium(V) chloride (eq. 3.6). The final chloride ligand could not be replaced even under reflux and extended reaction time. The difficulty associated with complete substitution of the chlorides with *tert*-butoxides in the examples above was attributed to steric restrictions.

$$(C_5H_5N)_2ZrCl_6 + \underset{\text{excess}}{4\ {}^{t}BuOH} + 5\ NH_3 \longrightarrow ZrCl({}^{t}BuO)_3 \cdot 2C_5H_5N + 5\ NH_4Cl\ (s) \quad (3.5)$$

$$Nb_2Cl_{10} + \underset{\text{excess}}{8\ {}^{t}BuOH} + \underset{\text{excess}}{10\ C_5H_5N} \longrightarrow 2\ NbCl(O^{t}Bu)_4(C_5H_5N) + 8\ C_5H_5N \cdot HCl \quad (3.6)$$

In the interaction of sodium tri(*tert*-butoxy)stannate, $[NaSn(O^tBu)_3]_2$, with group 4 metal tetrachlorides (Chapter I), we observed that instead of the transfer of one unit of the ligand to the group 4 metal, the preferential degradation of the stannate occurred. There was an exchange of ligands between the group 4 metals and tin/sodium metals. In other words, the stannate acted as a selective *tert*-butoxy transfer reagent for these metals.

Our goal was to exploit this selective transfer property of the ligand by using it as a catalyst for the selective synthesis of tri- and tetra-substituted alkoxides of group 4 and 5 metals from inexpensive starting materials (the metal chlorides and sodium *tert*-butoxide) in methylene chloride.

Experimental

Description of Techniques and Chemicals Used

General Procedures

All experiments were performed under an atmosphere of argon, using standard Schlenk techniques. Solvents were dried and freed of molecular oxygen by distillation under an atmosphere of nitrogen from sodium- or potassium-benzophenone ketyl immediately before use. NMR spectra were recorded on a Bruker AVANCE-500 NMR spectrometer at 25 °C. The ^{1}H, $^{13}C\{^{1}H\}$ NMR spectra are referenced relative to C_6D_5H (7.16 ppm) and C_6D_6 (128.39 ppm). Melting points were obtained on a Mel-Temp apparatus and are uncorrected. Columbia Analytical Services, Tucson, Arizona performed the elemental analysis. The reagents $NbCl_4(THF)_2$ and NaO^tBu were purchased from Aldrich, while $MCl_4(THF)_2$[57] (where M = Ti or Zr) were prepared according to published procedures.

Synthesis of $Ti(O^tBu)_4$, 24

A two-neck 100 mL flask was charged with $TiCl_4(THF)_2$ (2.50 g, 7.49 mmol), NaO^tBu (2.88 g, 29.95 mmol), and $[NaSn(O^tBu)_3]_2$ (0.27 g, 5 % mol) in a glove box. The flask was cooled to –78 °C and 30 mL of CH_2Cl_2 was then added. The resultant mixture was stirred overnight while it warmed to room temperature. The salt precipitated was filtered

over a medium porosity frit packed with celite. The solvent was removed by distillation. Distillation of the light yellow residue afforded the product as a clear, colorless liquid. Yield: 74 % (1.88 g, 6.43 mmol).

^{1}H NMR (C_6D_6): δ 1.37 (s, OC(C*H*$_3$)$_3$). ^{13}C NMR (C_6D_6): δ 80.5 (s, O*C*(CH$_3$)$_3$), 32.9 (s, OC(*C*H$_3$)$_3$).

Synthesis of Zr(O^{t}Bu)$_4$, 25

To a flask containing $ZrCl_4(THF)_2$ (1.83 g, 4.85 mmol), NaO^{t}Bu (1.86 g, 19.35 mmol), and [NaSn(O^{t}Bu)$_3$]$_2$ (0.17 g, 5 % mol) chilled to –78 ^{o}C was added 30 mL of methylene chloride. The reaction was stirred for 8 h while it gradually warmed to room temperature. The salt precipitated was filtered off to afford a colorless liquid. Distillation of the solvent and the resultant residue gave the product as a colorless liquid. Yield: 52 % (0.85 g, 2.53 mmol),.

^{1}H NMR (C_6D_6): δ 1.33 (s, OC(C*H*$_3$)$_3$). ^{13}C NMR (C_6D_6): δ 75.6 (s, O*C*(CH$_3$)$_3$), 33.4 (s, OC(*C*H$_3$)$_3$).

Synthesis of TiCl(O^{t}Bu)$_3$, 26

A two-neck 100 mL flask was charged with $TiCl_4(THF)_2$ (2.00 g, 5.99 mmol), NaO^{t}Bu (1.73 g, 17.97 mmol), and [NaSn(O^{t}Bu)$_3$]$_2$ (0.22 g, 5 % mol) in a glove box. The flask was cooled to –78 ^{o}C and 30 mL of CH_2Cl_2 was then added. The resultant mixture was stirred overnight while it warmed to room temperature. The salt precipitated was filtered over a medium porosity frit packed with celite. The solvent was removed by distillation. Distillation (79–85 ^{o}C, 0.75 mmHg) of the yellowish residue afforded the mixture of products as a clear colorless liquid, which solidified at room temperature. Yield: Mixture (^{1}H NMR): TiCl(O^{t}Bu)$_3$ (80 %), Ti(O^{t}Bu)$_4$ (20 %).

$TiCl(O^tBu)_3$: ^1H NMR (C_6D_6): δ 1.28 (s, $OC(CH_3)_3$). ^{13}C NMR (C_6D_6): δ 85.6 (s, $OC(CH_3)_3$), 32.2 (s, $OC(CH_3)_3$).

Synthesis of $ZrCl(O^tBu)_3$, 27

A two-neck 100 mL flask was charged with $ZrCl_4(THF)_2$ (1.00 g, 2.65 mmol), NaO^tBu (0.76 g, 7.95 mmol), and $[NaSn(O^tBu)_3]_2$ (0.1 g, 5 % mol) in a glove box. The flask was cooled to –78 °C and 30 mL of CH_2Cl_2 was then added. The resultant mixture was stirred overnight while it warmed to room temperature. The salt precipitated was filtered over a medium-porosity frit packed with celite. The solution was concentrated and stored at –4 °C.

^1H NMR (C_6D_6, 25 °C): δ 1.53 (s, $OC(CH_3)_3$). ^{13}C NMR (C_6D_6): δ 76.5 (s, $OC(CH_3)_3$), 32.4 (s, $OC(CH_3)_3$).

Synthesis of $Nb(O^tBu)_5$, 28

To a cold (–78 °C) solution of NaO^tBu (0.55 g, 5.70 mmol) and $[NaSn(O^tBu)_3]_2$ (0.10 g, 5 % mol) in methylene chloride (30 mL) was added drop-wise a solution of $NbCl_4(THF)_2$ (0.54 g, 1.43 mmol) in methylene chloride (20 mL). The precipitated NaCl was removed using a medium porosity frit and the filtrate was concentrated to 10 mL. Storage of the solution at –10 °C afforded colorless crystals. Yield: 45 % (0.29 g, 0.63 mmol).

^1H NMR (C_6D_6): δ 1.48 (s, $OC(CH_3)_3$). ^{13}C NMR (C_6D_6): δ 80.3 (s, $OC(CH_3)_3$), 32.0 (s, $OC(CH_3)_3$). Anal. Calcd for $C_{20}H_{45}O_5Nb$: C, 52.39; H, 9.89. Found: C, 52.18; H, 10.02.

Results and Discussion

1. Syntheses and Spectroscopic Analyses of $Ti(O^tBu)_4$, 24 and $Zr(O^tBu)_4$, 25

The syntheses of compounds **24** and **25** were achieved by treating the respective metal tetrachlorides with sodium *tert*-butoxide in the presence of catalytic amounts of tri(*ter*t-butoxy)stannate (Scheme 19). The tetra-*tert*-butoxides are monomeric due to the bulk of the *tert*-butoxy group and this structural feature makes them volatile. The compounds were, therefore, purified by vacuum distillation. The reactions were monitored by NMR spectroscopy. The NMR spectra of the crude reaction mixtures were similar to those of the isolated product, i.e., no other product was detected by NMR. The formation of stable heterobimetallic side-products is problematic in the syntheses of these alkoxides. Since these side-products were not observed, it was concluded that either these side-products were not formed or they were insoluble in the solvent used.

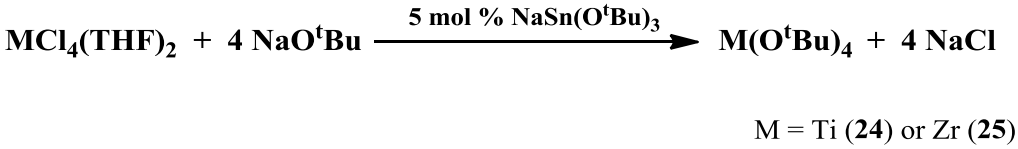

Scheme 19. Syntheses of compounds **24** and **25**.

The spectra obtained for the compounds matched those previously reported.[1] The ^1H NMR spectrum of **24** in benzene-d_6 is shown in Figure 41. The ^1H NMR spectrum is simple with a single peak for the equivalent protons of the *tert*-butoxy groups at 1.37 ppm. The $^{13}C\{^1H\}$ NMR spectrum has two peaks at 80.5 ppm and 32.9 ppm (Figure 42). The former peak was assigned to the quaternary carbons, while the latter was assigned to the primary carbons of the *tert*-butoxy groups.

The spectra obtained for compound **25** are similar to those of **24**, since these compounds are homologues. The *tert*-butoxy protons were observed as a singlet at 1.33 ppm. In the ^{13}C NMR spectrum the quaternary and primary carbons were observed at 75.6 and 33.4 ppm, respectively.

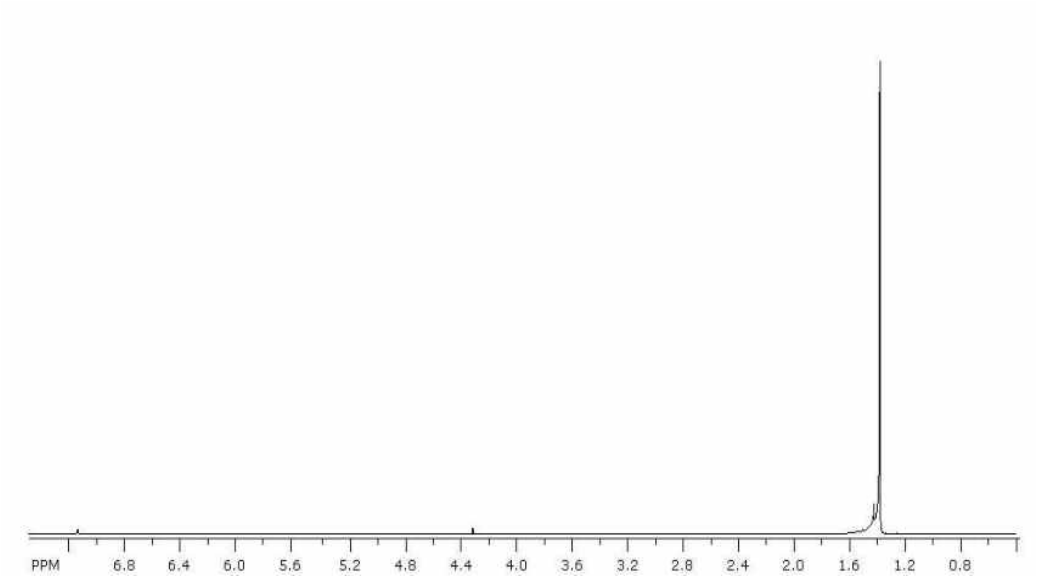

Figure 41. ^{1}H NMR spectrum of **24**.

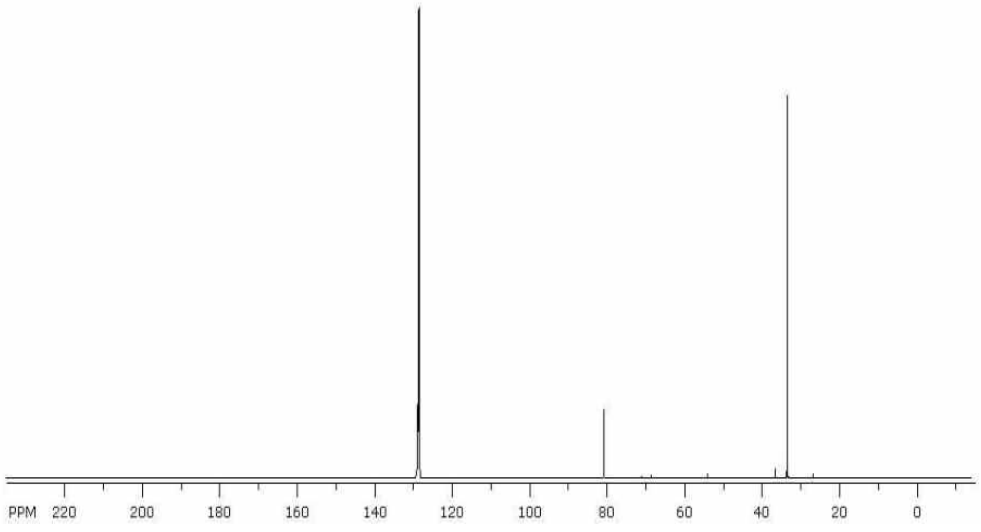

Figure 42. $^{13}C\{^{1}H\}$ NMR spectrum of **24**.

2. Syntheses and Spectroscopic Analysis of $TiCl(O^tBu)_3$ 26, and $ZrCl(O^tBu)_3$ 27

Preparation of compounds **26** and **27** is made important by the fact that they could be used as starting materials for the synthesis of other derivatives. No general method has been reported for the synthesis of monochloro *tert*-butoxides of group 4 metals. The pyridine adduct of **27** was accidentally isolated by Bradley *et al*. In their attempted synthesis of $Zr(O^tBu)_4$ **25**, from dipyridinium hexachlorozirconate, $(C_5H_6N)_2ZrCl_6$, the reaction stopped at the trisubstituted product $ZrCl(O^tBu)_3 \cdot 2C_5H_5N$.[139] Further treatment of the trisubstituted compound with sodium *tert*-butoxide did not lead to the replacement of the chloride, but the chloride was replaced when the less sterically bulky EtOH was used. Compound **26** has also been synthesized from the comproportionation of $TiCl_4$ and $Ti(O^tBu)_4$ (eq. 3.7), but the method requires heating, long reaction periods, the latter reagent is expensive and sometimes side products are obtained.[59] Unfortunately, the comproportionation method cannot be used for the synthesis of the chloro-tri-*tert*-butoxides of hafnium and zirconium.

$$\mathbf{TiCl_4 + 3\ Ti(O^tBu)_4 \longrightarrow 4\ TiCl(O^tBu)_3} \quad (3.7)$$

Compounds **26** and **27** were synthesized by treating the respective metal tetrachlorides with sodium *tert*-butoxide in the presence of catalytic amounts of tri(*tert*-butoxy)stannate (Scheme 20).

$$\mathbf{MCl_4(THF)_2 + 3\ NaO^tBu \xrightarrow{5\ mol\ \%\ NaSn(O^tBu)_3} MCl(O^tBu)_3 + 3\ NaCl}$$

M = Ti (**26**), Zr (**27**)

Scheme 20. Syntheses of compounds **26** and **27**.

In the synthesis of **26**, compound **24**, the tetrasubstituted complex, was obtained as a side product. Even when the amount of sodium *tert*-butoxide used was limiting, both compounds were still formed. Attempts at separating the two compounds by vacuum distillation were unsuccessful: the distillate had both compounds in the same ratio. The ^{1}H NMR spectrum of the mixture of compounds is shown in Figure 43. The best way of separating these compounds might be by crystallization. Since compound **26** is a solid and **24** is a liquid, the former could be crystallized out of the mixture. The difficulty in doing so lies in the fact that **26** is coordinatively unsaturated, hence a donor solvent is required to stabilize the metal and to effect crystallization. Currently, we have attempted to crystallize this compound from donor solvents such as pyridine and THF, but no crystals have yet been isolated.

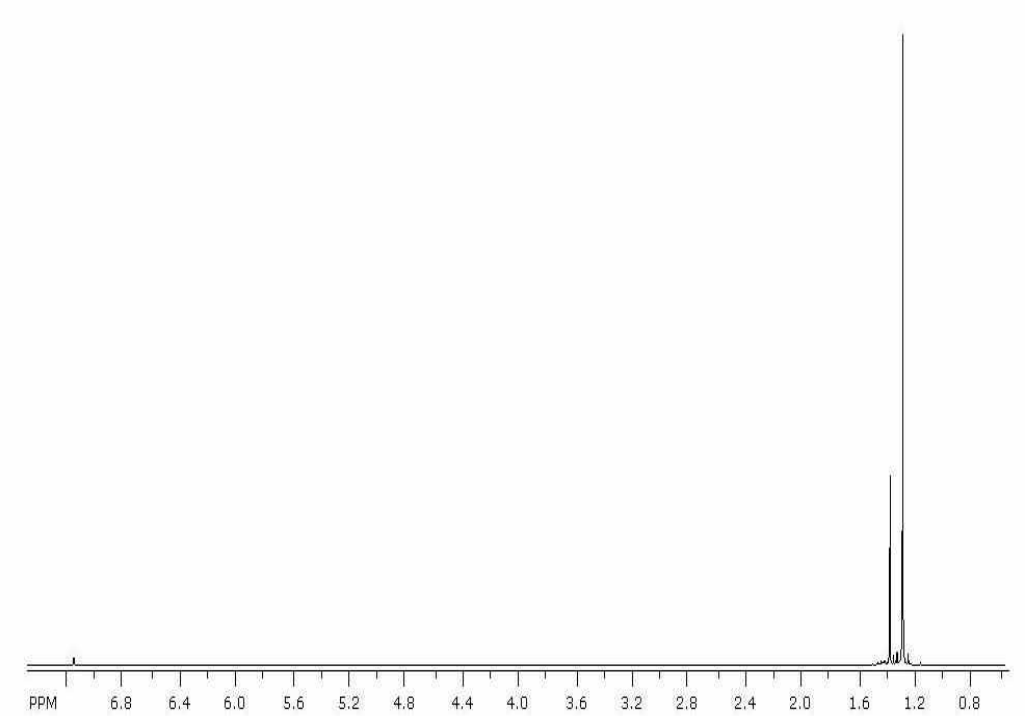

Figure 43. ^{1}H NMR spectrum of a mixture of **24** and **26**.

The synthesis of **27** was monitored by NMR spectroscopy. The ^{1}H NMR spectrum of the reaction mixture showed that compound **27** was the only product and no tetrasubstituted product was present (Figure 44). The protons of the *tert*-butoxy group were observed as a broad peak at 1.53 ppm. Attempts have been made at purifying this compound by crystallization from pyridine and THF, but no crystals have been isolated so far.

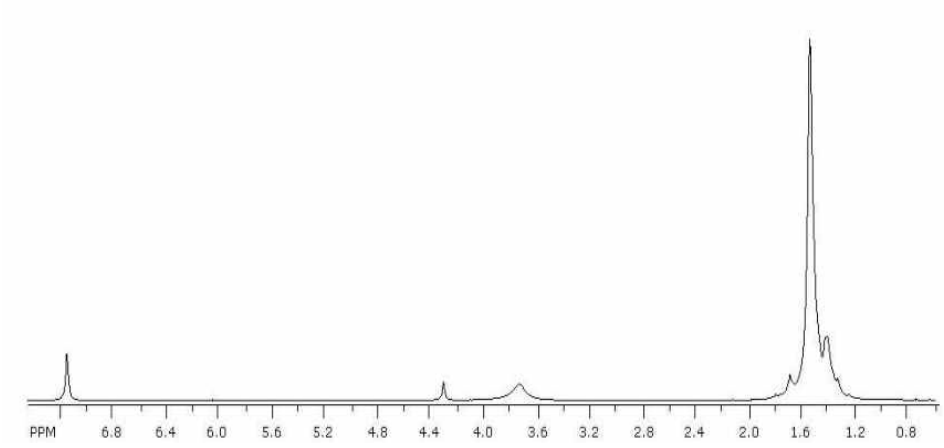

Figure 44. ^{1}H NMR spectrum of of **27**.

3. Synthesis and Spectroscopic Analysis of $Nb(O^{t}Bu)_5$, 28

The synthesis of compound **28** was achieved by treating $NbCl_4(THF)_2$ with sodium *tert*-butoxide in the presence of catalytic amounts of tri(*tert*-butoxy)stannate in methylene chloride (Scheme 21).

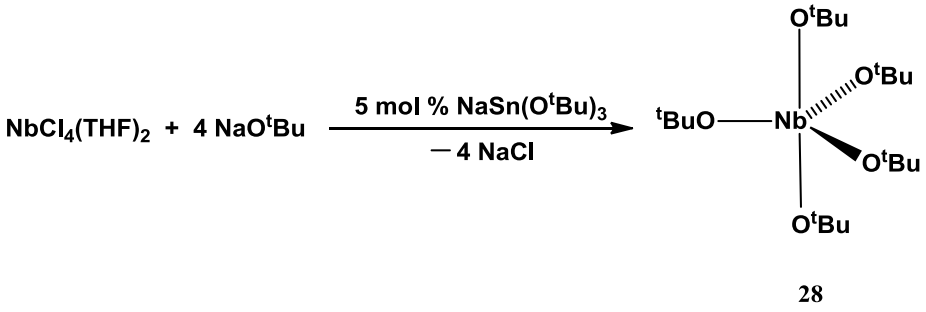

28

Scheme 21. Synthesis of compound **28**.

Although the reagents where employed in a 1:4 ratio, the product obtained had the reactants in a 1:5 ratio *i.e*. the oxidation of niobium occurred from Nb^{IV} to Nb^{V}. The reason for the formation of the observed product lies in the stability of the expected product, $Nb(O^tBu)_4$. During attempts to synthesize $Nb(OR)_4$ from $Nb(NEt_2)_4$ and the corresponding alcohol, Thomas observed the immediate oxidation of these tetra-substituted products to the penta-substituted alkoxides (eq. 3.8 and 3.9).[137] The oxidation of the expected products occurred even after the meticulous exclusion of oxygen. In our case, we believe that when the unstable tetrasubstituted alkoxide was formed, it disproportionated into a Nb^{V} and a Nb^{III} product. The trivalent niobium compound has not been identified so far. $Nb(O^tBu)_5$ might be best accessed via the oxidation of $NbCl_4$, since attempts at synthesizing this compounds via $NbCl_5$ always gives incomplete substituted products.[2,137]

$$Nb(NEt_2)_4 + 4\ ROH \longrightarrow Nb(OR)_4 + 4\ Et_2NH \qquad (3.8)$$

$$Nb(OR)_4 + ROH \longrightarrow Nb(OR)_5 + 1/2\ H_2 \qquad (3.9)$$

Compound **28** was characterized by NMR spectroscopy (Figures 45 and 46). The ^1H NMR spectrum of **28** in deteurated benzene contains a singlet peak at 1.48 ppm, which was assigned to the protons of the *tert*-butoxy group. The $^{13}C\{^1H\}$ NMR spectrum had two singlet peaks for the quaternary (80.3 ppm) and primary carbons (32.0 ppm) of the *tert*-butoxy groups, respectively.

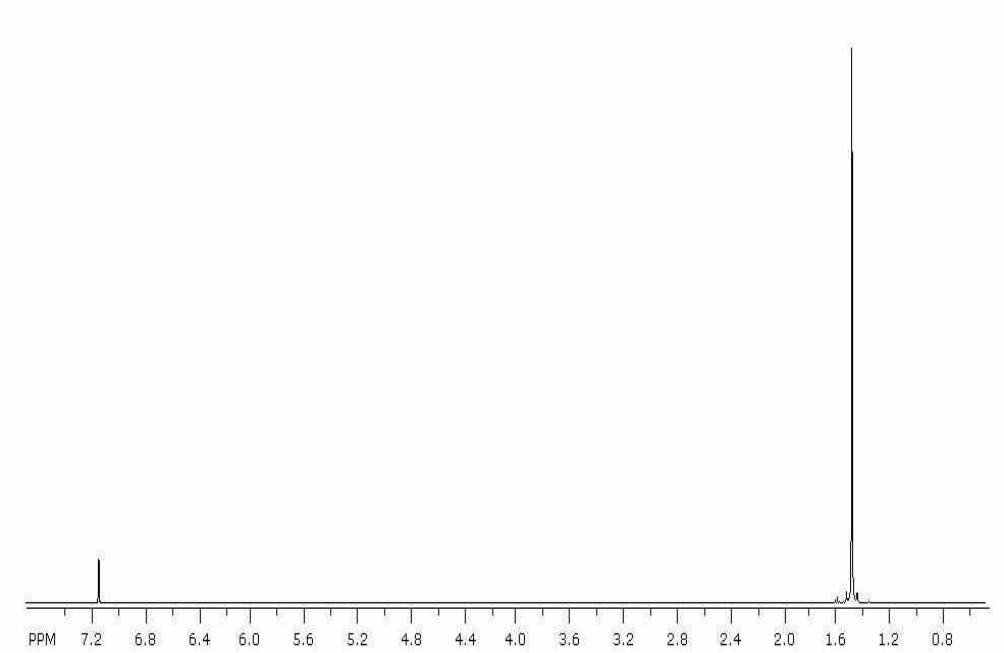

Figure 45. ^{1}H NMR spectrum of **28**.

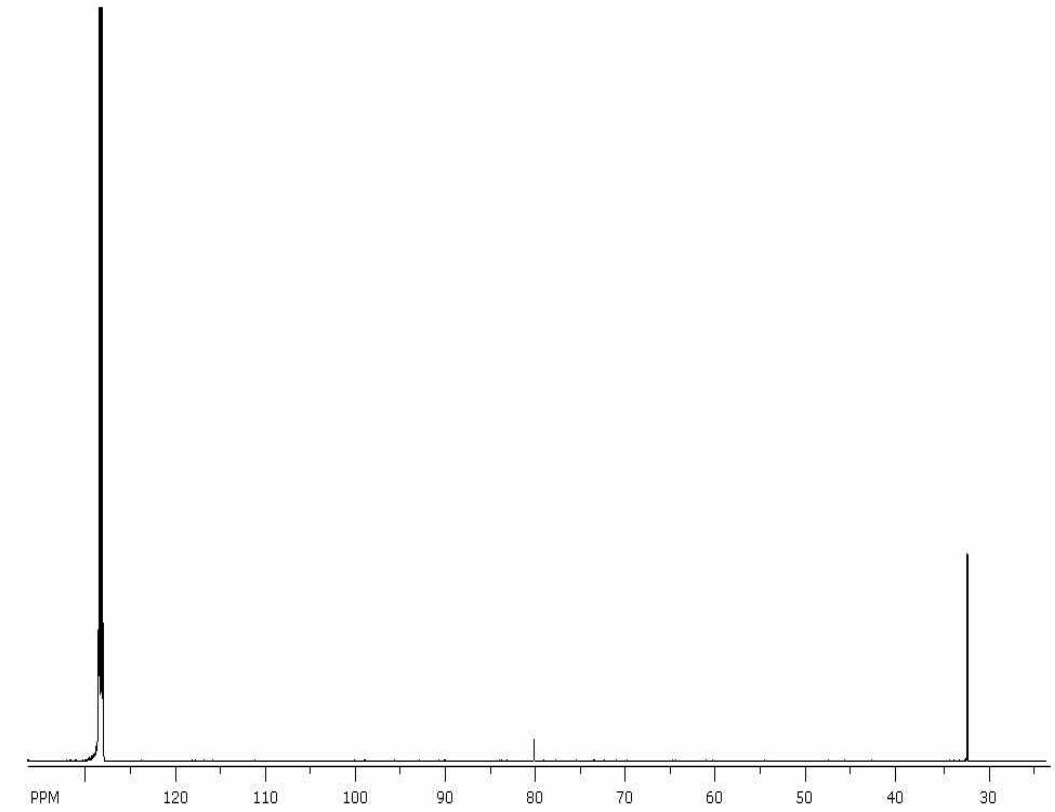

Figure 46. $^{13}C\{^{1}H\}$ NMR spectrum of **28**.

4. Solid-state Structure of $Nb(O^tBu)_5$, 28

Crystals from which the structure of **28** was obtained were grown from hexane. Complex **28** crystallizes in the orthorhombic crystal system with space group *Pnc*2 and four independent molecules in the unit cell. The structure of the compound is shown in Figure 47, while crystallographic data are given in Tables 24 and 25.

Structural characterization of niobium *tert*-butoxide derivatives is extremely rare and the only compound of this class that has been structurally characterized was done recently by Mathur *et al*.[140]

The structure of compound 28 was disordered and this made the structural refinement of the compound difficult. The disorder in the compound arises from the fact that there is a two-fold axis of rotation (C_2) that passes through the Nb1, O3 and the *tert*-butyl group attached to this oxygen atom. Since a *tert*-butyl group is C_3 symmetric and not C_2 symmetric, there is positional disorder of the carbon atoms of the methyl group. In other words, the two symmetry elements are not compatible. The geometry about niobium is that of a distorted trigonal bipyramid with the angle between the *tert*-butoxy group all deviating slightly from the expected 120^o (O1–Nb–O1$'$ = 125.70(2) and O1–Nb–O3 = 117.15(3)) and 180^o (O2–Nb–O2$'$ = 176.25(3)).

The Nb–O1 (1.87(3) Å), Nb–O2 (1.90(3) Å), and Nb–O3 (1.89(2) Å) bond distances are comparable with the terminal alkoxide groups in $Nb_2(O^iPr)_{10}$ (1.89–1.91 Å) and $NbCl(O^tBu)_4py$ (1.86–1.89 Å).[2]

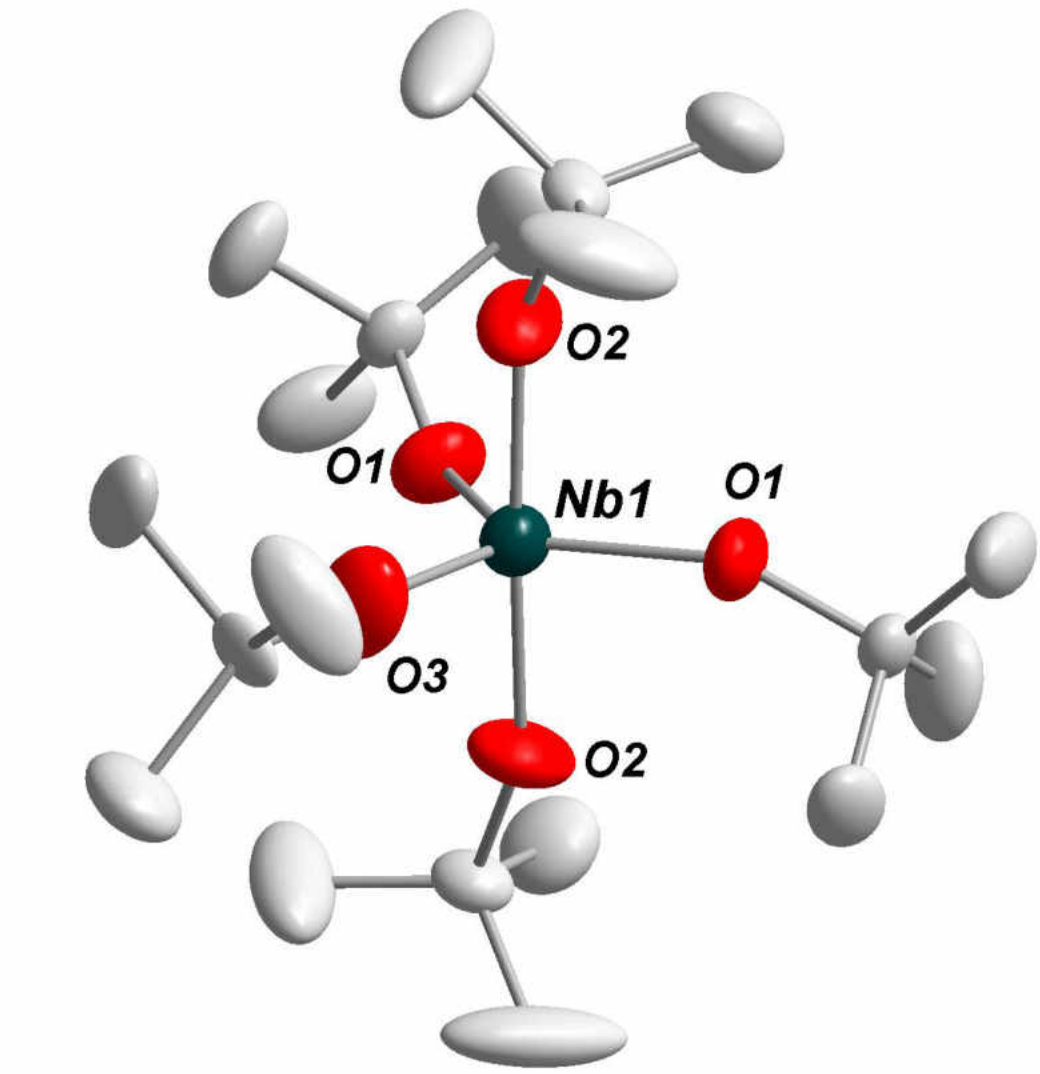

Figure 47. Solid-state structure and labeling scheme of **28**. With the exception of carbon (35%) all atoms are drawn at the 50% probability level.

Table 24. Crystal data for compound **28**

Molecular formula	$C_{20}H_{45}O_5Nb$
fw	458.48
Crystal system	orthorhombic
Space-group	*Pnc*2(30)
a, Å	16.3392(5)
b,Å	16.3394(8)
c,Å	9.9328(9)
α, deg	90
β, deg	90
γ, deg	90
V, Å^3	2651.79(28)
Z	4
F(000)	1140
ρ(calc), g cm^{-3}	1.1256
λ, Å	0.710 73
temp, K	173
μ, mm^{-1}	1.325
$R(F)^a$	0.0432
$R_W(F^2)^b$	0.0893

[a] $R = \sum|F_o - F_c| \quad |F|_o$. [b] $R_w = \{[\quad w(F_o^2 - F_c^2)] / [\sum w(F_o^2)^2]\}^{1/2}$; $w = 1/[\sigma^2(F_o)^2 + (xP)^2 + yP]$, where $P = (F_o^2 + 2F_c^2)/3$.

Table 25. Selected bond lengths (Å) and angles (°) for **28**

Bond Lengths			
Nb–O1	1.8703(1)	O–C10	1.4211(1)
Nb–O2	1.8983(1)	O–C20	1.432(1)
Nb–O3	1.8983(2)	O–C3O	1.3889(1)
Bond Angles			
O1–Nb–O1'	125.70(2)	O2–Nb–O2'	176.25(3)
O1–Nb–O2	88.05(4)	O2–Nb–O3	91.88(3)
O1–Nb–O2'	90.24(2)	O2'–Nb–O3	91.88(3)
O1' –Nb–O2	90.24(2)	Nb–O1–C10	152.02(3)
O1' –Nb–O2 '	88.05(4)	Nb–O2–C20	155.37(2)
O1–Nb–O3	117.15(3)	Nb–O3–C30	180
O1'–Nb–O3	117.15(3)		

Summary and Conclusion

Homoleptic tertiary alkoxides are difficult to synthesize due to steric restrictions. Hence, few routes are available for the synthesis of these compounds. We designed a synthetic method for the preparation of tertiary allkoxides of group 4 and 5 metals by exploiting the selective *tert*-butoxy transfer properties of tri(*tert*-butoxy)stannate towards these metals. An added advantage of the method is the fact that it could be modified to obtain heteroleptic chloride-*tert*-butoxides, a feat which is usually difficult to achieve, since substitution usually yields multiple products.

For group 4 metals, the above method gave both homoleptic ($Ti(O^tBu)_4$ **24** and $Zr(O^tBu)_4$ **25**) and heteroleptic ($TiCl(O^tBu)_3$ **26** and $ZrCl(O^tBu)_3$ **27**) alkoxides. Compounds **24** and **25** were volatile liquids which were purified by distillation *in vacuo*. The synthesis of **26** was made difficult by the formation of **24** as a side-product. Even the use of less than stoichiometric amounts of the alkoxide did not prevent the formation of **24**. In the synthesis of **27**, the reaction furnished the expected product and the tetrasubstituted product was not observed. Purification of **26** and **27** by crystallization from donor solvent are underway, but no crystals have been isolated at this time.

Niobium tetrachloridebis(tetrahydrofuranate), $NbCl_4(THF)_2$, reacted with NaO^tBu to give pentakis(*tert*-butoxy)niobium, $Nb(O^tBu)_5$ **28**, instead of the expected tetrakis(*tert*-butoxy)niobium, $Nb(O^tBu)_4$. It is believed that the initially formed tetrakis(*tert*-butoxy)niobium is unstable, hence it disproportionated to yield compound **28** and a trivalent niobium compound (which has not yet been identified). Complex **28** was X-ray structurally characterized and to the best of our knowledge is one of only two niobium *tert*-butoxides to have been structurally characterized to date.

Although the compounds (**24**–**28**) above have been previously reported, the method used for their syntheses was simple, inexpensive and versatile in that it allowed for controlled synthesis of the desired compound. Hence, the synthesis of desired chloro-*tert*-butoxides was achieved.

CHAPTER IV

SYNTHESIS AND CHARACTERIZATION OF COORDINATION POLYMERS BUILT FROM THE COMBINATION OF CpM and ME(O^tBu)$_3$ (M = Na or K and E = Ge or Sn)

Introduction

Coordination polymers are inorganic or organometallic structural networks (1D, 2D or 3D) containing metal cations linked together by multifunctional ligands. The synthesis of coordination polymers has attracted a lot of attention not only for the exciting new structures they form, but also for the fact that their design through the assembly of designed building blocks provides control over the solid-state structures obtained and hence functionality of the final material, a very desirable feature.[141−147]

The Cp ligand, which is ubiquitous in organometallic chemistry, is one of many ligands that have been employed in the synthesis of coordination polymers. The bonding in the Cp ring is such that there is an equal distribution of electron density above and below the ring. Hence, this ligand and its derivatives are easily used to tether metal centers, forming extended polymeric arrays. Many research groups have used a combination of ferrocene (Cp_2Fe) and group 1 and 2 metal salts to obtain polymeric structures, in which the metal cations are η^5-bound to the Cp ring, yielding extended geometries.[148−151] The planned synthesis of coordination polymer networks with alkali-metal ions is usually difficult to achieve, and most of these polymers are obtained by

serendipity.[152] The difficulty associated with the planned synthesis of coordination polymers containing alkali metals is the fact that, unlike transition metals with well-defined coordination numbers, there is a greater span of coordination numbers possible for alkali metal ions.[152] Few examples of cases where these metal organic frameworks are systematically generated are found in the literature.[148−152]

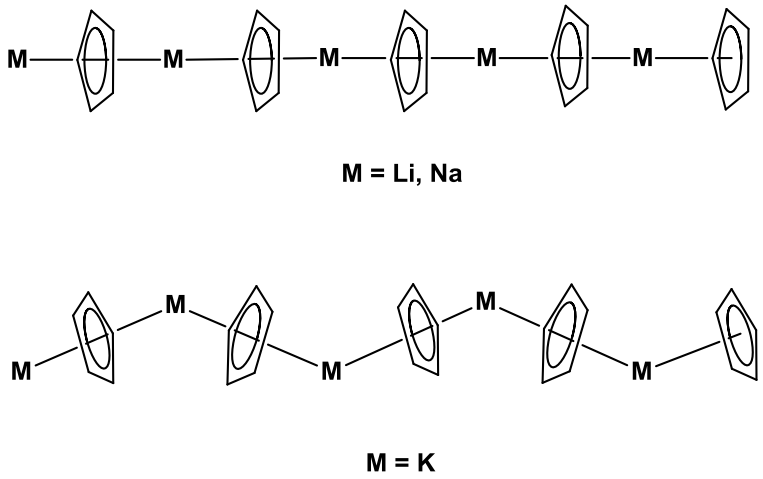

Figure 48. Structures of MCps as determined by powder X-ray diffraction.

The utility of alkali metal cyclopentadienides is largely limited to their use as precursors in the synthesis of other main group-, transition-, lanthanide- and actinide metal cyclopentadienyl complexes.[153] However, the structures of these important intermediates were only determined recently and single crystals of these compounds have never been grown.[154] Structural characterization of the compounds was made possible by developments in high resolution powder X-diffraction techniques. The difficulty in growing single crystals of these compounds lies in nature of the bonding in the compounds. The bonding in alkali metal cyclopentadienides has been established to be about 80–90% ionic in character.[155] Hence, the highly ionic compounds, which are

insoluble in non-polar solvents, can only be obtained as powders from these solvents. Structural characterization of the powders obtained showed that the compounds are polymeric and the structure adopted depends on the size of the alkali metal cation (Figure 48).[154] Coordinative saturation of the metal cations, hence stabilization, is needed to grow single crystals of alkali metal cyclopentadienides. This has been achieved by either growing the crystals in donor solvents such as ethers (Et_2O, THF) or in the presence of bases like TMEDA and pyridine, or furthermore by employing modified Cp ligands with donor site arms: (TMS)Cp, (benzyl)Cp, or (CN)Cp.[155−161]

In an attempt at synthesizing $CpSnO^tBu$ via salt metathesis by treating CpSnCl with NaO^tBu, instead of the desired product, we obtained the polymeric coordination polymer $\{(THF)NaCp{\cdot}NaCp{\cdot}[NaSn(O^tBu)_3]_2{\cdot}THF\}_\infty$ **20** (see chapter 2). Analysis of this coordination polymer showed that it was a double salt of NaCp and $NaSn(O^tBu)_3$. The coordination polymer was later synthesized by combining these two salts in THF. The NaCp and $NaSn(O^tBu)_3$ units were tethered by coordination of both metals to the Cp ligand (bilateral η^5-coordination) and by coordination to the *tert*-butoxides to give a unique new 1D polymeric coordination compound. The polymer can be considered as a crystallization of NaCp which is only made possible by $NaSn(O^tBu)_3$, that connects the NaCp units via its sodium atom and *tert*-butoxides. This form of crystallizing NaCp is unique and to the best of our knowledge only two other coordination polymers made up of alkali metal cyclopentadienides and group 14 alkoxometallates have been reported in the literature.[162] Only one of the two compounds previously reported was structurally characterized.[162]

We now report the fairly simple, planned synthesis and characterization of alkali/group 14 metal organic frameworks obtained by combining alkali metal cyclopentadienide salts (MCp) with alkali metal/Group 14 alkoxometalates ($ME(O^tBu)_3$) (where M = Na or K and E = Sn or Ge).

Experimental

Description of Techniques and Chemicals Used

General Procedures

All experiments were performed under an atmosphere of argon, using standard Schlenk techniques. Solvents were dried and freed of molecular oxygen by distillation under an atmosphere of nitrogen from sodium or potassium benzophenone ketyl immediately before use. NMR spectra were recorded on a Bruker AVANCE-500 NMR spectrometer at room temperature. The ^1H and $^{13}C\{^1H\}$ NMR spectra are referenced relative to C_6D_5H (7.16 ppm) and C_6D_6 (128.39 ppm), respectively. Columbia Analytical Services, Tucson, AZ, performed the elemental analyses. The reagents NaCp,[154] KCp,[154] $[NaGe(O^tBu)_3]_2$,[58] $[KSn(O^tBu)_3]_2$[58] were synthesized according to published procedures.

General Synthetic Route

The coordination polymers were generally synthesized by combining MCp and $[ME(O^tBu)_3]_2$ in 20 mL of THF at room temperature to give a clear solution. The solution was stirred for 4 h and then concentrated to about half of its original volume and then stored at −4 °C. Crystallization usually occurred after about two days.

Synthesis of [NaCp(THF) NaGe(O^tBu)$_3$]$_\infty$, 29

The synthesis was accomplished by combining [NaGe(O^tBu)$_3$]$_2$ (0.88 g, 1.40 mmol) and NaCp (0.25 g, 2.84 mmol). Crystallization afforded colorless rectangular crystals. Yield: 90 % (0.60 g, 1.26 mmol).

Mp: decomposes (200 °C). ^{1}H NMR (C_6D_6): δ 6.51 (s, C_5H_5), 3.58 (t, J = 13 Hz, OCH_2CH_2,), δ 1.41 (t, J = 13 Hz, OCH_2CH_2), δ 1.34 (s, $OC(CH_3)_3$). $^{13}C\{^1H\}$ NMR (C_6D_6): 105.4 (C_5H_5), 70.4 ($OC(CH_3)_3$), 68.4 (OCH_2CH_2), 34.8 ($OC(CH_3)_3$), 26.2 (OCH_2CH_2). Anal. Calcd for $C_{21}H_{40}O_4Na_2Ge$: C, 53.09; H, 8.49. Found: C, 53.06; H, 8.72.

Synthesis of [NaCp(THF) KGe(O^tBu)$_3$]$_\infty$, 30

As described above, compound **3** was synthesized by combining [NaGe(O^tBu)$_3$]$_2$ (0.73 g, 1.16 mmol) and KCp (0.24 g, 2.31 mmol). Yield: 91 % (0.52 g, 1.06 mmol).

Mp: 120–123 °C. ^{1}H NMR (C_6D_6): δ 6.37 (s, C_5H_5), 3.57 (t, J = 13 Hz OCH_2CH_2), 1.42 (t, J = 13 Hz, OCH_2CH_2), 1.36 (s, $OC(CH_3)_3$). $^{13}C\{^1H\}$ NMR (C_6D_6): δ 106.2 (C_5H_5), 70.8 ($OC(CH_3)_3$), 68.4 (OCH_2CH_2), 34.8 ($OC(CH_3)_3$), 26.2 (OCH_2CH_2). Anal. Calcd for $C_{21}H_{40}O_4NaKGe$: C, 51.34; H, 8.21. Found: C, 49.33; H, 8.23.

Synthesis of [NaCp(THF) KSn(O^tBu)$_3$]$_\infty$, 31

The double salt was synthesized by combining KSn(O^tBu)$_3$ (0.98 g, 2.60 mmol) and NaCp (0.23 g, 2.61 mmol). Yield: 87 % (1.22 g, 2.27 mmol).

Mp: 118–120 °C. ^{1}H NMR (C_6D_6): δ 6.36(s, C_5H_5), 3.56 (t, J = 13 Hz, OCH_2CH_2,), 1.42 (t, J = 13 Hz, OCH_2CH_2), 1.33 (s, $OC(CH_3)_3$). $^{13}C\{^1H\}$ NMR (C_6D_6): δ 106.0 (C_5H_5), 70.4 ($OC(CH_3)_3$), 68.3 (OCH_2CH_2), 36.0 ($OC(CH_3)_3$), 26.2 (OCH_2CH_2). Anal. Calcd for $C_{21}H_{40}O_4NaKSn$: C, 46.94; H, 7.50. Found: C, 47.13; H, 7.71.

Synthesis of $[KCp(THF)_2KSn(O^tBu)_3]_\infty$, 32

Compound **4** was synthesized by combining $KSn(O^tBu)_3$ (0.43 g, 1.14 mmol) and KCp (0.12 g, mmol). Yield: 90 % (0.64 g, 1.02 mmol).

Mp: 212–214 °C. ^{1}H NMR (C_6D_6): δ 6.33 (s, C_5H_5), 3.57 (t, J = 13 Hz OCH_2CH_2), 1.42 (t, J = 13 Hz, OCH_2CH_2), 1.36 (s, $OC(CH_3)_3$). $^{13}C\{^1H\}$ NMR (C_6D_6): δ 106.7 (C_5H_5), 70.2 ($OC(CH_3)_3$), 68.2 (OCH_2CH_2), 35.9 ($OC(CH_3)_3$), 26.2 (OCH_2CH_2). Anal. Calcd for $C_{50}H_{96}O_{10}K_4Sn_2$: C, 48.00; H, 7.73. Found: C, 46.25; H, 7.57.

Results and Discussion

1. Syntheses and Spectroscopic Analysis of Compounds 29–31

Alkali metal salts are predominantly ionic in nature. Syntheses employing these salts are mostly carried out in polar solvents, such as ethers, because these solvents are able to stabilize structural fragments of these compounds by acting as neutral donors. Therefore, THF was chosen as the solvent for combining MCp and $ME(O^tBu)_3$. When THF was introduced into a flask containing both salts, they quickly dissolved, and the desired product was usually obtained in about two hours. The resultant products were all polymeric and as expected had THF molecules coordinated (Scheme 22). These polymers are highly air- and moisture-sensitive and soluble in hydrocarbon solvents, such as benzene and hexane.

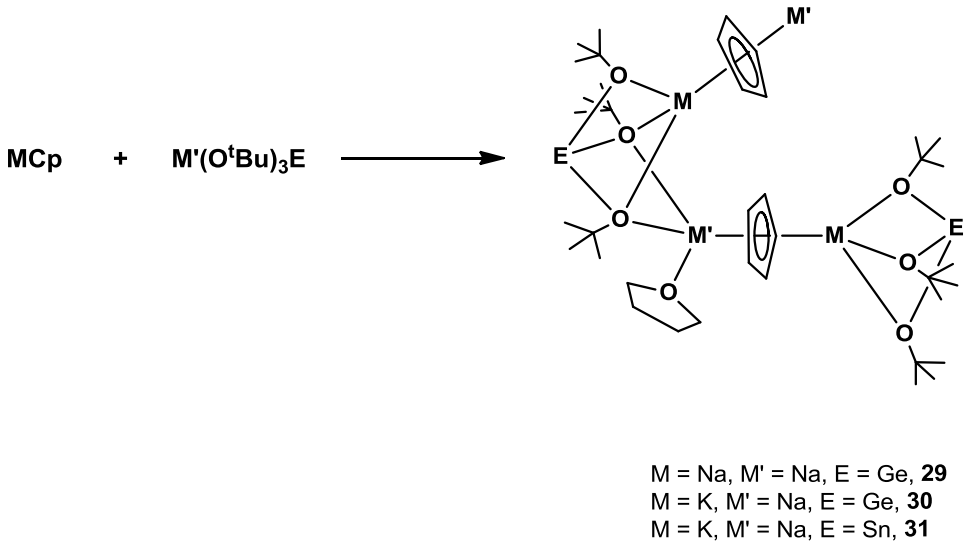

Scheme 22. Syntheses of compounds **29**–**31**.

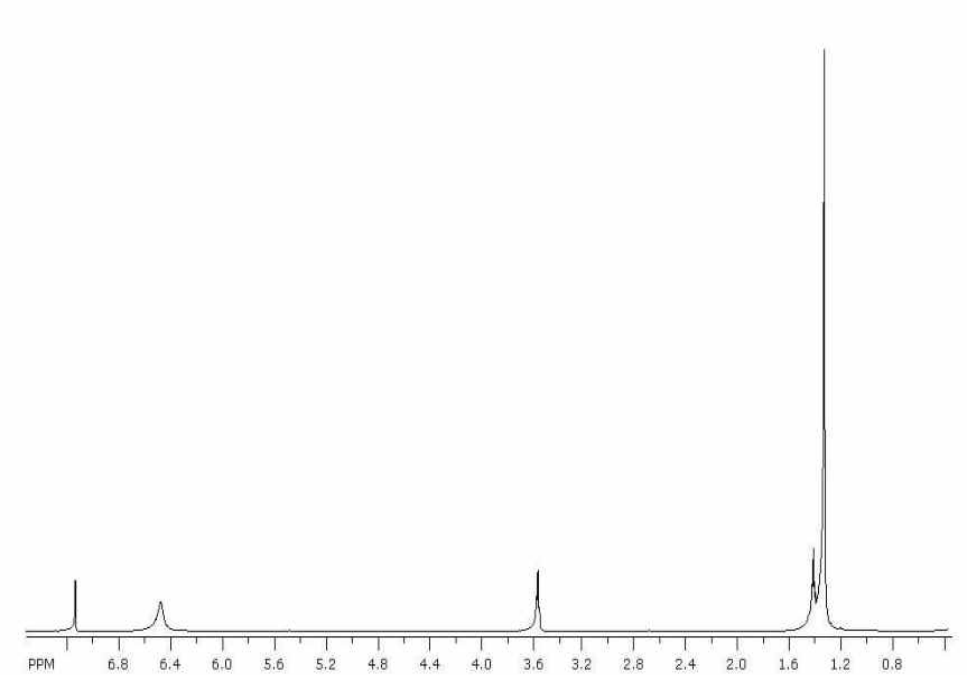

Figure 49. ^{1}H NMR spectrum of **29**.

The synthesis of the compounds was monitored by NMR spectroscopy. The spectra obtained for compounds **29**–**31** were similar to each other and to that of compound **20**, reported in Chapter 2. That for **29**, shown in Figure 49, will be used as the

sample for discussion. The ^{1}H NMR spectrum of compound **29** in deteurated benzene had four peaks in addition to that of the solvent. A broad peak, observed at 6.51 ppm was assigned to the Cp protons. Two triplet peaks at 3.58 and 1.41 ppm were assigned to the different methylene protons on the coordinated THF molecule. The protons on the different *tert*-butoxy groups were observed as a sharp singlet at 1.34 ppm. The equivalence of all different *tert*-butoxy and Cp groups in solution does not match the solid-state structures of the compounds obtained by X-ray crystallography. Hence, it is believed that in solution the NaCp and ME($O^{t}Bu$)$_3$ fragments remain separated.

2. Solid-state Structures of Compounds 29–31

X-ray quality crystals of compounds **29–31,** from which their structures were obtained, were grown from THF as colorless rectangular blocks. Compound **29** crystallized in the orthorhombic crystal system with space group $P2_12_12_1$ and had four molecules in the unit cell, while compounds **30** and **31** both crystallized in the monoclinic crystal system with space group $P2_1/n$ and four molecules in the unit cell. Additional crystallographic data for compound **29** are presented in Tables 26 and 27, while those for compound **30** are listed in Tables 28 and 29, and those for compound **31** are given in Tables 30 and 31.

The solid-state structure determinations of compounds **29–31** were much better than that of analogous **20** which was highly disordered. The inherent disorder in **20** was caused by the fact that every fourth Na ion was missing a coordinated THF molecule. In compounds **29–31** there were no missing THF molecules, hence there is no disorder, and the asymmetric unit was reduced from NaCp, NaSn($O^{t}Bu$), THF·NaCp, and NaSn($O^{t}Bu$)$_3$

as observed in **20** to just consisting of THF·NaCp and $NaGe(O^tBu)_3$ in **29** (Figure 50), THF·NaCp and $KGe(O^tBu)_3$ in **30** (Figure 51), and THF·NaCp and $KSn(O^tBu)_3$ in **31** (Figure 52). Similar to the structure of **20**, the repeating units in complexes **29**–**31** are arranged in a zig-zag fashion in the polymer backbone, but were linear through the Na–Cp–Na region of the polymer in **29** and the Na–Cp–K region in **30** and **31**.

In all three compounds, the Cp ligands are bilaterally η^5-coordinated by two alkali metal atoms, forming a supersandwiched structure. The Na–Cp interactions in the three compounds are very similar, whereby Na–Cp = 2.695(4) Å and 2.732(4) Å in **29**, Na–Cp = 2.784(4) Å in **30**, and Na–Cp = 2.783 (4) Å in **31**. The K–Cp bond lengths in **30** (3.072(4) Å) and **31** (3.068(4) Å) are also very close and are similar to those in CpK (3.056 Å) and $CpK{\cdot}Et_2O$ [3.012 (2) Å].[154,160] The Na–THF distances in all three compounds (2.352(3) Å in **29**, 2.316(3) Å in **30**, and 2.323(3) Å in **31**) are almost identical, but are shorter than that in polymeric $C_4H_7OCH_2C_5H_4Na{\cdot}THF$ (Na−THF = 2.424(3) Å).[157]

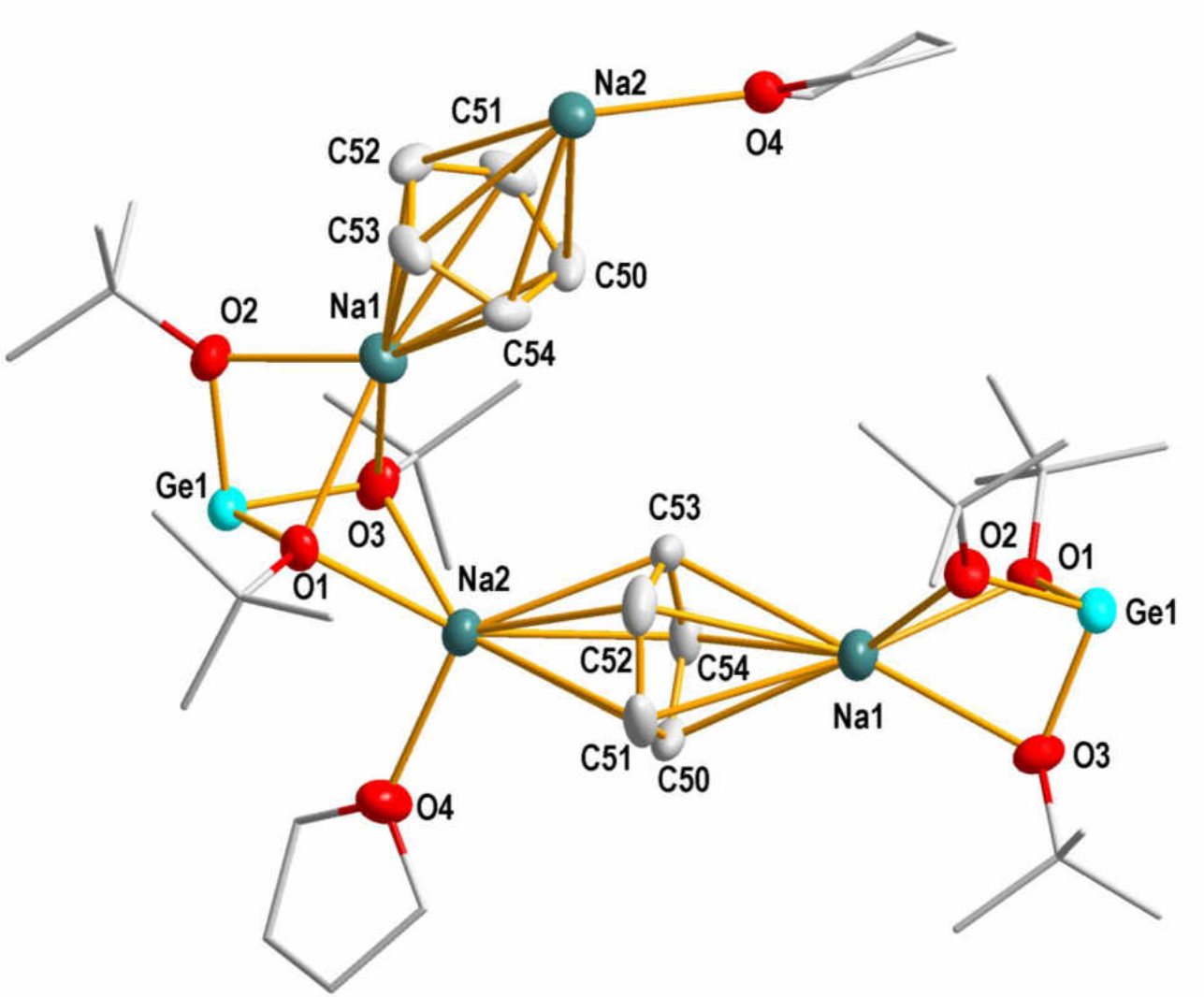

Figure 50. Solid-state structure and labeling scheme of **29**. With the exception of carbon (35%) all atoms are drawn at the 50% probability level.

Table 26. Crystal data for compound **29**

Molecular formula	$C_{21}H_{40}GeNa_2O_4$
fw	475.1
Crystal system	orthorhombic
Space-group	$P2_12_12_1$ (19)
a, Å	10.8074(6)
b,Å	14.7699(8)
c,Å	16.1477(9)
α, deg	90
β, deg	90
γ, deg	90
V, Å^3	2577.6(2)
Z	4
F(000)	1008
ρ(calc), g cm^{-3}	1.224
λ, Å	0.710 73
temp, K	173
μ, mm^{-1}	1.243
$R(F)^a$	0.0620
$R_W(F^2)^b$	0.0814

[a] $R = \sum|F_o - F_c| \quad |F|_o$. [b] $R_w = \{[\quad w(F_o^2 - F_c^2)] / [\sum w(F_o^2)^2]\}^{1/2}$; $w = 1/[\sigma^2(F_o)^2 + (xP)^2 + yP]$, where $P = (F_o^2 + 2F_c^2)/3$.

Table 27. Selected bond lengths (Å) and angles (°) for **29**

Bond Lengths			
Na1−O1	2.482(2)	Na1−C(50−54)	2.695(4)
Na1−O2	2.284(2)	Na2−C(50−54)	2.732(4)
Na1−O3	2.477(18)	Ge1−O1	1.909 (17)
Na2—O1	2.375(2)	Ge1−O2	1.880(19)
Na2−O3	2.383(19)	Ge1−O3	1.894(17)
Na2−O4	2.352(3)		
Bond Angles			
O2−Ge1−O1	92.82(9)	O1−Na1−O3	59.44(7)
O3−Ge1−O1	80.55(7)	O2−Na1−O3	68.82(7)
O3−Ge1−O2	91.15(8)	O1−Na2−O3	59.44(6)
O1−Na1−O2	70.19(7)		

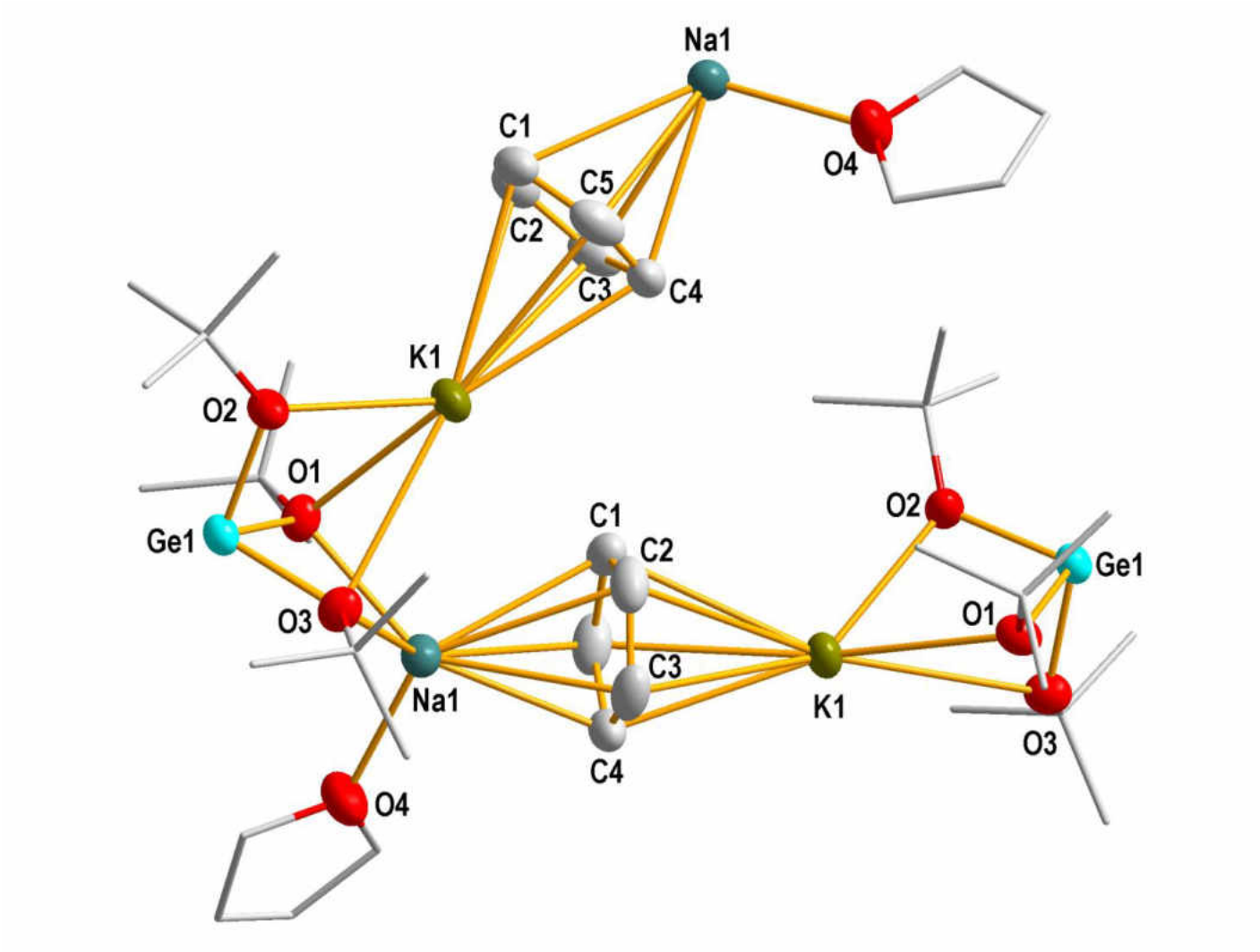

Figure 51. Solid-state structure and labeling scheme of **30**.With the exception of carbon (35%) all atoms are drawn at the 50% probability level.

Table 28. Crystal data for compound **30**

Molecular formula	$C_{21}H_{40}GeKNaO_4$
fw	491.25
Crystal system	monoclinic
Space-group	$P2_1/n$(14)
a, Å	9.3796(3)
b,Å	10.3730(3)
c,Å	27.1734(8)
α, deg	90
β, deg	93.949(2)
γ, deg	90
V, Å^3	2637.55(14)
Z	4
F(000)	1036
ρ(calc), g cm^{-3}	1.234
λ, Å	0.710 73
temp, K	173
μ, mm^{-1}	1.356
$R(F)$[a]	0.0578
$R_W(F^2)$[b]	0.1011

[a] $R = \sum|F_o - F_c| \quad |F|_o$. [b] $R_w = \{[\quad w(F_o^2 - F_c^2)] / [\sum w(F_o^2)^2]\}^{1/2}$; $w = 1/[\sigma^2(F_o)^2 + (xP)^2 + yP]$, where $P = (F_o^2 + 2F_c^2)/3$.

Table 29. Selected bond lengths (Å) and angles (°) for **30**

Bond Lengths			
K1−O1	2.814(2)	K1−C(1−5)	3.072(4)
K1−O2	2.583(2)	Na1−C(1−5)	2.784(4)
K1−O3	3.150(2)	Ge1−O1	1.919(2)
Na1—O1	2.365(3)	Ge1−O2	1.891(2)
Na1−O3	2.290(2)	Ge1−O3	1.895(2)
Na1−O4	2.316(3)		
Bond Angles			
O2−Ge1−O1	94.35(10)	O1−K1−O2	62.20(7)
O3−Ge1−O1	82.38(9)	O1−K1−O3	49.42(6)
O3−Ge1−O2	92.77(10)	O2−K2−O3	56.08(6)
O1−Na1−O3	65.29(8)		

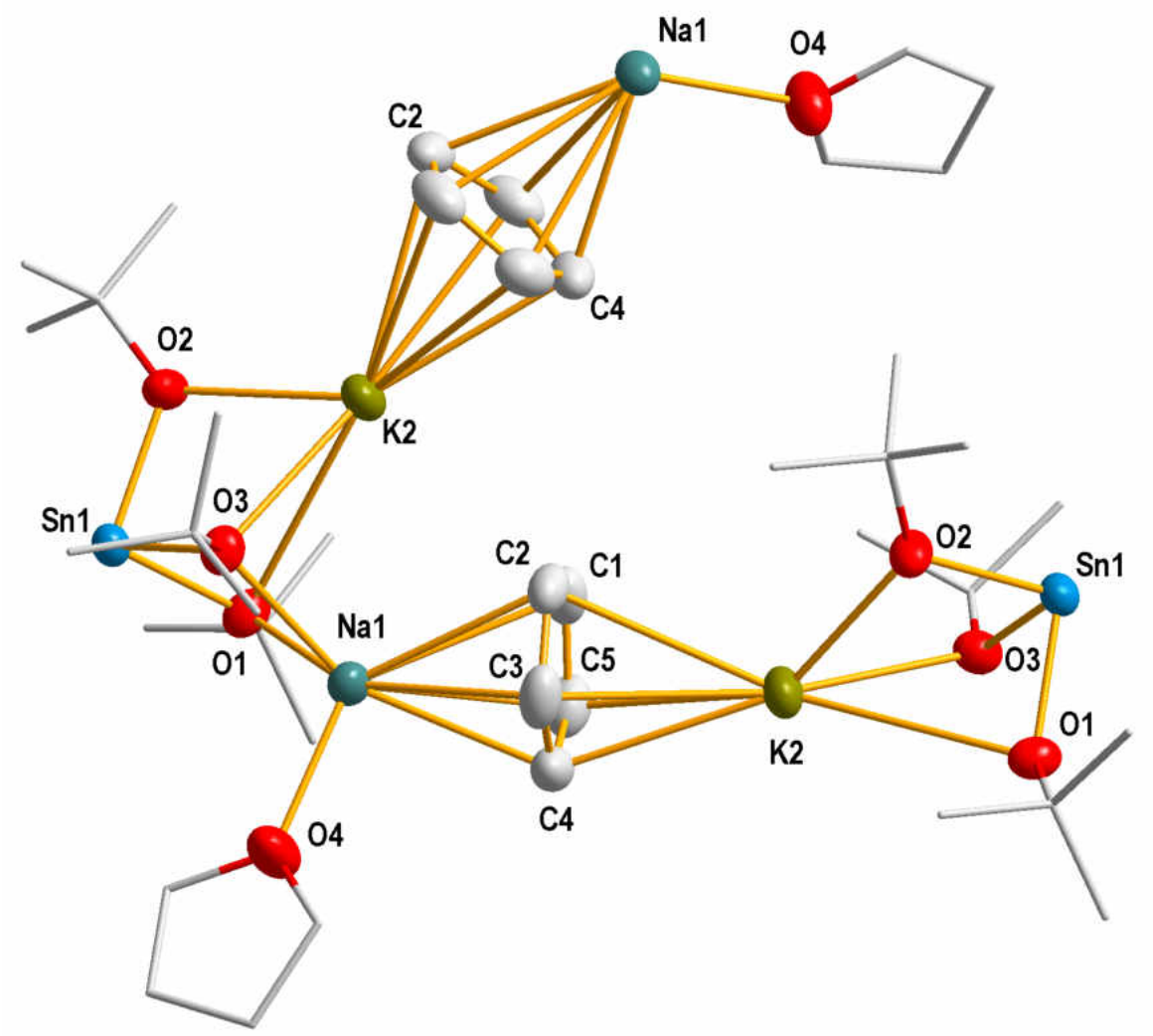

Figure 52. Solid-state structure and labeling scheme of **31**.With the exception of carbon (35%) all atoms are drawn at the 50% probability level.

Table 30. Crystal data for compound **31**

Molecular formula	$C_{21}H_{37}KNaO_4Sn$
fw	534.29 g/mol
Crystal system	monoclinic
Space-group	$P2_1/n$(14)
a, Å	9.3598(4)
b,Å	10.4865(4)
c,Å	27.3505(11)
α, deg	90
β, deg	92.985(2)
γ, deg	90
V, Å^3	2680.85(19)
Z	4
F(000)	1100
ρ(calc), g cm^{-3}	1.324
λ, Å	0.710 73
temp, K	173
μ, mm^{-1}	1.145
$R(F)$[a]	0.0452
$R_W(F^2)$[b]	0.1030

[a] $R = \sum|F_o - F_c| \quad |F|_o$. [b] $R_w = \{[\quad w(F_o^2 - F_c^2)] / [\sum w(F_o^2)^2]\}^{1/2}$; $w = 1/[\sigma^2(F_o)^2 + (xP)^2 + yP]$, where $P = (F_o^2 + 2F_c^2)/3$.

Table 31. Selected bond lengths (Å) and angles (°) for **31**

Bond Lengths			
K2−O1	3.273(3)	K2−C(1−5)	3.068(4)
K2−O2	2.586(3)	Na1−C(1−5)	2.783(4)
K2−O3	2.786(3)	Sn1−O1	2.074(2)
Na1—O1	2.286(3)	Sn1−O2	2.069(2)
Na1−O3	2.380(3)	Sn1−O3	2.094(2)
Na1−O4	2.323(3)		
Bond Angles			
O2−Sn1−O1	89.62(10)	O1−K1−O2	58.38(7)
O3−Sn1−O1	79.53(9)	O1−K1−O3	51.44(6)
O3−Sn1−O2	90.66(10)	O2−K2−O3	66.74(7)
O1−Na1−O3	69.65(9)		

3. Synthesis and Spectroscopic Analysis of $[KCp(THF)_2KSn(O^tBu)_3]_\infty$, 32

Compound **32** was synthesized by mixing equimolar amounts of KCp and $KSn(O^tBu)_3$ in THF (Scheme 23).

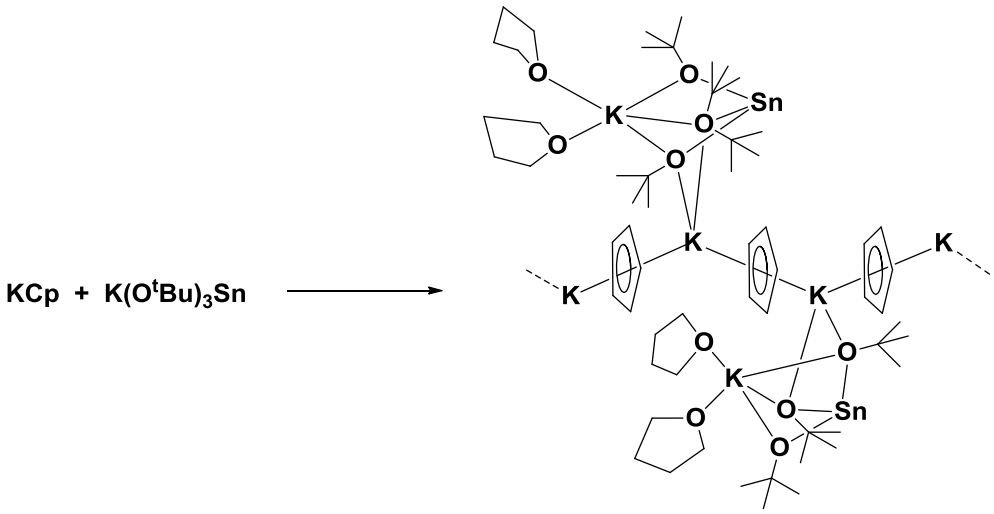

Scheme 23. Synthesis of compounds **32**.

Compound **32** was characterized by NMR spectroscopy (Figure 53). The ^1H NMR spectrum of **32** is very similar to that of **29**–**31**, except for the THF signals which were much more intense, reflecting of the greater number of coordinated THF molecules. The Cp protons were observed as a sharp singlet at 6.33 ppm, while the different *tert*-butoxy protons were observed as a singlet at 1.36 ppm, and the methylene protons of the coordinated THF molecules appeared as triplets at 3.57 and 1.42 ppm. The ^{13}C NMR spectrum had five peaks, with the signals at 106.7 ppm assigned to the Cp carbon atoms, those at 70.2 and 35.9 ppm assigned to the quaternary and primary carbons of the *tert*-butoxy group, respectively and those at 68.21 and 26.20 ppm attributed, respectively, to the different methylene carbons on the coordinated THF molecules.

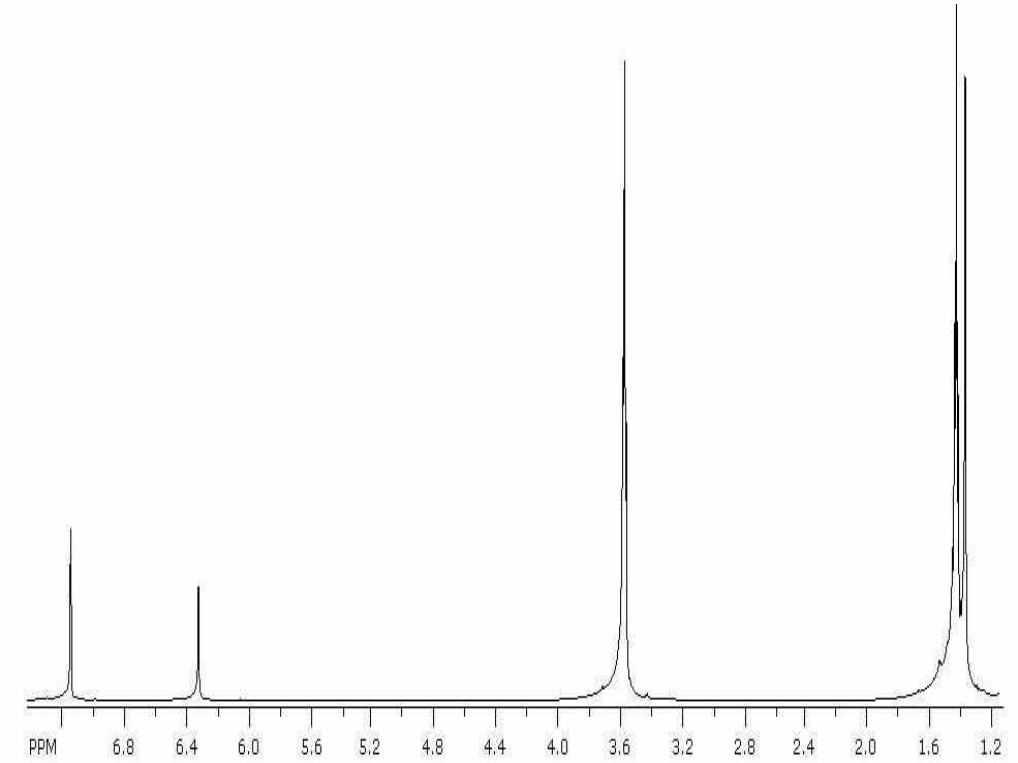

Figure 53. ^{1}H NMR spectrum of **32**

4. Solid-state Structure of $[KCp(THF)_2KSn(O^tBu)_3]_\infty$, 32

Compound **32** crystallized in the monoclinic crystal system with space group *Pn* and two molecules in the unit cell. Supplemental crystallographic data are given in Tables 32 and 33.

The solid-state structure of compound **32** is shown in Figure 54. The structure adopted by the compound is different from those of complexes **29**-**31**. The difference in structure between the compounds can be attributed to the larger size of potassium and hence a larger coordination number is needed to saturate the different potassium metal center and this is made possible by the observed structure. The asymmetric unit in the polymer is made up of $KSn(O^tBu)_3$, KCp, KCp, and $KSn(O^tBu)_3$. The backbone of the polymer is made up of repeating KCp units, which are arranged in a zig-zag manner.

There are therefore four crystallographically unique potassium atoms: K1, K2, K3 and K4. K1 and K4 are the potassium atoms of the two crystallographic different tri(*tert*-butoxy)stannate units. Hence, they are each coordinated to three *tert*-butoxides and to two additional THF molecules. K2 and K3, on the other hand, are bilaterally η^5-coordinated to two Cp ligands and to two additional *tert*-butoxides.

The two different $KSn(O^tBu)_3$ units in **32** are very similar, with equivalent K–O^{t}Bu (average K1–O^{t}Bu = 2.741(4), average K4–O^{t}Bu = 2.732(4)), Sn–O^{t}Bu (average Sn1–O^{t}Bu = 2.073(3), average Sn2–O^{t}Bu = 2.072(4)), and K–THF bonds (average K1–THF = 2.741(4), average K2–THF = 2.735(4)). The Sn–O^{t}Bu bonds are similar to those observed in polymeric $[KSn(O^tBu)_3]_\infty$ (average Sn–O^{t}Bu = 2.067(5) Å, average K–O^{t}Bu = 2.942(6) Å) and polymeric $[K_4(C_5H_5)_2Sn_2(O^tBu)_6(dme)_2]_\infty$ (average Sn–O^{t}Bu = 2.069(2) Å, average K–O^{t}Bu = 2.717(4) Å).[58,162] On the other hand, the K–O^{t}Bu bonds are longer than that in $[K_4(C_5H_5)_2Sn_2(O^tBu)_6(dme)_2]_\infty$ but are considerably shorter than those in $[KSn(O^tBu)_3]_\infty$. The different K–Cp interactions are also very close and they are similar to those observed in other compounds.

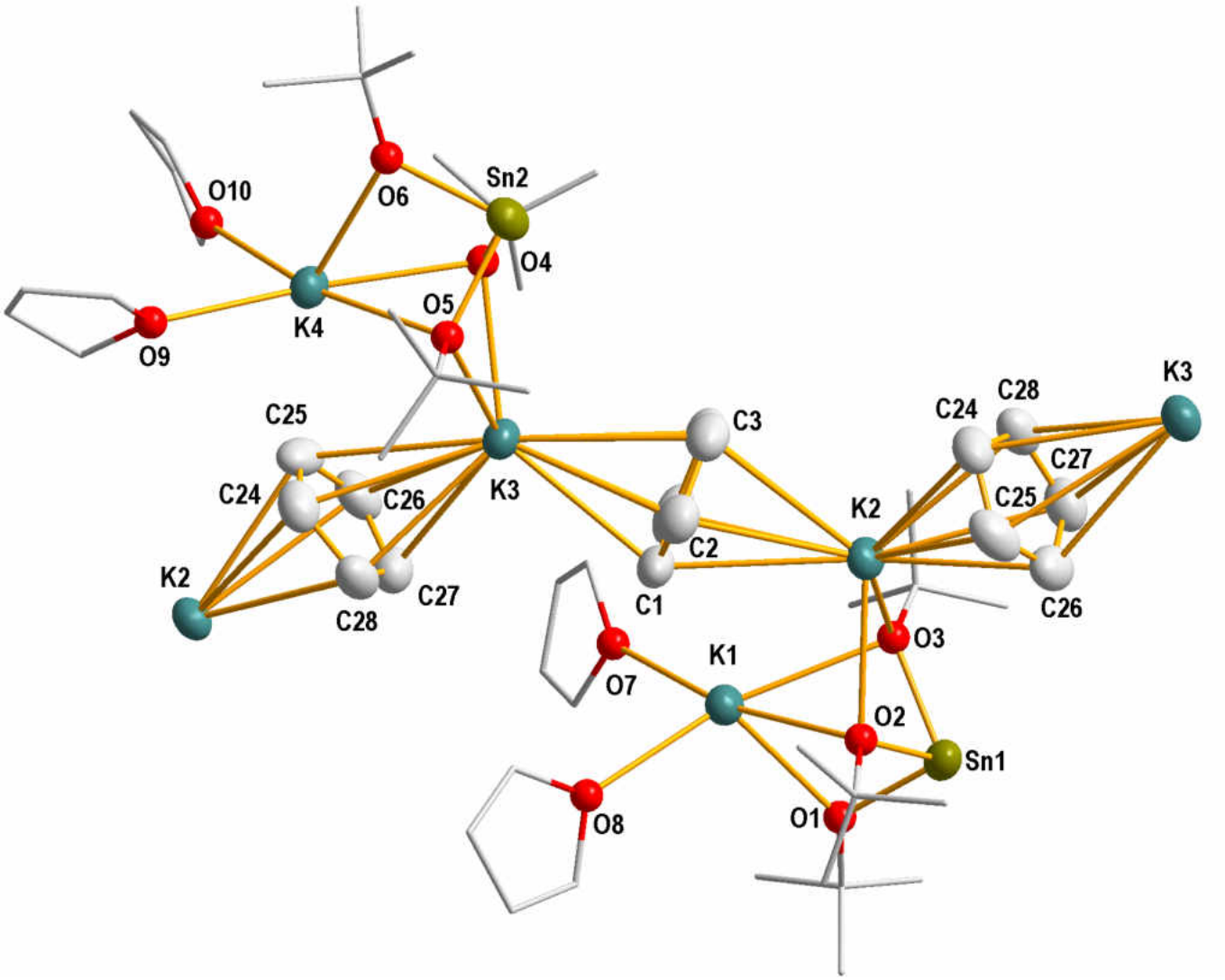

Figure 54. Solid-state structure and labeling scheme of **32**. With the exception of carbon (35%) all atoms are drawn at the 50% probability level

Table 32. Crystal data for compound **32**

Molecular formula	$C_{50}H_{96}K_4O_{10}Sn_2$
Fw	1251.12 g/mol
Crystal system	Monoclinic
Space-group	*Pn*(7)
a, Å	17.1071(6)
b,Å	10.3426(4)
c,Å	19.3863(7)
α, deg	90
β, deg	110.592(2)
γ, deg	90
V, Å^3	3210.9(2)
Z	2
F(000)	1286
ρ(calc), g cm^{-3}	1.285
λ, Å	0.710 73
temp, K	173
μ, mm^{-1}	1.082
$R(F)^a$	0.0381
$R_W(F^2)^b$	0.0920

[a] $R = \sum|F_o - F_c| \quad |F|_o$. [b] $R_w = \{[\quad w(F_o^2 - F_c^2)] / [\sum w(F_o^2)^2]\}^{1/2}$; $w = 1/[\sigma^2(F_o)^2 + (xP)^2 + yP]$, where $P = (F_o^2 + 2F_c^2)/3$

Table 33. Selected bond lengths (Å) and angles (°) for **32**

Bond Lengths			
K1−O1	2.616(3)	K4−O9	2.693(5)
K1−O2	2.784(3)	K4−O10	2.771(3)
K1−O3	2.802(3)	K2−C(1−5)	3.179(4)
K1−O7	2.758(4)	K2−C(24−28)	3.136(4)
K1−O8	2.723(4)	K3−C(1−5)	3.153(4)
K2−O2	2.802(3)	K2−C(24−28)	3.222(4)
K2−O3	2.782(3)	Sn1−O1	2.074(3)
K3−O4	2.741(3)	Sn1−O2	2.073(3)
K3−O5	2.763(3)	Sn1−O3	2.077(2)
K4−O4	2.770(3)	Sn2−O4	2.072(2)
K4−O5	2.784(2)	Sn2−O5	2.071(3)
K4−O6	2.642(3)	Sn2−O5	2.072(3)
Bond Angles			
O2−Sn1−O1	89.56(12)	O2−K1−O3	56.75(7)
O3−Sn1−O1	89.55(11)	O7−K1−O8	87.81(17)
O3−Sn1−O2	79.53(10)	O4−K4−O5	57.14(7)
O4−Sn2−O5	79.76(10)	O4−K4−O6	65.24(9)
O4−Sn2−O6	89.6(1)	O5−K4−O6	65.05(8)
O5−Sn2−O6	89.62(11)	O9−K4−O10	81.52(16)
O1−K1−O2	65.43(10)	O2−K2−O3	56.76(7)
O1−K1−O3	65.21(8)	O4−K3−O5	57.71(7)

Summary and Conclusion

The simple and straightforward combination of alkali-metal cyclopentadienides and alkoxometalates yields new mixed-ligand ($Cp^{-}/O^{t}Bu^{-}$) heterometallic coordination polymers, in which the alkoxide and Cp ligands serve as linkers between metal centers. Two structures are possible based on the group 1 metal cation present in both salts. A combination of salts of sodium and potassium gave similar structures, $[MCp(THF)ME(O^{t}Bu)_3]_\infty$ **29–31**, in which the NaCps, which had a THF molecule coordinated to the sodium atoms, were linked by the potassium salts, a mode of crystallization of NaCp which has never been observed before. On the other hand, when both salts contained the larger potassium cation, a different structure was obtained, $[MCp(THF)_2ME(O^{t}Bu)_3]_\infty$ **32,** in which the KCps were linked together in the polymer backbone and the coordination requirements of the potassium was fulfilled by coordination to two of the *tert*-butoxides of the alkoxometallate unit. The difference in the adopted structures was due to the larger size of potassium.

The utility of group 1 salts as synthetic precursors highlights the syntheses of the double salts reported. The double salts could also be used to synthesize mixed half-sandwiched metal complexes of the type $CpM[(O^{t}Bu)_3E$.

Appendix

List of Synthesized Compounds

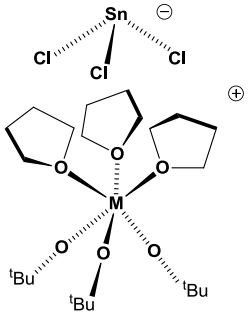

M = Zr (**6**), M = Hf (**7**)

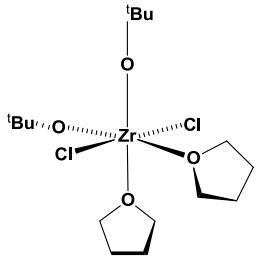

M = Zr (**8**), M = Hf (**9**)

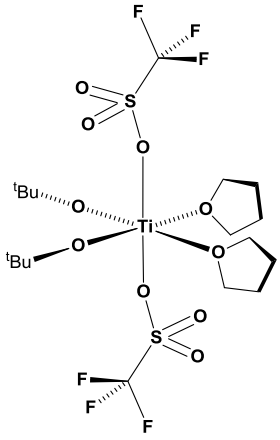

10

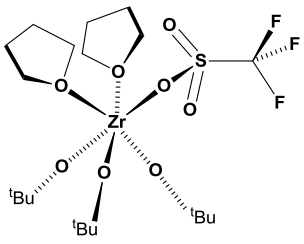

11

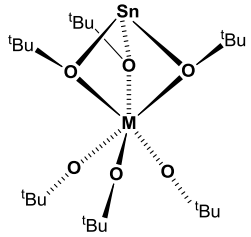

M = Zr (**12**), M = Hf (**13**)

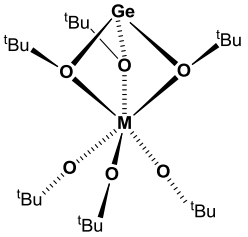

M = Zr (**14**), M = Hf (**15**)

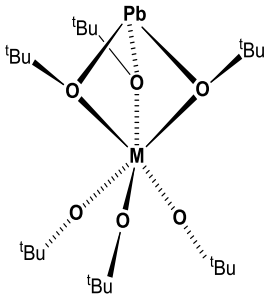

M = Zr (**16**), M = Hf (**17**)

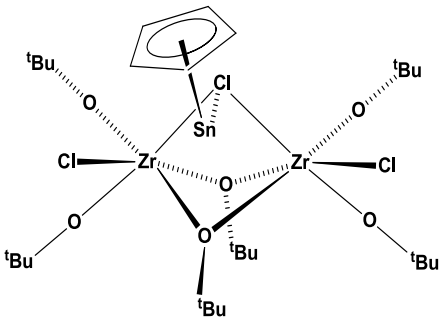

19

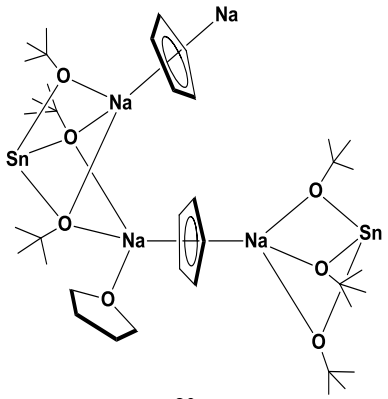

20

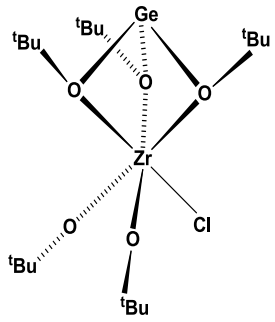

21

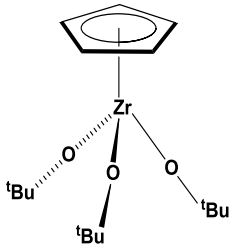

22

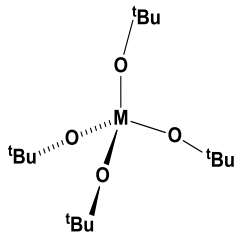

M = Ti (**24**), Zr (**25**)

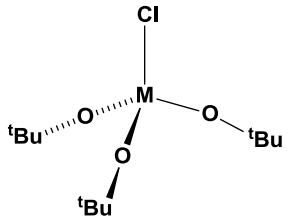

M = Ti (**26**), Zr (**27**)

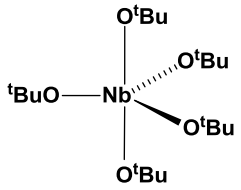

28

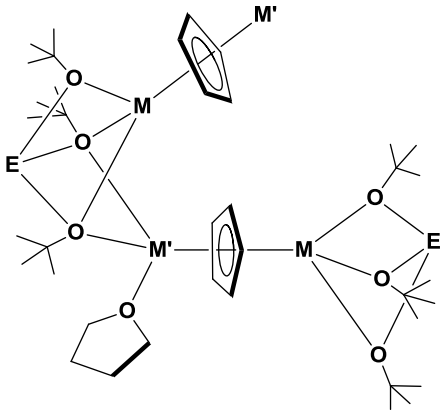

M = Na, M' = Na, E = Ge, **29**
M = K, M' = Na, E = Ge, **30**
M = K, M' = Na, E = Sn, **31**

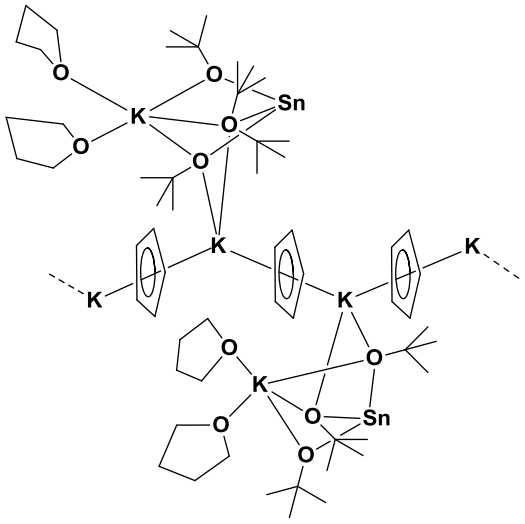

32

References

1. Bradley, D. C.; Mehrotra, E. C.; Rothwell, I. P.; Singh, A. *Alkoxo and Aryloxo Derivatives of Metals*; Academic Press: San Diego, 2001.

2. Turova, N. Y.; Turevskaya, E. P.; Kessler, V. G.; Yanovskaya, M. I. *The Chemistry of Metal Alkoxides*; Kluwer Academic Publishers: Dordrecht, 2002.

3. Mäntymäki, M.; Ritala, M.; Leskelä, M. *Coord. Chem. Rev*. **2012**, *256*, 854–887.

4. Ottley, L. A. M.; Boyle, T. J. *Chem. Rev*. **2008**, *108*, 1896–1917.

5. King, S. J.; Carmalt, C. J. *Coord. Chem. Rev*. **2006**, *250*, 682–709.

6. Hubert-Pfalzgraf, L. G. *Coord. Chem. Rev*. **1998**, *178–180*, 967–997.

7. Veith, M.; Mathur, S.; Mathur, C. *Polyhedron* **1998**, *17*, 1005−1034.

8. Mehrotra, R. C.; Singh, A.; Sogani, S. *Chem. Rev*. **1994**, *94*, 1643–1660.

9. Veith, M.; Weidner, S.; Kunze, K.; Käfer, D.; Hans, J.; Huch, V. *Coord. Chem. Rev*. **1994**, *137*, 297–322.

10. Chandler, C. D.; Roger, C.; Hampden-Smith, M. J. *Chem. Rev*. **1993**, *93*, 1205–1241.

11. Caulton, K. G.; Hubert-Pfalzgraf, L. G. *Chem. Rev*. **1990**, *90*, 969–995.

12. Terry, K. W.; Tilley, T. D.; Rheingold, A. L. *Polyhedron* **1998**, *17*, 891−897.

13. Athar, T.; Kwon, J. O.; Seok, S. *Appl. Organometal. Chem*. **2005**, *19*, 964−970.

14. John, L.; Sobota, P. *Alkoxide Molecular Precursors for Nanomaterials: A One Step Strategy for Oxide Ceramics*; Ceramic Materials; Intech: September 2010.

15. Krishnan, V.; Gross, S.; Müller, S.; Armelao, L.; Tondello, E.; Bertagnolli, H. *J. Phys. Chem.* B **2007**, *111*, 7519−7528.

16. Veith, M.; Haas, M.; Huch, V. *Chem. Mater*. **2005**, *17*, 95−101.

17. Kuhlman, R.; Vaartstra, B. A.; Streib, W. E.; Huffman, J. C.; Caulton, K. G. *Inorg. Chem.* **1993**, *32*, 1272−1278.

18. Hofman, R.; Westheim, J. G. F.; Haanappel, V. A. C.; Fransen, T.; Gellings, P. J. *Thermochimica Acta* **1993**, *215*, 329−335.

19. Cui, D.; Nishiura, M.; Tardif, O.; Hou, Z. *Organometallics* **2008**, *27*, 2428−2435.

20. Schrock, R. R. *Polyhedron* **1995**, *22*, 3177−3195.

21. Njua, E. Y.; Steiner, A.; Stahl, L. *Inorg. Chem.* **2010**, *49*, 2163−2172.

22. Katsuki, T.; Sharpless, K. B. *J. Am. Chem. Soc.* **1980**, *102*, 5974–5976.

23. Wengrovius, J. H.; Sancho, J.; Schrock, R. R. *J. Am. Chem. Soc.* **1981**, *103*, 3932–3934.

24. Lubben, T. V.; Wolczanski, P. T.; Duyne, G. D. *J. Am. Chem. Soc.* **1984**, *3*, 977–983.

25. LaPointe, R. E.; Wolczanski, P. T.; Duyne, G. D. *J. Am. Chem. Soc.* **1985**, *4*, 1810–1818.

26. Yamasaki, S.; Kanai, M.; Shibasaki, M. *Chem. Eur. J.* **2001**, *7*, 4066–4072.

27. Marquet, N.; Kirillov, E.; Roisnel, T.; Razavi, A.; Carpentier, J-F. *Organometallics* **2009**, *28*, 606−620.

28. Ruhlandt-Senge, K.; Bartlett, R. A.; Olmstead, M. M.; Power, P. P. *Inorg. Chem.* **1993**, *32*, 1724−1728.

29. Bell, N. A.; Coates, G. E.; Shearer, H. M. M.; Twiss, J. *J. Chem. Soc., Chem. Commun*. **1983**, 840–841.

30. Centinkaya, B.; Gümrükcü, I.; Lappert, M. F.; Atwood, J. L.; Rogers, R. D.; Zaworotko, M. J. *J. Am. Chem. Soc.* **1980**, *102*, 2088–2089.

31. Chisholm, M. H.; Clark, D. L.; Folting, K.; Huffman, J. C.; Hampden-Smith, M. *J. Am. Chem. Soc.* **1987**, *4*, 7750–7761.

32. Veith, M.; Töllner, F. *J. Organomet. Chem.* **1983**, *246*, 219–226.

33. Veith, M.; Kunze, K. *Angew. Chem. Int. Ed. Engl.* **1991**, *30*, 95–97.

34. Veith, M.; Rösler, R. *Angew. Chem. Int. Ed. Engl.* **1982**, *21*, 858–859.

35. Beck, G.; Hitchcock, P. B.; Lappert, M. F.; Mackinnon, I. A. *J. Chem. Soc., Chem. Commun*. **1989**, 1312–1314.

36. Pinkerton, A. A.; Schwarzenbach, D.; Hubert-Pfalzgraf, L. G.; Riess, J. G. *Inorg. Chem.* **1976**, *15*, 1196−1199.

37. Yanovsky, A. I.; Turevskaya, E. P.; Turova, N. Y.; Dolgushin, F. M.; Pisarevsky, A. P.; Batzanov A. S.; Stuchkov, Y. T. *Russ. J. Inorg. Chem*. **1994**, *39*, 1307–1315.

38. Goel, S. C.; Chiang, M. Y.; Buhro, W. E. *Inorg. Chem.* **1990**, *29*, 4640−4646.

39. Veith, M.; Mathur, S.; Huch, V.; Decker, T. *Eur. J. Inorg. Chem.* **1998**, 1327−1332.

40. Weiss, E.; Alsdorf, H.; Kühr, H. *Angew. Chem. Int. Ed. Engl.* **1967**, *6*, 801–802.

41. Sadurski, E. A.; Ilsley, W. H.; Thomas, R. D.; Glick, M. D.; Oliver, J. P. *J. Am. Chem. Soc.* **1978**, *100*, 7761–7762.

42. Drake, S. R.; Streib, W. E.; Chisholm, M. H.; Caulton, K. G. *Inorg. Chem.* **1990**, *29*, 2707−2708.

43. Goel, S. C.; Hollingsworth, J. A.; Beatty, A. M.; Robinson, K. D.; Buhro, W. E. *Polyhedron* **1998**, *17*, 781−790.

44. Neumüller, B. *Chem. Soc. Rev*. **2003**, *32*, 50−55.

45. Atwood, D. A.; Jieger, J. A.; Liu, S.; Rutherford, D.; Wei, P.; Tucker, R. B. *Organometallics* **1999**, *18*, 976−981.

46. Wijk, M.; Norrestam, R.; Nygren, M.; Westin, G. *Inorg. Chem.* **1996**, *35*, 1077−1079.

47. Westin, G.; Moustiakimov, M.; Kritikos, M. *Inorg. Chem.* **2002**, *41*, 3249−3258.

48. Evans, W. J.; Golden, R. E.; Ziller, J. W. *Inorg. Chem.* **1993**, *32*, 3041−3051.

49. Hubert-Pfalzgraf, L. G.; Daniele, S.; Bennaceur, A.; Daran, J.-C.; Vaisermann, J. *Polyhedron* **1997**, *16*, 1223−1234.

50. Wolczanski, P. T. *Polyhedron* **1995**, *14*, 3335−3362.

51. Steffey, B. D.; Fanwick, P. E.; Rothwell, I. P. *Polyhedron* **1990**, *9*, 963−968.

52. Veith, M.; Hobein, P.; Rösler, R. *Z. Naturforsch.* **1989**, *44b*, 1067–1081.

53. Veith, M.; Hans, J.; Stahl, L.; May, P.; Huch, V.; Sebald, A. *Z. Naturforsch.* **1991**, *46b*, 403−424.

54. Veith, M. *Chem. Rev*. **1990**, *90,* 3−16.

55. Veith, M.; Kafer, D.; Koch, J.; Stahl, L.; Huch, V. *Chem. Ber*. **1992**, *125*, 1033−1042.

56. Teff, D. J.; Huffman, J. C.; Caulton, K. G. *Inorg. Chem.* **1996**, *35*, 2981−2987.

57. Manzer, L. E. *Inorg. Syn.* **1982**, *21*, 135−140.

58. Veith, M.; Rösler, R. *Z. Naturforsch.* **1986**, *41b*, 1071−1080.

59. Selent, D.; Ramm, M.; Janiak, C. *J. Organomet. Chem.* **1995,** *501*, 235–244.

60. Siemens Analytical X-ray Systems, Madison, WI, 1995.

61. SADABS program for absorption corrections using the Bruker CCD Detector System. Based on: Blessing, R. H. *Acta Crystallogr., Sect. A,* **1995**, *51*, 33–38.

62. G. M. Sheldrick, *Acta Crystallogr., Sect. A,* **2008**, *64*, 112–122.

63. SHELXTL 5.10 (PC-Version*),* Siemens Analytical X-Ray Instruments, Inc. Madison, WI, 1998.

64. SHELXTL NT Version 5.10, Program Library for Structure Solution and Molecular Graphics*,* Bruker Analytical X-ray Systems, Madison, WI, 1999.

65. Teff, D. J.; Huffman, J. C.; Caulton, K. G. *Inorg. Chem.* **1994**, *33*, 6289−6292.

66. Heyn, R. H.; Tilley, T. D. *Inorg. Chem.* **1989**, *28*, 1768−1769.

67. Collins, S.; Koene, B. E.; Ramachandran, R.; Taylor, N. J. *Organometallics* **1991**, *10*, 2092–2094.

68. Jia, A.-Q.; Jin, G.-X. *Dalton Trans*. **2009**, 8838–8845.

69. Veith, M.; Mathur, S.; Huch, V. *Chem. Commun*. 1**997**, 2197–2198.

70. Williams, P. A.; Roberts, J. L.; Jones, A. C.; Chalker, P. R.; Bickley, J. F.; Steiner, A.; Davies, H. O.; Leedham, T. J. *J. Mater. Chem*. **2002**, *12*, 165–167.

71. Saha, T. K.; Ramkumar, V.; Chakraborty, D. *Inorg. Chem.* **2011**, *50*, 2720−2722.

72. Yasuda, H.; Nakayama, Y.; Takei, K.; Nakamura, A.; Kai, Y.; Kanehisa, N. *J. Organomet. Chem.* **1994,** *473*, 105–116.

73. Wu, Z.; Diminnie, J. B.; Xu, Z. *Organometallics* **1998**, *17*, 2917–2920.

74. Cole, S. C.; Coles, M. P.; Hitchcock, P. B. *Organometallics* **2005**, *24*, 3279–3289.

75. Rivard, E.; McWilliam, A. R.; Lough, A. J.; Manners, I. *J. Chem. Soc., Dalton Trans*. **2002**, 2173–2179.

76. Galeffi, B.; Simard, M.; Wuest, J. D. *Inorg. Chem.* **1990**, *29*, 955−958.

77. Schweder, B.; Görls, H.; Walther, D. *Inorg. Chim. Acta* **1999**, *286*, 14−23.

78. Loo, Y. F.; O'Kane, R.; Jones, A. C.; Aspinall, H. C.; Potter, R. J.; Chalker, P. R.; Bickley, J. F.; Taylor, S.; Smith, L. M. *J. Mater. Chem.* **2005**, *15*, 1896−1902.

79. Williams, P. A.; Roberts, J. L.; Jones, A. C.; Chalker, P. R.; Bickley, J. F.; Steiner, A.; Davies, H. O.; Leedham, T. J. *J. Mater. Chem.* **2002**, *12*, 165−167.

80. Alvanipour, A.; Atwood, J. L.; Bott, S. G.; Junk, P. C.; Kynast, U. H.; Prinz, H. *J. Chem. Soc., Dalton Trans*. **1998**, 1223–1228.

81. Liu, F.-Q.; Usón, I.; Roesky, H. W. *Z. Anorg. Allg. Chem*. **1996**, *622*, 819–822.

82. Donzelli, A.; Potvin, P. G. *Inorg. Chem.* **2009**, *48*, 4171−4178.

83. Boyle, T. J.; Ottley, L. A. M.; Rodriguez, M. A. *Polyhedron* **2008**, *27*, 3079−3084.

84. Kessler, M.; Hansen, S.; Hollman, D.; Klahn, M.; Beweries, T.; Spannenberg, A.; Rosenthal, U. *Eur. J. Inorg. Chem*. **2001**, 627−631.

85. Kongprakaiwoot, N.; Armstrong, J. B.; Noll, B. C.; Brown, S. N. *Dalton Trans*. **2010**, *39*, 10105−10115.

86. Bos, K. D.; Bulten, E. J.; Noltes, J. G.; Spek, A. L. *J. Organomet. Chem.* **1975,** *99*, 71–77.

87. Bos, K. D.; Bulten, E. J.; Noltes, J. G. *J. Organomet. Chem.* **1972,** *39*, C52–C55.

88. Herber, R. H.; Carrasquillo, G. *Inorg. Chem.* **1981**, *20*, 3693−3697.

89. Hough, E.; Nicholson, D. G.; Vasudevan, A. K. *J. Chem. Soc., Dalton Trans.* **1989**, 2155−2159.

90. Hermann, H.; Gehrman, T.; Wadepohl, H.; Gade, L. H. *Dalton Trans*. **2008**, *39*, 6231−6241.

91. Dorn, H.; Shah, S. A.; Noltemeyer, M.; Schmidt, H.-G.; Roesky, H. W. *J. Fluorine Chem*. **1998**, *88*, 195−199.

92. Hernandez-Gruel, M. A.; Pérez-Torente, J. J.; Ciriano, M. A.; López, J. A.; Lahoz, F. J.; Oro, L. A. *Eur. J. Inorg. Chem*. **1999**, 2047−2050.

93. Lee, W.-Y.; Hsieh, C.-C.; Hsu, J.-W.; Datta, A.; Lin, Y.-C.; Huang, J.-H.; Lee, T.-Y. *J. Organomet. Chem.* **2011,** *696*, 3816–3821.

94. Siemeling, U. *Chem*. *Rev*. **2000**, *100*, 1495–1526.

95. Maynadie, J.; Berthet, J-C.; Thuery, P.; Ephritikhine, M. *Chem. Comm.* **2007**, 486−488.

96. Xie, Z. *Acc*. *Chem*. *Res*. **2003**, *36*, 1−9.

97. Hsiao, T-J.; Tsai, J.-C. *J*. *Appl*. *Polym*. *Sci*. **2010**, *116*, 2040−2049.

98. Pupi, R. M.; Coalter, J. N.; Petersen, J. L. *J*. *Organomet*. *Chem*. **1995**, *495*, 17−25.

99. Sanz, M.; Cuenca, T.; Mikhail, G.; Grassi, A.; Bott, R. K.; Hughes, D. L.; Lancaster, S. J.; Bochmann, M. *Organometallics* **2004**, *23*, 5324−5331.

100. Dove, A. P.; Xie, X.; Waymouth, M. *Chem. Comm.* **2005**, 2152−2154.

101. Sabota, P.; Utko, J.; John, Ł.; Jerzykiewciz, L. B.; Drąg-Jarząbek, A. *Inorg*. *Chem*. **2008**, *47*, 7939−7941.

102. Tsai, J.-C.; Kuo, J. C.; Chen, Y.-C. *J. Polym. Sci. Part A*: *Polym. Chem.* **2005**, *43*, 2304–2315.

103. Elschenbroich, C. *Organometallics 3rd Ed.*; Wiley-VCH: Weinheim, 2006.

104. Wailes, P. C.; Coutts, R. S.; Weigold, H. *Organometallic Chemistry of Titanium, Zirconium and Hafnium*; Academic Press: New York and London, 1974.

105. Lebedev, A. Y.; Izmer, V. V.; Asachenko, A. F.; Tzarev, A. A.; Uborsky, D. V.; Humotova, Y. A.; Shperber, E. R.; Canich, J. A. M.; Voskoboynikov, A. Z. *Organometallics* **2009**, *28*, 1800−1816.

106. Napoli, M.; Ricciardi, R.; Memoli, A.; Longo, P. *J. Polym. Sci. Part A*: *Polym. Chem.* **2008**, *46*, 1476–1487.

107. Knobloch, D. J.; Lobkovsky, E.; Chirik, P. J. *J. Am. Chem. Soc.* **2010**, *132*, 10553–10564.

108. Chirik, P. J. *Organometallics* **2010**, *29*, 1500−1517.

109. Stoebenau, E. J.; Jordan, R. F. *J. Am. Chem. Soc.* **2006**, *128*, 8162–8175.

110. Gott, A. L.; Clark, A. J.; Clarkson, G. J.; Munslow, I. J.; Wade, A. R.; Scott, P. *Organometallics* **2008**, *27*, 2706−2714.

111. Njua, E. Y.; Steiner, A.; Stahl, L. *J. Organomet. Chem.* **2011**, *696*, 3301−3306.

112. Schäfer, A.; Karl, E.; Zsolnai, L.; Huttner, G.; Brintzinger, H. H. *J. Organomet. Chem.* **1987**, *328*, 87–89.

113. Deck, P. A.; Fisher, T. S.; Downey, J. S. *Organometallics* **1997**, *16*, 1193−1196.

114. Sobota, P.; Drąg-Jarząbek, A.; John, Ł.; Utko, J.; Jerzykiewciz, L. B.; Duczmal, M. *Inorg. Chem.* **2009**, *48*, 6584–6593.

115. Toney, J. H.; Marks, T. J. *J. Am. Chem. Soc.* **1985**, *107*, 947–953.

116. Alvarez, C. S.; Bond, A. D.; Harron, E. A.; Layfield, R. A.; McAllister, J. A.; Pask, C. M.; Rawson, J. M.; Wright, D. S. *Organometallics* **2001**, *20*, 4135–4137.

117. Casado, M. A.; Ciriano, M. A.; Edwards, A. J.; Lahoz, F. J.; Perez-Torrente, J. J.; Oro, L. A. *Organometallics* **1998**, *17*, 3414–3416.

118. Gorsich, R. D. *J. Am. Chem. Soc.* **1960**, *82*, 4211–4214.

119. Reger, D. L.; Mahtab, R.; Baxter, J. C.; Lebioda, L. *Inorg. Chem.* **1986**, *25*, 2046–2048.

120. Kim, Y.; Jnaneshwara, G. K.; Verkade, J. G. *Inorg. Chem.* **2003**, *42*, 1437–1447.

121. Johnson, J. S.; Bergman, R. G. *J. Am. Chem. Soc.* **2001**, *123*, 2923–2924.

122. Augustin, D.; Rima, G.; Gornitzka, H.; Barrau, J. *Organometallics* **2000**, *19*, 4276–4282.

123. Michalczyk, L.; de Gala, S.; Bruno, J. W. *Organometallics* **2001**, *20*, 5547–5556.

124. Werner, H. *Angew. Chem. Int. Ed. Engl.* **1977**, *16*, 1–9.

125. Casey, C. P.; O'Conner, J. M.; Haller, K. J. *J. Am. Chem. Soc.* **1985**, *105*, 1241–1246.

126. Veith, M.; Mathur, C.; Mathur, S.; Huch, V. *Organometallics* **1997**, *16*, 1292–1299.

127. Lorber, C.; Choukroun, R.; Vendier, L. *Organometallics* **2008**, *27*, 5017–5024.

128. Dinnebier, R. E.; Behrens, U.; Olbrich, F. *Organometallics* **1997**, *16*, 3855–3858.

129. Aoyagi, T.; Shearer, H. M. M.; Wade, K.; Whitehead, G. *J. Organomet. Chem.* **1979**, *175*, 21–31.

130. Scribelli, J. V.; Curtis, M. D. *J. Am. Chem. Soc.* **1973**, *95*, 924–925.

131. Dusausoy, Y.; Prots, J.; Renaut, P.; Gautheron, B.; Tainturier, G. *J. Organomet. Chem.* **1978**, *157*, 167–172.

132. Bradley, D. C.; Mehrotra, R. C.; Wardlaw, W. *J. Chem. Soc.* **1952**, 4204–4209.

133. Mehrotra, R. C. *J. Am. Chem. Soc.* **1954**, *76*, 2266–2267.

134. Mehrotra, R. C.; Kapoor, P. N. *J. Less-Common Met.* **1964**, *7*, 98–101.

135. Kapoor, P. N.; Mehrotra, R. C. *J. Less-Common Met.* **1966**, *10*, 66–70.

136. Lappert, M.; Power, P.; Protchenko, A.; Seeber, A. Metal Amide Chemistry; John Wiley and Sons, Ltd: West Sussex, 2009.

137. Thomas, I. M. *Can. J. Chem*. **1961**, *39*, 1386–1388.

138. Bradley, D. C. *Chem. Rev*. **1989**, *89*, 1317–1322.

139. Bradley, D. C.; Halim, F. M. A.-E.; Sadek, E. A.; Wardlaw, W. *J. Chem. Soc.* **1952**, 2032–2035.

140. Appel, L.; Fiz, R.; Tyrra, W.; Sanjay, M. *Dalton Trans*. **2012**, *41*, 1981–1990.

141. Tong, M.-L.; Hu, S.; Wang, J.; Kitagawa, S.; Ng, S. W. *Cryst. Growth Des.* **2005**, *5*, 837–839.

142. Silva, M. R.; Gwengo, C.; Lindeman, S. V.; Smith, M. D.; Gardinier, J. R. *Inorg. Chem.* **2006**, *45*, 10998–11007.

143. Ye, B.-H.; Tong, M.-L.; Chen, X.-M. *Coord. Chem. Rev*. **2005**, *249*, 545–565.

144. Knaust, J. M.; Keller, S. W. *Inorg. Chem.* **2002**, *41*, 5650–5652.

145. Wen, M.; Munakata, M.; Suenaga, Y.; Kuroda-Sowa, T.; Maekawa, M.; Yan, S. G. *Inorg. Chim. Acta* **2001**, *322*, 133–137.

146. Carlucci, L.; Ciani, G.; Proserpio, D. M. *Chem. Commun*. **1999**, 449–450.

147. Carlucci, L.; Ciani, G.; Macchi, P.; Proserpio, D. M.; Rizzato, S. *Chem. Eur. J.* **1999**, *5*, 237–243.

148. Morris, J. J.; Noll. B. C.; Honeyman, G. W.; O' Hara, C. T.; Kennedy, A. R.; Mulvey, R. E.; Henderson, K. W. *Chem. Eur. J.* **2007**, *13*, 4418–4432.

149. Ilkhechi, A. H.; Scheibitz, M.; Bolte, M.; Lerner, H.-W.; Wagner, M. *Polyhedron* **2004**, *23*, 2597–2604.

150. Ilkhechi, A. H.; Scheibitz, M.; Bolte, M.; Lerner, H.-W.; Wagner, M. *J. Organomet. Chem.* **2005**, *690*, 1971–1977.

151. Ilkhechi, A. H.; Mercero, J. M.; Silanes, I.; Bolte, M.; Scheibitz, M.; Lerner, H.-W.; Ugalde, J. M.; Wagner, M. *J. Am. Chem. Soc.* **2005**, *127*, 10656–10666.

152. Fromm, K. M. *Coord. Chem. Rev*. **2008**, *252*, 856–885.

153. Erker, G.; Kehr, G.; Fröhlich, R. *Organometallics* **2008**, *27*, 3–14.

154. Dinnebier, R. E.; Behrens, U.; Olbrich, F. *Organometallics* **1997**, *16*, 3855–3858.

155. Lambert, C.; Schleyer, P. von R. *Angew. Chem. Int. Ed. Engl.* **1994**, *33*, 1129–1140.

156. Jutzi, P.; Leffers, W.; Hampel, B.; Pohl, S.; Saak, W. *Angew. Chem. Int. Ed. Engl.* **1987**, *26*, 583–584.

157. Zhang, S.; Liu, J.; Wei, G.; Lin, G.; Chen, W. *Polyhedron* **1993**, *12*, 2771–2774.

158. Herberich, G. E.; Fischer, A. *Organometallics* **1996**, *15*, 58–67.

159. Rabe, G.; Roesky, H. W.; Stalke, W.; Pauer, F.; Sheldrick, G. M. *J. Organomet. Chem.* **1991**, *403*, 11–19.

160. Jordan, V.; Behrens, U.; Olbrich, F.; Weiss, E. *J. Organomet. Chem.* **1996**, *517*, 81–88.

161. Herdtweck, E.; Köhler, F. H.; Möller, R. *Eur. J. Inorg. Chem.* **2005**, 952–958.

162. Veith, M.; Mathur, C.; Mathur, S.; Huch, V. *Inorg. Chem.* **1999**, *38*, 5650–5652.